Plasma biomass gasification in a 15 kW pilot facility

by

Keabetswe Maseko

CVD 800

2020/2/09

Plasma biomass gasification in a 15 kW pilot facility

by

Keabetswe Maseko

Student Number: 27067514

A dissertation submitted in partial fulfilment of the requirements for the degree of Master's in Engineering

Department of Chemical Engineering

FACULTY OF ENGINEERING, BUILT ENVIRONMENT AND INFORMATION TECHNOLOGY

UNIVERSITY OF PRETORIA

Supervisor: Prof. P.L. Crouse

Co-supervisor: Dr I.J. van der Walt

Synopsis

Plasma gasification experiments were conducted on sucrose and crushed macadamia nutshells. The pilot-scale plasma gasification system used comprises a 15 kW DC plasma torch fitted to a 5 L gasification reactor. The DC plasma torch has an efficiency of ~30 % with most of the energy lost in the torch anode.

For the macadamia nutshells, the plasma input-power was set at 9, 11 and 14 kW. At each power input setting, four different feed rates were investigated, namely 0.5, 0.7, 1.04 and 1.14 kg/h. It was observed that as the power increases, conversion increases from 48 % at 9 kW to higher than 80 % at 14 kW. It was also observed that higher mass feed rates increase the conversion. The lower heating values of the syngas produced during gasification increased with higher power inputs and higher feed rates. At a feed rate of 1 kg/h, the maximum calorific power value was 3.45 kW, at a torch setting of 14 kW. The highest power values obtained was slightly more than 4 kW.

The effect of equivalence ratio (ER) was evaluated on the plasma gasification of sucrose. ER values of 1 and 2 were investigated. With an ER of 1, the CO/H_2 ratio was 1.8 and the CO/CO_2 ratio was 109. With an ER of 2, the CO/H_2 ratio was 1.73, and the CO/CO_2 ratio 18. As expected, an increase in ER enhances the formation of CO_2. A low ER thus results in higher syngas quality.

At equivalent conditions the homogenous, crystalline sucrose yielded a CO/CO_2 ratio of 109, significantly higher than the 29 for plasma gasification of the macadamia nut shells. A contributing factor to having better quality syngas, was the smaller the average particle diameter of the sucrose, 0.4 mm, compared to the 10 mm of the crushed macadamia nut shells was. Another contributing factor could be that the available carbon in the macadamia nut shells structure are more strongly bonded than in sucrose.

For additional insight, kinetic data for the pyrolysis of sucrose, fructose and glucose were obtained using a TGA-FTIR hyphenated system, at much lower heating rates than anticipated in plasma system, and TGA-DTG experiments on macadamia nut shells. Dynamic studies were performed on sucrose, fructose and glucose at heating rates of 5, 10, 15, 20 and 50 °C/min in an atmosphere of nitrogen flowing at 50 mL/min, and for the macadamia shell at heating rates of 5, 10 and 20 °C/min in an atmosphere of nitrogen flowing at 50 mL/min. The sugars yielded

80 % to 85 % conversion into gaseous products, while the conversion of the shells approached 90 %; the residue was biochar. The FTIR spectra showed the major products that form from the pyrolysis of sugars to be CO_2, H_2O, along with large quantities C-H-O-containing compounds, amongst them $C_5H_4O_2$ and $C_6H_6O_3$. The latter two compounds are probably condensible.

Keywords: Plasma gasification; pyrolysis of macadamia nut shells; equivalence ratio; calorific value; conversion

Acknowledgements

I would like to thank the National Research Foundation which gave me wonderful financial support and aided me in achieving my goal. As President Nelson Mandela once said, “Education is the most powerful weapon which you can use to change the world.”

I wish to thank my mother, who has always taught me to be persistent and face difficulties head on. She has always highlighted the importance of adversity. She would occasionally say, “You cannot grow without adversity, it enriches progress”.

I’m also grateful for the support and encouragement from my family, friends and colleagues. To Lesego Wakhaba, Nkateko Makaringe, and Gerard Puts – sincere thanks for your contribution to my research work. I’m forever grateful to Jaco van der Walt, whose vast knowledge of and passion for plasma gasification strengthened my interest to pursue initiatives for waste treatment.

To my God, words can’t even describe my gratitude. Your grace, mercy and love have carried me through this journey. I will continuously pray for wisdom and knowledge, trusting you to lead me to prosperous heights in all aspects of my life.

I thank Professor Philip Crouse most sincerely for his kindness, availability to discuss my research status and being a good listener. Your deep knowledge of all subject matters has always guided me to complete tasks with due diligence. I thank you for the encouragement, support and constant belief which reminded me that I’m capable beyond measure. It has been an honour to be mentored by you and I hope you will continue to guide me in obtaining higher education levels.

Table of Contents

List of figures

List of tables

Nomenclature

α	Defined as the conversion of pyrolysis.
g(α)	Denotes the integral form of the rate expression
TGA	Thermogravimetric analyser
FTIR	Fourier-transform infrared spectroscopy
MSW	Municipal solid waste
SWI	Solid waste incinerators
DTG	Differential thermogravimetry
RF	Radio frequency
DC	Direct current
AC	Alternating current
SASA	South African Sugar Association
GC	Gas chromatography
MS	Mass spectrometry
H-NMR	Proton nuclear magnetic resonance
slpm	Standard liters per minute
LHV	Low heating value
ΔQr	Power available for gasification
η	Efficiency
W*torch*	Power of the torch
*Q*losses	Power losses carried out of the gasification reactor

Chapter 1 Introduction

Current energy sources worldwide may be categorised as fossil fuels, nuclear fuels, and renewables. Fossil fuels are coal, petroleum and natural gas. These hydrocarbon-based fuels possess great utility due to their inherent energy density and ease of use. They are essentially chemical compounds which contain hydrogen and carbon atoms. Fossil fuels are the ubiquitous form of hydrocarbon fuels in the world today and it is common knowledge that our current way of life would not exist without them (Curley, 2011). A major disadvantage of the use of fossil fuels is the vast amount of carbon dioxide and other pollutants released into the atmosphere, which, according to current climate science, cause global warming and other environmental ills (Ozcan, 2014). Over the years, there has also been a worldwide decline in available fossil fuel resources and a substantial growth in their price. Figure 1.1 shows the annual cost increase of coal in South Africa (The Chamber of Mines Coal Leadership Forum, 2018).

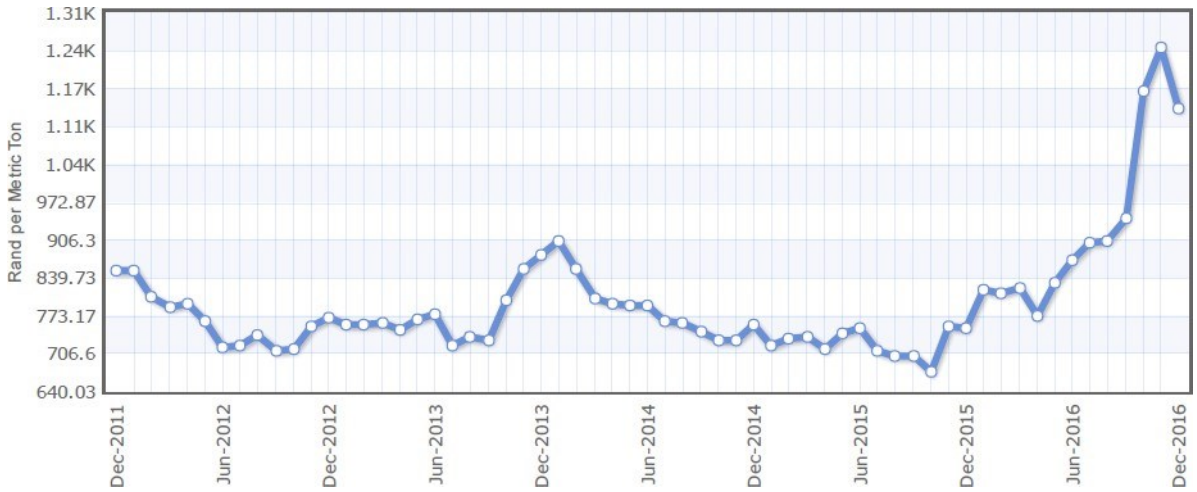

Figure 1.1: Monthly price of South African coal export*s*

The renewable energy sources include solar, wind, hydroelectric, biomass, and geothermal power. Renewable energy has swiftly become favourable as an alternative energy source to fossil fuels (Koçar and Civaş, 2013). Hydrocarbon fuels derived from biomass are an effective, practical and most reliable alternative to fossil fuels. Biomass effectively stores solar energy, and is the only renewable source of carbon that can be converted into convenient solid, liquid, and gaseous fuels. The use of biomass as a general source of heat and power has numerous benefits (Fiorese, Catenacci *et al.*, 2014), including, but not limited to, a carbon-neutral production cycle (Bridgwater and Peacocke, 2000), and globally abundant sources of raw materials (McKendry, 2002).

Different types of product can be derived from biomass, depending on the nature of the organic matter present in the starting material (Srirangan, Akawi *et al.*, 2012). A further advantage of using biomass is that reliance on conventional waste disposal methods such as landfills can be reduced, as both natural and synthetic organic waste material can be pyrolysed or burned to produce useful products or energy (Popp, Lakner *et al.*, 2014).

Biomass resources include wastes, forest products, energy crops and aquatic plants. The major constituents of energy crops are starch and sugar. The South African sugar industry constitutes a major part of the national economy because of its agricultural and industrial activities. It is estimated that the industry produces an average of 18.8 million tons of sugar annually(SASA, 2014). The sugarcane sector is situated primarily on farms in KwaZulu-Natal, along with substantial farming operations in Mpumalanga and the Eastern Cape (SASA, 2014). Since the South African sugar industry produces a large excess of sugar cane crops, the conversion of this excess into biomass-derived hydrocarbons is an economically attractive undertaking that is free from the environmental or sociological concerns that plague the bio-energy sector.

(Govender, 2011) pointed out that the sugarcane industry in South Africa has the potential to minimize non-beneficial climate changes by producing renewable cogeneration electricity and fuel ethanol. (Smithers, 2014) undertook a review of sugarcane trash recovery systems for energy cogeneration in South Africa. He highlighted the potential of biomass as a sustainable source of energy. It has been calculated that approximately one-third of the energy available from sugarcane is contained in its off-cuts (tops and leaves), which are generally burned or not recovered from the field. Based on the results reported in the literature and assuming 50% off-cut recovery efficiency, it is estimated that 1.53 million tons of sugarcane off-cuts are available annually for the cogeneration of electricity in South Africa, which would essentially produce 180 MW over a 200-day milling season. In South Africa, more than 90% of the sugarcane crop is manually harvested and the off-cuts burned; therefore, a case could be made for re-evaluating this industry's waste handling methods for possible energy generation.

(Wienese and Purchase, 2004) investigated the prospects for the South African sugar industry producing renewable energy. They reported that South African sugar factories have the potential to export the excess electricity generated during production, above their own demand, to the grid. The key factors that largely affect the possibility of exporting electricity are: increasing boiler and turbine efficiencies; reducing process steam; and improving biomass-based integrated gasification combined-cycle technology.

Biomass gasification is the process of converting organic matter into syngas, i.e., the production of mainly carbon monoxide (CO), carbon dioxide (CO_2) and hydrogen (H_2). Gasification takes place at temperatures above ~900 °C. In the case of plasma gasification, a plasma torch is used as energy source for reaching the high temperature required. The overall aim of this study was to investigate the effects of solid feed rates and different plasma power inputs (and the resulting reactor operating temperatures) on product quality and yield, using well-defined materials, viz, sucrose and crushed macadamia nut shells, in 30 kW pilot facility. Both sucrose and macadamia nuts are classified as energy crops, comprising mainly cellulose, hemicellulose and lignin (Bridgwater, 2003).

Previously (Makaringe, van der Walt *et al.*, 2017) investigated four biomass materials, namely peach pips, pine wood, bamboo and Napier grass. TGA-FTIR (thermogravimetric analysis–Fourier transform infrared spectroscopy) analyses were conducted in addition to the plasma gasification studies. Bamboo and Napier grass were eventually excluded from the investigation because of their fluffy nature which led to intractable feeding problems. The conversion efficiency was found to increase with increasing reactor temperature. The effect of feed rate on conversion efficiency and the produced gas concentration was minimal. The gaseous products obtained were predominately carbon monoxide and hydrogen, which is attributed to the high operating temperature, greater than 1 000 °C, in the plasma reactor. For the TGA-FTIR experiments, the predominant gas was carbon dioxide, with small traces of carbon monoxide. Most of the heat loss occurred at the torch anode; energy conversion efficiency for the plasma process was between 30 and 40 %. One objective of this study, was to complement this work. Similarly, TGA-FTIR experiments were conducted to analyse the thermal behaviour of the biomass samples, namely sucrose, as well as fructose and glucose, followed by macadamia nut shells. The TGA-FTIR experiments were performed using both nitrogen and oxygen. After that plasma gasification experiments were conducted. In the plasma gasification of sucrose, feeding problems were experienced. This was caused by the nature of the sugar, which decomposes at temperatures above 186 °C clogging the screw feeder.

Chapter 2 Literature review

Biomass (essentially organic materials) is a sustainable source of renewable energy such as electricity and biofuel. Biomass is organic material derived from living organisms. It is composed of a mixture of organic molecules containing hydrogen, oxygen and nitrogen. The carbon in the plant material is absorbed from the atmosphere as CO_2 by plant life using the energy from the sun. The biomass carbon reacts with oxygen when burned and forms carbon dioxide, which is then released into the atmosphere.

When complete combustion occurs, the amount of CO_2 that is produced equals the amount that was originally absorbed from the atmosphere. The process is regarded as carbon neutral because there is no net addition of CO_2. This effect is known as the carbon cycle or zero carbon emissions. Fossil fuels such as oil, coal and gas are also derived from biological material, but they were obtained from underground sources. They have a higher energy density, but when they are burned and the products are released into the atmosphere, fossil fuels render a carbon positive scenario (Demirbas, 2004).

2.1 Biomass resources

Biomass resources include wood, wood waste, agricultural crops and their waste by-products, municipal solid waste (MSW), animal wastes, waste from food processing, aquatic plants and algae. The majority of biomass energy production is wood and waste at 64 %, second is MSW at 24 %, then agricultural waste at 5 % and landfill gases at 5 % (Demirbas, Balat *et al.*, 2011). In landfills, methane is used as fuel in waste-to-energy plants. The waste-to-energy process reduces the MSW dumped in landfills by 60–90%, also causing the cost of landfills to be reduced. A key element about biomass is that it differs from other alternative energy sources because it is not homogeneous. Biomass resources can be divided into three basic categories:

1. Wastes
2. Standing forests
3. Energy crops

A wide range of materials can be used as biomass resources for energy production. Biomass energy is further separated into two categories: modern biomass and traditional biomass. Modern biomass is mainly used on a large scale and aims to substitute for conventional energy sources. It includes wood, agricultural residues, urban wastes, biofuels and energy crops.

Traditional biomass is classified as being typical of developing countries and has small-scale uses. It includes fuel wood, charcoal for domestic use, rice husks, plant residues and animal waste (Yanik, Kornmayer *et al.*, 2007).

Due to the exponential growth of the world population, the demand for energy is also increasing at an exponential rate. The fact that fossil fuels are being depleted over the years, and the growth in awareness of the need for preventing environmental degradation, have led to the search for alternative energy sources which will be renewable. Currently, biomass contributes about 12 % of the world's primary energy supply, with the percentage being higher in many developing countries, ranging between 40 and 50 %. The production of biomass worldwide is estimated at 146 billion metric tons a year, mostly biomass being wild plant growth. Some farm crops and trees can produce up to 20 metric tons per acre of biomass a year. Various types of algae and grasses may produce 50 metric tons a year (Serio, Kroo *et al.*, 2003).

2.2 Energy from biomass

The energy content of different plant materials determines their calorific value. The calorific value is a function of the percentage of carbon and hydrogen, which are the main contributors to the energy value of a biomass material. To obtain maximum energy, the biomass material should be air dried because the amount of energy contained varies with the moisture content. The amount of water has an effect on the recoverable energy. A study on Indian firewood found that the calorific value decreases linearly with increasing moisture content. There are five ways in which energy can be obtained (Ruiz, 2013):

1. Production of crops yielding starch, sugar, cellulose and oil
2. Solid waste which can be burned
3. Anaerobic digesters producing biogas which can be used to generate heat/electricity
4. Landfill production for methane
5. Biofuel production which includes ethanol, methanol, biodiesel and their derivatives

2.2.1 Wood fuels

Wood fuels are fuel sources originating from natural forests, natural woodlands and forestry plantations, specifically fuel wood and charcoal from these sources. The fuels include sawdust and residues from both forestry and wood-processing activities. Fuel wood is the fuel source for particularly small-scale industrial energy, used in the rural areas of developing countries.

As the demand for energy grows due to an increase in world population, reforestation programmes will be required to ensure that the required energy demand is met. The principal wood fuels used in industrialized countries are derived from wood-processing activities. The main advantage of having the energy production near its source is that it avoids the expenses associated with transport costs. Land clearing and logging residues provide domestic wood fuels (Funino, Yamaji *et al.*, 1999).

2.2.2 Agricultural residues

A large amount of agricultural plant residues is produced worldwide but is under-utilized. Rice husk is third the most common agricultural residue, making up 25 % of rice by mass. Sugarcane fibre, also known as bagasse, is the other main plant residue, along with coconut husks, groundnut (peanut) shells and straw. Wastes such as animal manure are included in agricultural residue, and in many developing countries they are used to generate heat or electricity (Funino, Yamaji *et al.*, 1999).

2.2.3 Sugarcane as an energy crop

The primary purpose of energy crops is to produce energy. These crops include energy plantations such as eucalyptus, willows, poplars, herbaceous crops, sugarcane, vegetable oil-bearing plants and sunflowers. Plant oils are important because they have a high energy density. Figure 2.1 shows the sugarcane plant undergoing the photosynthesis process (Koçar and Civaş, 2013).

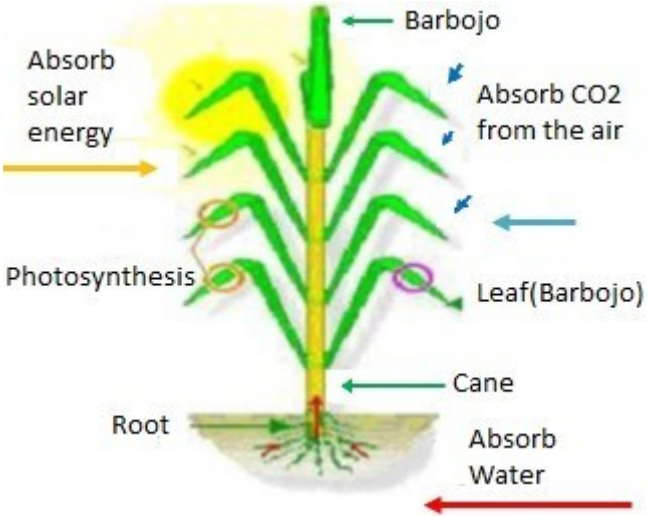

Figure 2.1: Sugarcane and the process of photosynthesis (Koçar and Civaş, 2013)

Sugarcane is the most abundant energy crop produced worldwide and its resources are increased by harvesting the sugarcane leaves and tops. Sugarcane is any of several species of grass, belonging to the genus *Saccharum,* tribe *Andropogoneae.* It originates from the grass family *Poaceae*. Sucrose is produced during the process of photosynthesis. Sugarcane's stout, jointed fibrous stalks are rich in sucrose, which accumulates in the stalk internodes. It typically grows in tropical regions. It is initially harvested and thereafter undergoes a crushing process to extract the liquid or juice. The liquid then goes through a heating process until all the water has evaporated and a syrup is formed. The syrup is boiled until sugar crystals form, producing a raw product of sucrose (Loh, Sujan *et al.*, 2013). Figure 2.2 shows the top 10 produced commodities in South Africa for 2013. From the figure it is evident that sugarcane is the most produced energy crop, followed by maize (Department of Agriculture, 2017).

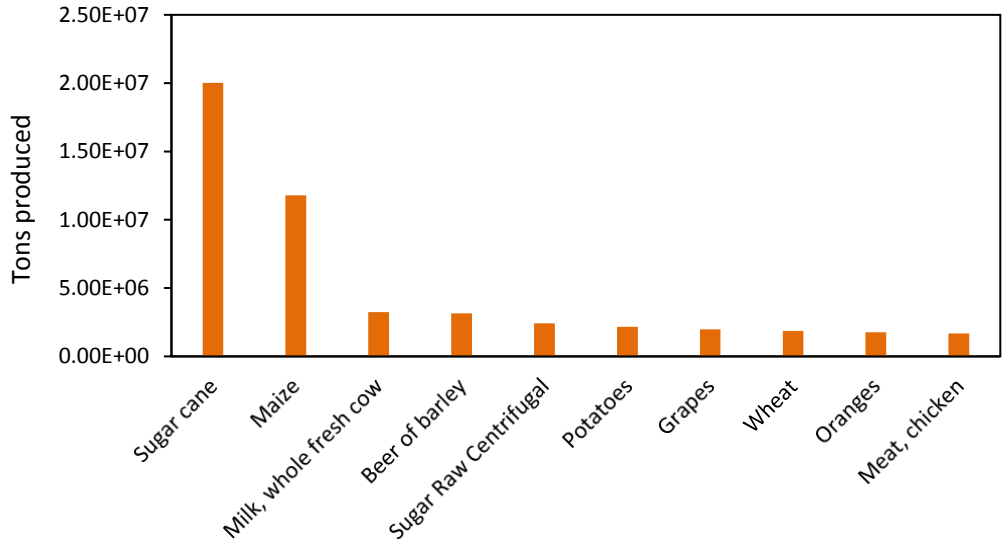

Figure 2.2: Top 10 produced commodities in South Africa for 2013 (Department of Agriculture, 2017)

(Alonso Pippo, Luengo *et al.*, 2011) explored energy recovery from sugarcane biomass residues by making use of sugarcane agricultural residues as boiler feedstock. They are of the opinion that energy recovery from sugarcane residues disposal would enhance social developments relating to minimizing environmental issues. With the improvements in sugarcane harvesting and cogeneration technology, bagasse and sugarcane trash have become important sources of bio-energy. A further advantage of using sugarcane trash is the additional benefit of it not competing as a food source. (Bocci, Di Carlo *et al.*, 2009) considered possible initiatives to improve the efficiency of sugarcane processing plants, such as increasing the pressure and temperature in the Rankine cycle of the plant, innovative configuration based on a gasifier plus hot gas conditioning, and gas turbine fuel cells. Figure 2.3 shows the increase in production of sugarcane and sugar beet across the world during the last decade.

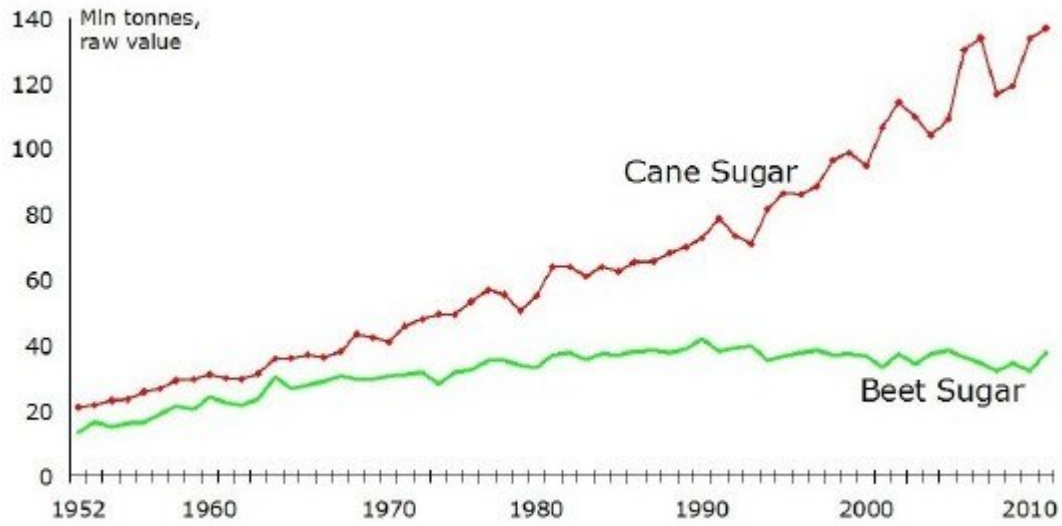

Figure 2.3: World sugar beet and sugarcane sugar production for the period 1952–2012

(Bocci, Di Carlo *et al.*, 2009) concluded that sugarcane bagasse and sugarcane trash have the potential to provide a significant amount of biomass for electricity production, and that the potential is increased by using the advanced cogeneration technologies. (Leal, Galdos *et al.*, 2013) investigated the importance of the various impacts on sugarcane residues left on the ground to decay during the production of sugar. They considered the availability, quality and economics of recovery which were used as the main criteria to determine the amount of residue that can be recovered for bioenergy or biofuels production. They also stated that sugarcane residues can be used as feedstock for energy production, soil protection against erosion, increase of soil organic carbon content, inhibition of weed growth, nutrient recycling and reduction of soil water losses.

Through the years there has been a growth in world population, resulting in an increase in energy consumption. This has also led to a rise in industrial development and socio-development. Life with electricity has expanded and we have become dependent on it. The main benefits of sustainable energy for waste management are to reduce landfill disposal and unmanageable waste, as well as to minimize the dangerous impact of waste on the environment. South Africa faces waste management challenges, especially with regard to hazardous and industrial waste. It is estimated that the waste generated in 2011 amounted to 108 million tons. It was also estimated that the amount of waste generated in 2015 would increase by an alarming 33 million ton. The lack of efficient waste treatment systems is due to insufficient waste

disposal facilities, and perhaps due to still making use of old technology for treatment purposes. Various thermal processes have been developed for treating waste and to obtain by-products that will essentially be useful in meeting the aims of energy production (Oelofse and Nahman, 2013).

Traditionally, the biochemical conversion of biomass into liquids such as ethanol has been undertaken using sugar/starch feedstocks, such as cereals. The conversion of cellulose into glucose via acid/enzymatic hydrolysis and the subsequent conversion of glucose into alcohol, using fermentation, is more easily undertaken with high-cellulose-content biomass than with lignin-rich biomass, i.e. woody species, which are not so easily converted (Coombs, 1996). There are three major processes for the conversion of biomass: thermal, chemical and biochemical conversion. Thermochemical processes convert biomass into viable biofuels and industrially useful chemical products. The different processes for thermal conversion vary according to their operating conditions, with the main parameters being the oxygen content and the temperature condition. These thermochemical processes include torrefaction, liquefaction, gasification and supercritical fluid extraction methods (Basu, 2013). Pyrolysis and gasification are the commercially used biomass thermal conversion processes. Among the thermochemical processes, pyrolysis has received increasing attention since the process conditions may be optimized to produce high-energy-density pyrolytic oils, in addition to the derived char and gas (Luo, Wang *et al.*, 2004).

2.2.4 Macadamia as an energy crop

Macadamia nuts originate from Australia and constitute part of the plant family *Proteaceae*. Macadamia is an evergreen species that can grow 19 m tall, with a width of 13 m. The *M. integrifolia*, which is referred to as “smooth shell macadamia”, and the *M. tetraphylla,* which is referred as “rough shell macadamia”, are regarded as the most important members of the family because of their economic viability. Their kernels are edible. The productive life of the tree is on average 40 to 60 years. However, this can be extended depending on suitable soil management and climates (Nagao, 2011).

Flowering occurs in mid-winter, with the development of nutlets into spherical nuts encased in green fibrous husks. Thereafter, a very hard, brown shell surrounds the macadamia nut kernels. Figure 2.4 shows the nutlets developing into spherical nuts encased in green fibrous husks (Garbelini, Ono *et al.*, 2016).

Figure 2.4: The development of macadamia nutlets into spherical nuts encased in green fibrous husks

The nuts are then harvested 7 to 8 months later. The macadamia nut has the hardest shell of any edible nuts. It's been estimated that a carefully applied pressure of 300 psi is required to shatter the shell without damaging the nut inside. Figure 2.5 shows the final product of matured ripe macadamia nuts (Garbelini, Ono *et al.*, 2016).

Figure 2.5: Matured ripe macadamia nuts

The world's larger producer of macadamia nuts is Australia, followed by Hawaii. South Africa is the third largest macadamia nut producer. Data from the macadamia industry in South Africa indicate a rapid growth rate, as seen in Figure 2.6. The growth rate of new plantings of macadamia nuts is increasing in all provinces (Southern African Macadamia Growers's Association, 2018).

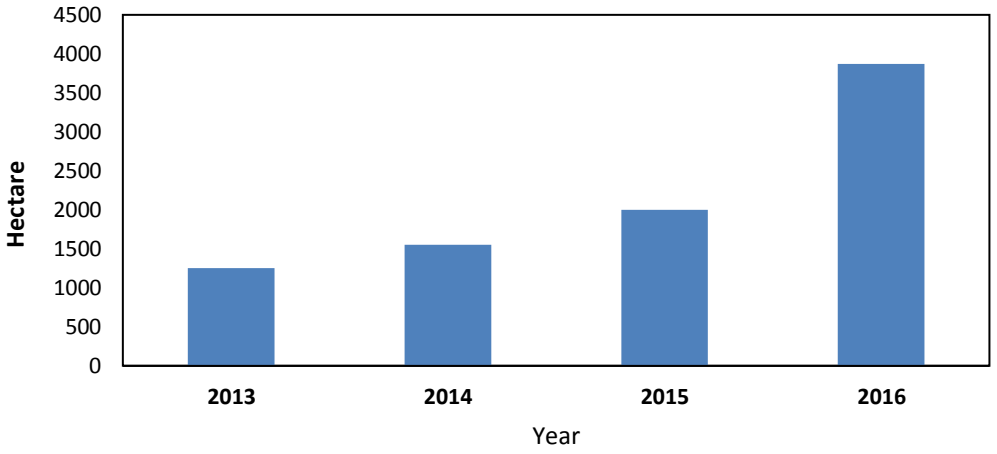

Figure 2.6: New plantings (ha) in the South African macadamia nut industry

Mpumalanga is the largest producing province of macadamia nuts in South Africa, as seen in Figure 2.7. The planting of macadamia nut trees near the coastal region of KwaZulu-Natal has increased tremendously (Southern African Macadamia Growers's Association, 2018).

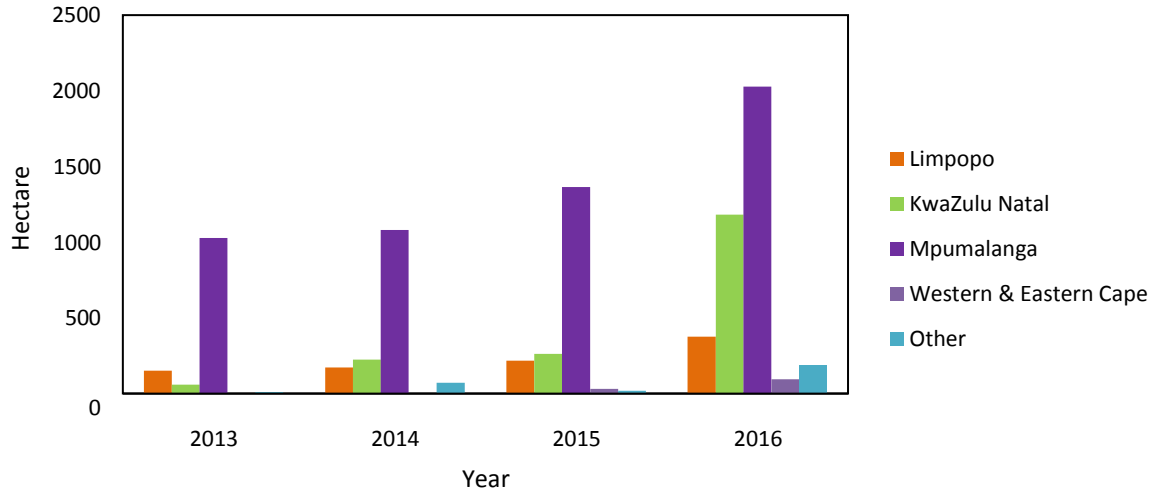

Figure 2.7: New plantings (ha) of macadamia nuts in South Africa relative to provinces

Based on the rapid growth of macadamia nut plantings, the production of macadamia nuts is also expected to increase. Figure 2.8 shows the total macadamia nuts production in South Africa, which is expressed in metric tons on a shell basis at 1.5 % kernel moisture content (Southern African Macadamia Growers's Association, 2018).

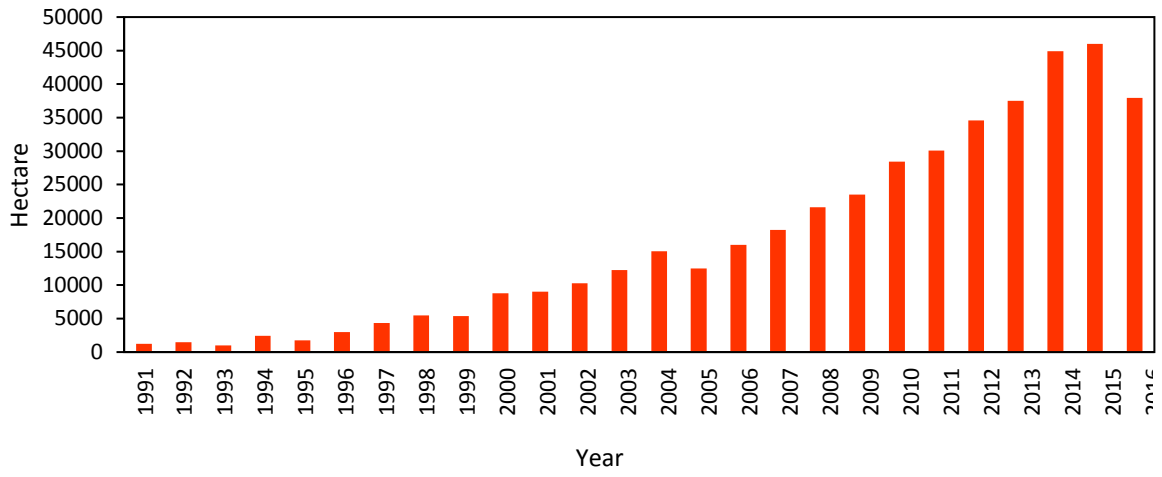

Figure 2.8: History of macadamia nuts production

The shells and other waste comprise about 70 % by weight of the macadamia nuts. In the past, waste produced from macadamia nut shells was merely placed in dumpsters, along with the rest of the trash to be disposed at landfills. Ergon Energy and Suncoast Gold Macadamias, Australia's biggest nut supplier, collaborated to build a plant generating electricity from macadamia nut shell waste. Suncoast Gold Macadamias produces over 5 000 tons annually of macadamia waste shells. The plant became fully commissioned and operational in 2005. A 6 MW steam boiler is powered by burning nut shells, producing 9 ton/h of high-pressure steam. A small fraction of the steam is used to dry the macadamia nut shells to reduce the moisture content in the kernels. Most of the steam is transferred to a 1.5 MW steam turbine, which generates 9 500 MWh annually of clean renewable energy (Energy, 2003).

Farmers have also recently started using waste from macadamia nut shells to produce biochar. Using biochar provides a method of increasing soil organic matter in a way that is stable for centuries. There are also agricultural benefits in using biochar for farmers. These benefits include (Trazzi, Leahy *et al.*, 2016):

- Biochar is effective in retaining water and nutrients in the root zone where it is available to plants.
- It increases soil tilth.
- It supports microbial communities.

- Biochar is highly recalcitrant and does not easily decay. It can sequester organic carbon for millennia – a benefit to soil fertility and a benefit to humanity in helping to reduce atmospheric carbon.

2.3 Structural composition of biomass

The three major constituents of biomass are cellulose, hemicellulose and lignin. There are also inorganic constituents and some fraction of water. The combination of cellulose, hemicellulose and lignin is known as lignocellulose, which comprises the parts of the plant matter produced by photosynthesis. The relative proportions of cellulose and lignin is one of the determining factors in identifying the suitability of plant species for subsequent processing as energy crops. The constituents are bonded by non-covalent forces or by covalent cross-linkages. Cellulose and hemicellulose are macromolecules constructed from different sugars, while lignin is an aromatic polymer synthesized from phenylpropanoid precursors (Lede and Bouton, 1999).

Cellulose is a glucose polymer, consisting of linear chains of (1,4)-D-glucopyranose units, where the units are linked 1-4 in the β-configuration, having an average molecular weight of 100 000. Hemicellulose is a mixture of polysaccharides, being composed mostly of sugars such as glucose, mannose, xylose, arabinose, methylglucuronic and galaturonic acids, with an average molecular weight of <30 000. The difference between cellulose and hemicellulose is the heterogeneous branched polysaccharide that binds strongly but non-covalently to the surface of each cellulose microfibril. Hemicellulose differs from cellulose in that it consists primarily of xylose and other five-carbon monosaccharides. Lignin arises from a group of amorphous high-molecular-weight, chemically related compounds. A three-carbon chain attached to the rings of six carbon atoms, called phenyl propane, is the building block of lignin (Yang, Yan *et al.*, 2007).

These building blocks of lignin may have zero, one or two methoxyl groups attached to the rings, giving rise to the three structures termed I, II and III respectively. The source of the polymer determines the proportions of each structure. Structure I is found in plants such as grasses, structure II in the wood of conifers and structure III in deciduous wood. Cellulose has the biggest fraction, representing about 40–50 % of biomass by weight, and hemicellulose represents 20–40 % of the material by weight. In combustion, the structural analysis of the biomass is important as it is one of the key factors determining the composition of the products.

The structural analysis is also vital for estimating the higher heating value (Yang, Yan *et al.*, 2007).

Carbohydrates are the simplest form of sugars. They are called carbohydrates because they contain carbon, oxygen and hydrogen atoms with a general typical formula of $C_n(H_2O)$, proportional to forming water. Glucose is produced during the photosynthesis process during which plants make their own food in the presence of sunlight, carbon dioxide, water and chlorophyll. Glucose acts as a form of fuel in the body of living organisms for the processes of growth, fertilization, stimulation of the immune system, and the development of blood cells. Carbohydrates are also saccharides, consisting of aldehydes and ketones. The various types of saccharide include monosaccharides, disaccharides and polysaccharides. A monosaccharide is the simplest form of sugar unit; examples include glucose, fructose and galactose. The most important monosaccharide is glucose, which is the human body's preferred energy source. It is commonly referred to as blood sugar because it circulates in the blood, relying on the enzymes hexokinonase or glucokinase to initiate metabolism. The body processes most of the carbohydrates ingested into glucose, which can either be used immediately as a source of energy or stored in the muscle cells or the liver as glycogen for later usage. Insulin is primarily secreted to respond to elevated blood concentration of glucose and also facilities the entry of glucose into the cells (Giudicianni, Cardone *et al.*, 2013).

Glucose is an aldehyde and has two isomers, D-glucose and L-glucose. D-glucose is the only biologically active isomer and its mirror image L-glucose cannot be used by cells. In a solution, the open-chain form of either D-glucose or L-glucose exists in equilibrium with several cyclic isomers, each containing a ring of carbons closed by one oxygen atom. The D-glucose isomer can exist in two forms, alpha-D-glucose and beta-D-glucose. The difference is only in the direction that the -H and -OH groups point on carbon 1. As seen in Figure 2.9, the designation alpha means that the hydroxyl groups attached to the C-1 and the CH_2OH groups at C-5 lie on opposite sides of the ring's plane, a trans arrangement. Figure 2.10 represents the beta-D-glucose molecule, showing that the hydroxyl group attached to the C-1 and the CH_2OH groups at C-5 lies on the same side of the ring's plane, a cis arrangement. When alpha-D-glucose molecules are joined chemically to form a polymer, starch is formed. When beta-D-glucose molecules are chemically joined to form a polymer, cellulose is formed. For acyclic systems, the trans isomers are more stable than the cis isomers. The instability of the cis isomers is normally due to the steric interaction of the substituents. The trans isomers are normally stable

due to their being less exothermic during combustion, making them thermodynamically stable (Bassilakis, Carangelo *et al.*, 2001).

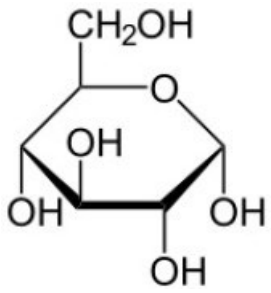

Figure 2.9: Alpha-D-glucose molecule

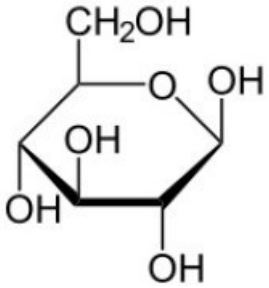

Figure 2.10: Beta-D-glucose molecule

Fructose is mostly found in vegetables and fruits. Fructose, however, has a different metabolic pathway and is not the preferred energy source for muscles or the brain. It is only metabolized in the liver and relies on fructokinase to initiate metabolism. In comparison to glucose, fructose acts more like a lipogenic, producing fat. It also does not cause insulin to be released or stimulate the production of leptin, a key hormone for regulating the energy intake. Thus, fructose behaves more like a fat in the body than the other carbohydrates. Fructose is a six-carbon polyhydroxyketone as seen in Figure 2.11, and its stability is due to its six-membered structure. Galactose is found in milk and dairy products (Ponder and Richards, 1993).

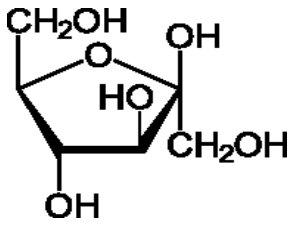

Figure 2.11: Molecular structure of fructose

Disaccharides are two monosaccharides bonded together; examples are sucrose, maltose and lactose. As shown in Figure 2.12, sucrose is formed by binding a molecule of glucose and fructose together. Sucrose is known in table sugar and is found in sugar beet and sugarcane. Vegetables and fruits also naturally contain sucrose. When sucrose is consumed, the enzyme beta-fructosidase separates sucrose into its individual sugar units of glucose and fructose. Both the sugars are taken up by their specific transport mechanisms to perform their respective duties in the body. The body responds to the glucose content of a meal in its usual manner and the fructose uptake occurs at the same time. The body uses glucose as its main energy source and the excess fructose, when not needed, will be poured into fat synthesis (Bulut and Karagoz, 2013).

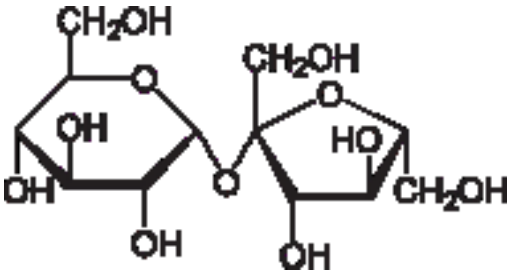

Figure 2.12: Molecular structure of sucrose

Polysaccharides are a chain of two or more monosaccharides and are classified as polymers. The two primary polysaccharides are cellulose and starch. Both the molecules consist of a long chain containing thousands of glucose molecules attached end on end. The difference between starch molecules and cellulose molecules is in the way in which the glucose structures are attached to each other. The difference in configuration of the molecules accounts for the very different properties of starch and cellulose. Because of the bond angles in the alpha acetal linkage, the starch molecule that forms is a spiral structure. The molecular structure of starch is presented in Figure 2.13. Starch is mainly used as storage for excess food reserves and is found in most plants. Due to the bond angles in the beta acetal linkage, the cellulose structure is mostly a linear chain. The molecular structure of cellulose in presented in Figure 2.14. Once

the glucose molecules are bonded into cellulose molecules, cellulose is no longer available as a food source. It is used primarily for structural support (Yang, Liu *et al.*, 2013).

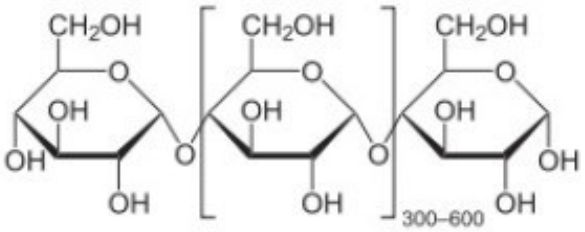

Figure 2.13: Starch molecule

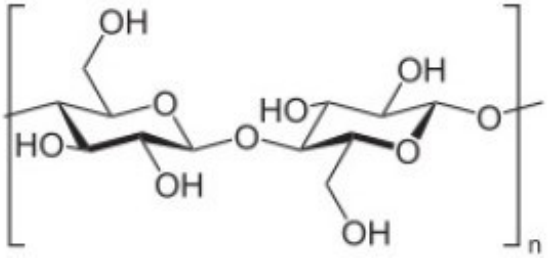

Figure 2.14: Cellulose molecule

2.4 Advantages and disadvantages of biomass fuels

The raw materials of biomass are readily available and are a relatively cheap fuel source. Biomass captures some of the hazardous components during combustion and has great reactivity during combustion processes. Typical examples of the materials that make up biomass fuels are manure and crops. Biomass is used as a renewable source of fuel to produce energy because there will always be waste residues in terms of scrap wood and forest resources. It presents a greater opportunity for new job creation as there is a diversification of fuel supply and sufficient energy security. Biomass can combine with conventional fossil fuels to reduce emissions and confer economic benefits. However, the natural decomposition of biomass produces methane, which is more active as a greenhouse gas than carbon dioxide. There is an additional greenhouse gas emission benefit in burning biogas, landfill gas and biomass residues to produce carbon dioxide. Biomass fuels have a limited sulphur content and do not contribute to sulphur dioxide emissions which can cause acid rain. Landfill disposals are reduced when waste material is used as biomass. Using biomass as an energy source does, however, have disadvantages. Biofuels do not compete economically with conventional fuels such as coal

because it is costlier to generate electricity from biomass in comparison with coal. There is also a great deal of potential competition with food and feed production. Biomass requires large harvesting and the collection, transport and storage of biomass is costly (Ahrenfeldt, Thomsen *et al.*, 2013).

The key aspects that play a role in the decision to employ a certain reactor design for the gasification process are: the scale of operation; the flexibility of the feedstock in terms of size and composition; the sensitivity to the amount of the ash and its composition; and the tar yield. The scale of the operation is the primary criterion since small decentralized systems tend to favour a basic simple design that is easy to control and maintain and utilizes a cheap reactor. The flexibility of the feed is crucial because biomass is quite fibrous and can become difficult to pulverize. Reducing the biomass in size is not desirable due to the adverse effect on the energy efficiency of the entire process. Raw biomass contains varying amounts of moisture, which has a huge impact on the composition of the final product. It is of the utmost importance that the gasification reactor should be able to handle any changes in fuel supply characteristics, both physically and chemically (Merola, 2011).

Each type of biomass contains an amount of inorganic matter, normally referred to as ash, in addition to the moisture and volatile fraction. Ash accumulation can become problematic, leading to difficulties in the operation of the gasifier. The downstream equipment can be negatively affected by the tar produced in the gasifier. Tar is defined as various kinds of larger hydrocarbon that are produced during the gasification process. It is basically all organic compounds with a molecular weight larger than that of benzene, excluding soot and char. Tar formation is a well-known problem in the gasification process. The main issue with tar formation is that it contributes significantly to the heating value of the product gas (Gómez-Barea, Ollero *et al.*, 2013).

Physically removing the tar from the gas will largely reduce the net carbon conversion efficiency of the process. The conversion route that is preferred is where tar is broken into smaller molecules such as CO and H_2. Combustion applications have a higher tolerance for tar in comparison with fuel cell applications. The concentration of tar produced during gasification should be limited to prevent the fouling of the downstream equipment and to enable the chemical energy stored in the tar molecules to be available to the conversion process (Battacharya, Siddique *et al.*, 1999).

2.5 Thermochemical processes

The conversion of biomass into biofuels can be achieved primarily via biochemical and thermochemical processes. These processes include a number of possible routes for converting the initial bio-renewable feedstocks into useful fuels and chemicals, including solid fuels, liquids and gases to produce electric power, heat, chemicals or gaseous and liquid fuels. Thermochemical conversion processes proceed via combustion, pyrolysis and gasification. Figure 2.15 shows a schematic diagram for biomass thermal conversion processes (Demirbas, 2009).

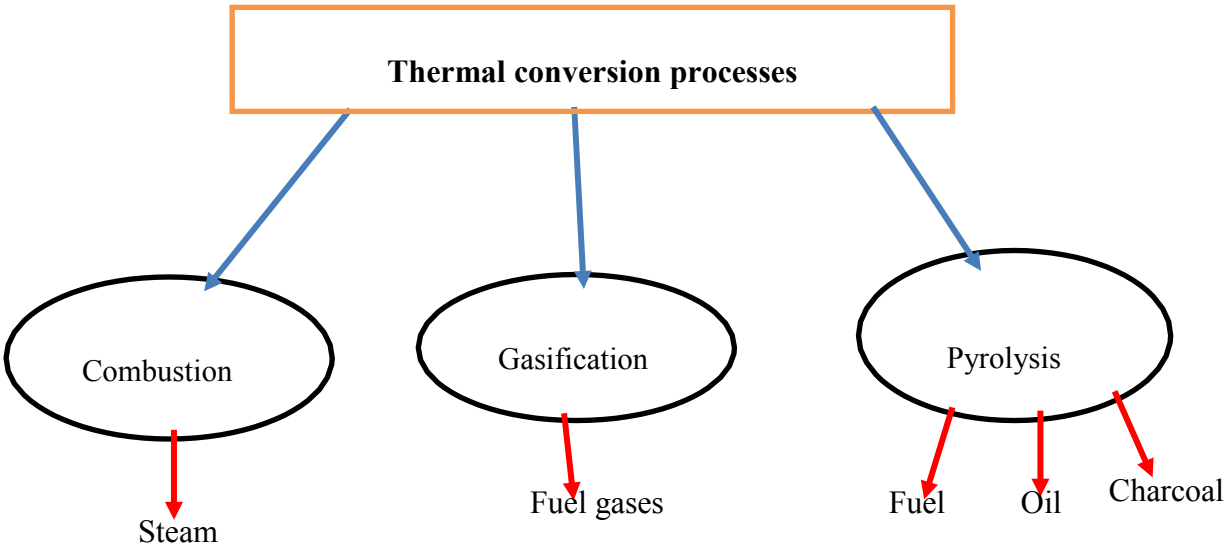

Figure 2.15: Schematic diagram of thermal conversion processes

Gasification occurs at moderately high temperatures and converts solid biomass into combustible gas mixtures known as syngas. The main components of the gas are CO, H_2, CO_2, CH_4, H_2O and N_2. There are also traces of tars which are produced during the gasification reaction. The syngas produced can be used to produce heat or liquid fuels. Different gasifying agents can be used, such as air, oxygen and steam. The use of air as a gasifying agent is relatively common in industry, but subsequently yields syngas with a low heating value (4–7 MJ/Nm^3) which can only be applied for heat and power usage. The use of steam and oxygen as gasifying agents increases the heating value of syngas (10–18 MJ/Nm3) and the H_2/CO ratio. For the purpose of producing liquid fuels through the Fischer-Tropsch process and for the production of H_2 to be used in fuel cells, a high H_2/CO ratio is required (Canabarro, Soares *et al.*, 2013).

Pyrolysis is an advanced thermal treatment that converts material into syngas at temperatures around 1 000 °C in the absence of oxygen. It can be described as the direct thermal decomposition of the material or organic matter to obtain solid, liquid and gas products. The operating temperature plays a vital role in the composition of the gas produced. The charcoal yield decreases with increasing temperature and low heating rates. The yield of a liquid product is maximized with a low temperature, high heating rate and short gas residence time process. A high yield of fuel gas is obtained with a high temperature, low heating rate and long gas residence time process (Mohan, Pittman *et al.*, 2006).

2.5.1 Gasification

The gasification process was first established in the 19th century by Dean Clayton. He implemented the process in factories to supply the town with its very own produced gas. The first plant became operational in London in 1812. Later the Fischer-Tropsch process was discovered in 1923 by Franz Fischer and Hans Tropsch, which made it possible to convert coal to liquid fuel. The German army wanted to improve the gasification process for fuel and chemical production. Towards the end of World War II, fossil fuels became cheaper and more readily available. Thereafter, gasification was halted until recently when it was realized that fossil resources were becoming depleted and fuel prices were on the rise. Gasification has now once again become favourable as means for energy production. The oxygen contained in the gasifying or oxidizing agent used for the gasification (air, oxygen, CO_2, steam H_2O) reacts with waste or organic material to produce syngas. The produced syngas can be used as feedstock in (Hrabovsky, 2011):

- The Fischer-Tropsch process for the production of liquid fuel
- Gas turbines or fuel cells for electricity production
- Chemical products

2.5.1.1 Conversion steps inside the gasifier

A solid organic fuel undergoes a process of thermochemical conversion when it passes through several conversion steps. The fuel is dried, heated, pyrolyzed, partially oxidized and reduced inside the reactor. The four basic processes of gasification are (Siedlecki, De Jong *et al.*, 2011):

1. Drying of the fuel
2. Pyrolysis

3. Oxidation
4. Reduction

2.5.1.1.1 Drying of the fuel

The moisture contained in the fuel is first removed to a level below 20 %. The solid fuel pellets are heated and dried at the top of the gasifier unit. The process is expressed as in Equation 1.

$$fuel_{raw} \rightarrow fuel_{dry} + H_2O_{(g)} \quad (1)$$

2.5.1.1.2 Pyrolysis

The dried fuel pellets now enter the second zone, called the pyrolysis zone. The gaseous products from the devolatilization are partially burned by the existing air. The volatile fraction of the fuel constituents is released into the gas phase and the remaining solids are the char, fixed carbon and ash. Equation 2 describes the pyrolysis process.

$$fuel_{dry} \rightarrow gases + vapours + char \quad (2)$$

2.5.1.1.3 Oxidation

The products of the pyrolysis step react with an externally supplied oxidant, which is normally O_2. The O_2 supplied is either from the enriched air or in the pure form. Steam and CO_2 can also act as oxidants. The oxidation process is as shown in Equations 3, 4 and 5.

$$C_{(s)} + {}^1/_2\, O_2 \rightarrow CO \quad (3)$$

$$CO + {}^1/_2\, O_2 \rightarrow CO_2 \quad (4)$$

$$H_2 + {}^1/_2\, O_2 \rightarrow H_2O \quad (5)$$

2.5.1.1.4 Reduction

The reduction step only proceeds when there is local depletion of oxygen and does not apply to combustion processes with sufficient excess air. Unlike the oxidation reactions, most of the gasification/reduction reactions are endothermic. It is necessary to provide the required amount of heat to maintain the desired gasification temperature. In the “direct gasification” concept this is achieved by supplying more oxygen so that the heat of combustion of the oxidation reactions will balance the heat required by the reduction reactions. In the “indirect gasification”

concept, the heat from outside the gasification reactor is usually transferred by a circulating heat carrier. The reduction process is as shown in Equations 6 to 11.

$$CH_4 + CO_2 \rightarrow 2CO + 2H_2 \quad (6)$$

$$CH_4 + H_2O \rightarrow CO + 3H_2 \quad (7)$$

$$CO + H_2O \rightarrow CO_2 + H_2 \quad (8)$$

$$C_{(s)} + H_2O \rightarrow CO + H_2 \quad (9)$$

$$C_{(s)} + CO_2 \rightarrow 2CO \quad (10)$$

$$C_{(s)} + 2H_2 \rightarrow CH_4 \quad (11)$$

2.5.1.2 Main reactor configurations

There are currently several types of gasification process configuration. The main reactor configurations are fixed bed gasifiers, circulating fluidized beds and entrained flow, as discussed below. Each of these reactors can carry out the gasification process. There is a compromise with each different type of reactor configuration between the quality of the produced gas, the conversion efficiency, the sustainability of handling of feedstock with varying physical and chemical properties, investment costs, as well as the complexity of the design and the operating conditions (Molino, Chianese *et al.*, 2016).

2.5.1.2.1 Fixed bed/moving bed gasifiers

Fixed bed gasifiers are the customary reactors for gasification and they normally operate at temperatures of approximately 1 000 °C or lower. The biomass is fed into the reactor at the top and forms a packed bed on a grate at a lower fixed position. The gasification air is injected from below the grate and passes through the fuel bed. Since the biomass fuel falls downwards in the gasifier as a moving plug, this type of gasifier is also called a moving bed gasifier. Depending on the flow direction of the gasifier, fixed bed gasifiers can be further classified into four groups, namely updraft, downdraft, side draft and open core. A major advantage of fixed bed gasifiers is that large particles and coarse biomass can be processed. The produced gas is at lower temperatures, minimizing the amount of control needed for the cooling system. The main drawback with fixed bed gasifiers is the high consumption of the gasifying agent and the large content of dust in the produced gas (Molino, Chianese *et al.*, 2016).

Updraft gasifiers

The updraft gasifier is the oldest and simplest type of all designs. The biomass is fed at the top, while air, the gasifying agent, is inserted at the bottom via a grate. The biomass and the air move in a countercurrent direction. The biomass fuel drops downwards and passes through other processes, such as drying and pyrolysis, to obtain the desired products. The pyrolytic solid char and volatile gases are further converted into combustible syngas, with most of the components being CO and H_2. The residue of char that remains is combusted by air and produces heat. The heat is then reused within the process to maintain the reduction, pyrolysis and drying zone processes. An advantage of using the fixed bed gasifier is that the moisture and ash content in the biomass do not affect the reaction. These gasifiers are relatively insensitive towards varying particle size (5–100 mm) and towards varying moisture content of the fuel – up to 55 wt% is possible. The process also yields high carbon conversions and has high thermal efficiency. However, it also results in high tar formation and is only ideal for small feed sizes (Mandl, Obernberger *et al.*, 2009). (See Figure 2.16.)

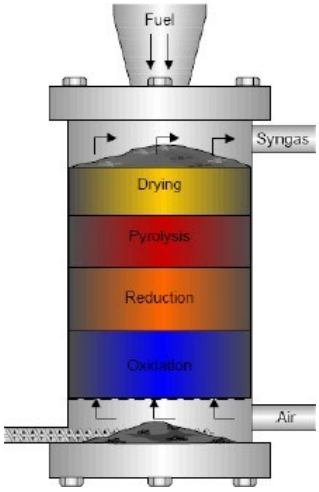

Figure 2.16: Scheme and operating principle of updraft fixed bed gasification

Downdraft gasifiers

For power generation from biomass gasification, a downdraft gasifier is the most favourable method for small-scale production. Both the waste and the gasifying agent (air, O_2, N_2 or steam)

are fed at the bottom part of the reactor. Most of the tar that is formed is burned for pyrolysis of the waste. The level of tar in this reactor configuration is extremely low, approximately 0.1 %. This is because the tar is reused to supply energy for the gasification reaction of the waste, and thus this process is known as "flaming pyrolysis". The downdraft reaction configuration is ideal for producing clean gas needing only a small amount of post-treatment for use in electricity generation with gas turbines. A disadvantage of this configuration is that the operating time is long, resulting in longer residence times of about 1–3 hours (Obernberger and Thek, 2008). (See Figure 2.17.)

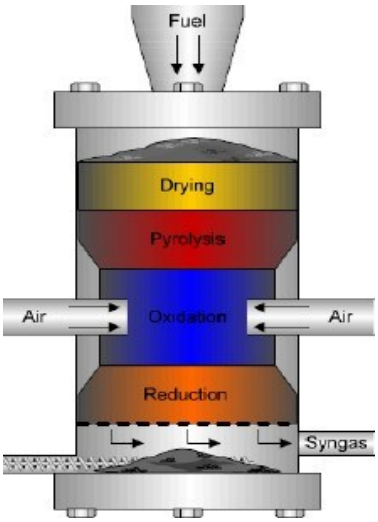

Figure 2.17: Scheme and operating principle of downdraft fixed bed gasification

Fluidized bed gasifiers

In fluidized bed gasifiers, the biomass (fuel) and gasifying agents such as air, steam or oxygen are mixed in a hot bed of solid material such as sand. The different zones (drying, pyrolysis, oxidation, reduction) cannot be isolated and distinguished due to the intensity of the mixing. In contrast to fixed bed gasifiers, the ratio of the gasifying agents can be changed, allowing the bed temperature to be controlled. The produced syngas contains traces of tars and high dust concentrations which need to be removed. There are two basic reactor designs, namely bubbling and circulating fluidized beds. Circulating fluidized bed gasifiers are the preferred choice for nearly all medium- to large-scale gasification for power production. This is due mainly to their high throughput, adaptability and easy adjustment for various types of biomass material. To maintain the bed material circulation, fluidized bed gasifiers should operate at full load. The hot bed material and solid char are circulated in the reactor and cyclone, while the

ash is separated and removed from the circulating stream (Obernberger and Thek, 2008). (See Figure 2.18.)

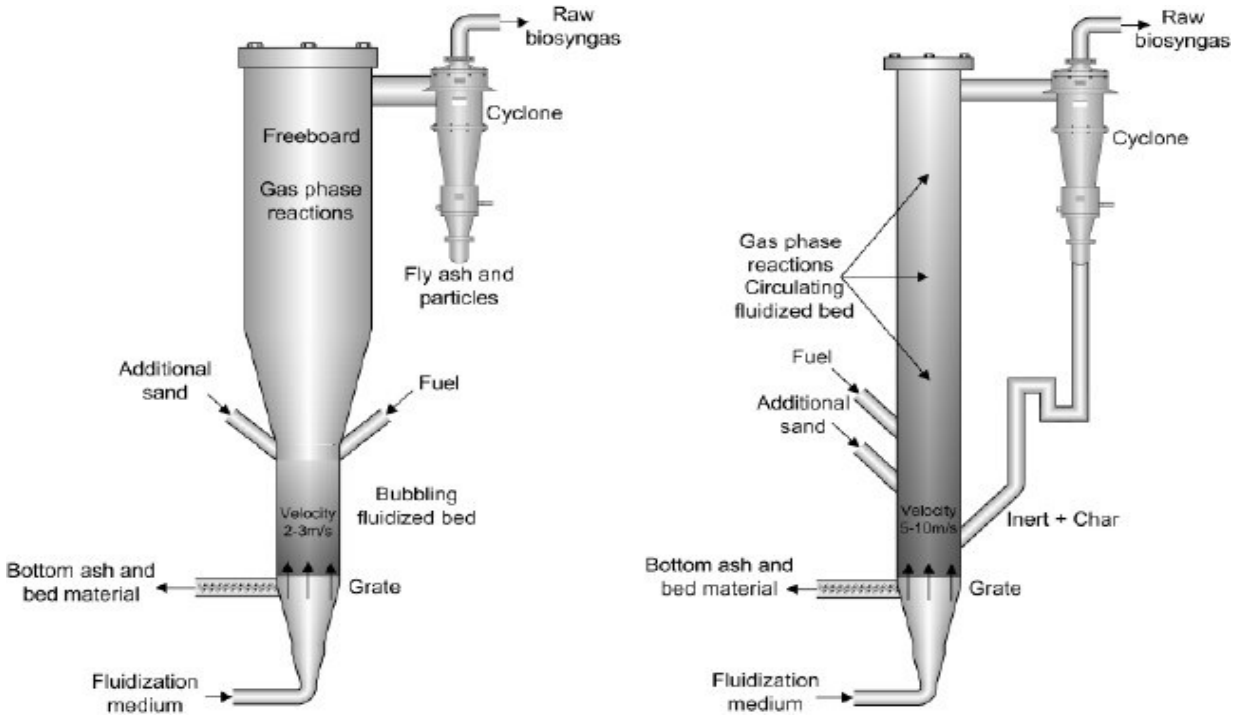

Figure 2.18: Scheme and operating principle of fluidized bed gasification and incineration

(Chang, Chang *et al.*, 2011) investigated biomass gasification to produce bio-hydrogen and syngas in a fluidized bed. The gasification zone consists of a tubular reactor and heater. The heater is used to ensure that the temperature is evenly controlled and there are three heating systems that can be independently controlled. The feedstock was used as reactant and bed material. The researchers used the theoretical minimum fluidization velocities of α-cellulose, bagasse and mushroom wood of 0.418, 1.02 and 2.81 L/min respectively. For α-cellulose, it was observed that at 247–280 °C, dehydration occurs. Within a temperature range of 280– 305 °C, the first combustive pyrolysis process begins and between 419 and 452 °C residual biomass pyrolysis occurs, depending on different heating rates. The heating rates investigated in the study for all biomass were 5, 10 and 20 °C/min, and the various temperatures of the reactor tried were 600, 700, 800, 900 and 1 000 °C. Bagasse and mushroom wood are composed of complex agricultural waste, such as cellulose, hemicellulose, lignin, fertilizer and other inorganic components. This is what caused the order of the reactions to differ from one another. At higher temperatures and higher heating rates, all three-biomasses produced a syngas with a higher composition of CO and H_2.

Entrained flow gasifiers

In entrained flow gasifiers, a dry pulverized solid (e.g. biomass), an atomized liquid fuel or a fuel slurry is gasified with oxygen (sometimes air) in co-current flow. The fuel (feedstock) particles must be much smaller than for other types of gasifier. This means the fuel must be pulverized, which requires more energy.

The gasification reactions take place in a dense cloud of very fine particles. Most coals are suitable for this type of gasifier. The high temperatures and pressures mean that a higher throughput can be achieved. However, the thermal efficiency is somewhat lower as the gas must be cooled before it can be cleaned with existing technology. The high temperatures also mean that tar and methane are not present in the product gas. However, the oxygen requirement is higher than for the other types of gasifier. All entrained flow gasifiers remove the major part of the ash as a slag as the operating temperature is well above the ash fusion temperature.

2.5.2 Incineration

Incineration is a waste treatment process, including the combustion of organic substances in waste materials for optimal energy recovery. Incineration entails operation at high temperatures and thus is characterized as a thermal treatment. The waste organic material treated during the incineration process is converted into gases, ash and heat, which is used for the generation of electricity (Eff, 1973).

Solid waste incineration plants are relatively expensive compared with other waste management options. The plants also require skilled operators and the maintenance costs are extremely high. Due to the high capital costs, developing countries might not consider them as an alternative for energy generation. Incineration plants are extremely complex, and the cleaning of the flue gas can contaminate the environment if not properly handled. The residues must be properly disposed of in well-operated and controlled landfills to prevent ground and surface water pollution.

Municipal solid waste incineration plants are only appropriate and applicable when the extensive requirement criteria are met. The criteria are:

- Solid waste must be disposed of at controlled and well-operated landfills.
- A properly functioning waste management system must have been operational over a number of years.

- There must be a stable supply of combustible waste of at least 50 000 metric tons per year.
- The lower calorific value must never be less than 7 MJ/kg.
- Technically skilled staff must be employed.
- The environment of the community must be stable enough to allow future planning for more than 15 years.

Various factors are involved in the assessment of municipal incineration as a basic refuse disposal method. Municipal incineration is an economical, nuisance-free, sanitary refuse disposal method. The most suitable method on which to base a decision as to whether incineration is the best solution to a city's refuse problem is by comparing the advantages and disadvantages of all other refuse disposal methods. There are ten advantages expressed by various authors in the refuse disposal field (Rubel, 1974):

1. Sanitary landfills require large plots of land compared with municipal incinerators.
2. Incinerators can easily be placed in industrial areas, near service areas and collection routes.
3. The operation of incinerators is not affected by inclement weather.
4. The operating time of a municipal incinerator is usually 24 hours a day to accommodate the variations in refuse generation.
5. The residue from an incinerator is normally stable and inorganic.
6. Incinerators can be in or near residential areas.
7. Incinerators are generally less expensive than sanitary landfills.
8. Incinerators are usually located near sewage treatment plants, which can complement the plants by burning malodorous gases and by drying and burning sludge.
9. Incinerators can burn practically any kind of refuse.
10. Income can be realized if there is a market for steam, hot water, electricity, salvage metals, residue and incineration service to industry.

The disadvantages of municipal incineration are:

1. The capital cost of an incinerator facility is high. Although incineration has a greater turnover than landfills, the initial cost can cause a substantial burden to a municipality.

2. Municipal incinerators emit pollutants into the atmosphere. There are efficient methods to reduce the air pollutants released into the atmosphere, but they are rather expensive.
3. The operating costs are expensive. The maintenance and repair costs can be high due to the system operating at high temperatures.

(Cangialosi, Intini *et al.*, 2008) evaluated the possible health effects of emissions from solid waste incinerators (SWI). Most studies have used the spatial distribution of incinerators and health endpoints to analyze exposure and risk. Lung and liver cancers have been shown as those with the strongest associations with proximity to SWIs. Emissions from incinerators include lead, arsenic, dioxin and cadmium. The latter two are considered carcinogenic to humans (Group 1) by the International Agency for Research on Cancer.

2.5.3 Pyrolysis

2.5.3.1 Pyrolysis of sucrose

The pyrolysis of biomass is essentially the heating of the organic material in the absence of oxygen. The mechanism of cellulose breakdown during the pyrolysis process reflects that of the whole biomass as cellulose is the most abundant component in biomass. The products from the process are biochar, bio-oils, low molecular weight hydrocarbons and gases such as CO_2, CH_4, CO and H_2O (Jin, Singh *et al.*, 2013). The composition of the product streams is largely dependent on the pyrolysis temperature, the material's geometry and the residence time in the pyrolysis reactor (Bassilakis, Carangelo *et al.*, 2001).

The pyrolysis of biomass consists of two types, namely primary and secondary. Primary pyrolysis is the decomposition of the major constituents in the biomass material. The secondary pyrolysis reaction involves the decomposition products of the primary reactions. The type of biomass in the feedstock is also a major factor in determining product composition. The heat of reaction, that is whether the pyrolysis reaction is endothermic or exothermic, plays a major role in modelling the pyrolysis reaction. When the reaction is exothermic, secondary pyrolysis reactions are more favourable (Sinha, Jhalani *et al.*, 2000). High heating rates (above 50 °C/min) and high temperatures (above 300 °C) generally maximize the gas and liquid product yields (Koumi Ngoh and Njomo, 2012).

At lower heating rates or temperatures, the yield of the solid char product is maximized. Biochar is an ideal tool for environmental management as its physical properties enhance the

soil's functionality. (Tang, Zhang *et al.*, 2013) reported that the addition of biochar to the soil increases its organic matter. This has several advantages: it improves the structure of the soil; there is less soil erosion; and it enhances the water-holding capacity of soil. It also makes the soil crumbly and less compact so that water and air can easily move through it and plant roots can easily penetrate it. In addition, it helps keep nutrients such as nitrogen and phosphorus from washing away during heavy rains. Another key benefit is that it absorbs an increased amount of carbon dioxide, which gets stripped from the atmosphere, thereby encouraging more plant growth.

The presence of biochar in the soil mixture influences its texture, structure, porosity, bulk surface area, etc. The physical properties of biochar in the soil may also have a direct impact on the plant growth. This is because both the penetration depth and the availability of air and water within the root zone of the plant are largely determined by the physical make-up of the soil horizon. The presence of biochar in the soil has a direct effect on the soil's response to water. The swelling-shrinking dynamics, permeability, the capacity to retain cations and the soil's response to ambient temperatures are also affected (Downie, Crosky *et al.*, 2009).

(Kim, Kim *et al.*, 2012) investigated the influence of pyrolysis temperature on the physiochemical properties of biochar from the fast pyrolysis of pitch pine. Biochar was produced using a fluidized bed reactor at different pyrolysis temperatures of 300, 400 and 500 °C. The results showed that the yield of biochar decreased sharply from 60.7 to 14.4 % with increasing pyrolysis temperatures. The produced biochar was characterized by elemental analysis, which indicated that the carbon content had increased from 63.9 to 90.5 % with increasing pyrolysis temperature, while the hydrogen and oxygen contents had decreased. The particle size distribution was also investigated, and the results indicated that the size reduction of biochar increases with pyrolysis temperature.

(Demirbas, 2004) experimentally investigated the slow pyrolysis of agricultural residues in a cylindrical batch reactor and how different conditions such as temperature and particle size affect the yield and reactivity of biochar. The agricultural residues he considered were olive husks, corn cobs and tea waste, pyrolyzed at high temperatures of 950–1250 K. The results indicated that as the pyrolysis temperature increased, the biochar yield decreased. The biochar yield increased with increasing particle size of the sample. Olive husks, having a higher lignin content than corncobs, resulted in a higher biochar yield. The bio-char produced from olive

husks was more reactive in gasification than the biochar from corncobs because of the higher ash content.

(Wang, Liu *et al.*, 2007) studied the pyrolysis behaviour of cellulose at a heating rate of 20 K/min by TGA analysis coupled with FTIR spectroscopy. The experimental results showed that the decomposition of cellulose occurs mainlyin the temperature range of 550–670 K. The FTIR analysis showed that free water is first released during the pyrolysis of cellulose, which is then followed by dehydration**,** depolymerization, and decarboxylation and decarbonylation. The glycosidic and carbon-carbon bonds break into a series of hydrocarbons, alcohols, aldehydes and acids. The large-molecule compounds decompose further into gases such as CH_4, CO_2 and CO.

(Yang, Yan *et al.*, 2007) studied the pyrolysis characteristics of the three main components of biomass, namely hemicellulose, cellulose and lignin, using TGA-FTIR in a packed bed. All samples were heated to 900 °C at a constant heating rate of 10 °C/min. The major gas products from the analysis of the different three component samples were H_2, CO, CO_2 and CH_4. Due to the difference in the chemical structure of the three samples, decomposition occurred at different temperatures and also caused a difference in the yields of the composition of the gas products.

Cellulose is essentially polysucrose and the fundamental chemical reactions that give rise to the products in cellulose pyrolysis are approximately the same as those of sucrose. Sucrose is a disaccharide carbohydrate which is extracted from cane or beet sugar. When sucrose is heated or treated with an acid, it hydrolyzes to form glucose and fructose (Pennington and Baker, 1990). In recent years, the focus of biomass conversion has shifted towards the use of sucrose-rich feedstocks, including refined and partially refined sucrose from the sugar industry. The thermal degradation of cellulose occurs via a two-step reaction. The first reaction is a gradual degradation, decomposition and formation of char at lower heating rate temperatures. This is then followed by rapid volatilization accompanied by the formation of levoglucosan at higher heating rate temperatures.

Most sugar-producing countries use large-scale plants for the conversion of sucrose into bio-ethanol or other hydrocarbons. A major constraint for the production of sugar biomass-derived products is the fear of an increase in food prices and a negative environmental impact from the

agricultural undertakings. There are also concerns regarding farmers sacrificing food crops in favour of the production of so-called “energy crops”.

The South African sugar industry constitutes a major part of the national economy because of its agricultural and industrial activities. It is estimated that the industry produces an average of 18.8 million tons of sugar annually (SASA, 2014). The sugarcane sector is situated primarily in farms in KwaZulu-Natal, along with substantial farming operations in Mpumalanga and the Eastern Cape (SASA, 2014). Since the South African sugar industry produces a large excess of sugarcane crops, the conversion of this excess into biomass-derived hydrocarbons is an economically attractive undertaking that is free from the environmental or sociological concerns that plague the bio-energy sector.

(Johnson, Alford et al., 1969) discovered that the major constituent for the pyrolysis of sucrose at high boiling points is 5-hydroxymethylfurfural, and that at lower boiling points the major product that is formed is furfural. (Šimkovic, Šurina et al., 2003) analysed the primary reactions of sucrose thermal degradation at 185 °C. They revealed the formation of glucopyranose isomers and the splitting of the glycosidic bond. (Yang, Liu et al., 2013) reported that levoglucosan is the primary product from the fast pyrolysis of sugar. (Chen, Dou et al., 2012) pyrolyzed sucrose at a heating rate of 10 °C/min in a tubular reactor and found that the primary gases produced are CO, CO_2, H_2 and CH_4. They modelled the kinetics of the reaction using TGA analysis and predicted that the model that best describes the pyrolysis of sucrose is presented in Equation 12. The integral form of the rate expression is denoted as g(α) and the conversion of pyrolysis is defined as α.

$$g(\alpha) = -In(1-\alpha) \tag{12}$$

with the activation energy reported as 35.8 kJ/mol and the frequency factor reported as 8.12×10^2 min^{-1}.

(Wang, Dou *et al.*, 2014) undertook a study on the pyrolysis characteristics of sucrose at different heating rates of 5, 10, 15, and 25 °C/min and using TGA-GC/MS. The gas products from the pyrolysis of sucrose were analysed and consisted mainly of CO, CO_2, H_2 and CH_4, similar to the gaseous products discovered by (Chen, Dou *et al.*, 2012) in their analysis. They stipulate that the Avrami-Erofeev equation can accurately predict the kinetics of the pyrolysis of sucrose. They found that activation energy and the frequency factor vary with the heating rate. (Bulut and Karagoz, 2013) conducted a study on the pyrolysis of table sugar at different

temperatures of 300, 400 and 500 °C in a fixed bed reactor. The bio-oils were extracted with diethyl ester and the various gaseous products were identified using GC-MS, H-NMR and FTIR. The major constituents from the pyrolysis of table sugar at 500 °C are: 1,4:3,6-dianhydro-α-d-glucopyranose, 5-(hydroxymethyl) furfural, 5-acetoxymethyl-2-furaldehyde and cyclo-tetradecane (Bulut and Karagoz, 2013).

2.5.3.2 Pyrolysis of macadamia nuts

(Xavier, Lira *et al.* ,2016) studied the pyrolysis of macadamia nut shells and the parameters that affect the sensitivity analysis. The thermogravimetric data were obtained with a Shimadzu TGA-50H. The experiments were repeated three times, under similar experimental conditions. The dynamic tests were performed starting at room temperature to reach 1 173 K at various heating rates: 5, 10, 20 and 30 $K.min^{-1}$. The kinetic parameters of macadamia nut shell pyrolysis were determined using the Independent Parallel Reaction (IPR) model. The results indicated that the maximum rate of pyrolysis increases with increasing heating rate. (Xavier, Lira *et al.* ,2016)

From the differential thermogravimetry (DTG) curves it was observed that the macadamia nut shell devolatilization consists of two visible peaks, and a flat tailing section. Each peak corresponds to the maximum degradation of one subcomponent of biomass. The lower temperature shoulder represents the decomposition of hemicellulose present in the macadamia nut shell, and the higher temperature peak corresponds to the decomposition of cellulose. The flat tailing section of the conversion rate curves at higher temperatures corresponds to lignin. Lignin is known to decompose slowly and in a wider range of temperatures. Among the parameters investigated, the highest sensitivities were those with respect to activation energies; mass fractions of subcomponents and pre-exponential factors of the Arrhenius equation resulted in a moderate sensitivity, while reaction orders gave the lowest sensitivities.

(Bada, Falcon *et al.*, 2015) studied the combustion and co-combustion behaviour of macadamia nut shells, high-ash coal and anthracite using thermogravimetry. All samples were analysed in air, oxygen and CO_2 atmospheres at different heating rates from 10 to 40 ºC. The combustion and co-combustion of the macadamia nut shells, coal, anthracite and their blends in different weight ratios were investigated using a TGA 701 Leco thermogravimetric analyzer. The three raw samples were combusted at heating rates of 10, 20, 30 and 40 °C/min in an oxygen atmosphere from a temperature of 25 ºC up to 950 °C. Macadamia shells were discovered to have the lowest ash content of 0.36 %, while the ash content of coal was 27.49 %. They both

had similar calorific values of 19.4 MJ/kg. The DTG results indicated that high combustion rates are influenced by high heating rates.

(Kumar, Maroufi *et al*, 2017) investigated the pyrolysis of macadamia nuts. The experiments were conducted in a horizontal alumina tube furnace, with reactor temperatures of 500, 650, 800, 1 000 and 1 300 ºC respectively in an argon atmosphere. They concluded that higher pyrolysis temperatures decrease the char surface area because the temperature is high enough to cause structural ordering and merging of pores. The results also suggested that biochar derived from the pyrolysis of macadamia nuts can be used as a valuable carbon resource to sustain and produce cleaner iron.

2.5.4 Plasma gasification

The fourth state of matter is plasma, consisting of a mixture of electrons, ions and neutral particles. Overall, it is electrically neutral. The degree of ionization of a plasma is proportional to that of atoms that have lost or gained electrons. The creation of a sustained electrical arc via a movement of electric current through a gas is a process known as electrical breakdown. Excess heat is generated due to the electrical resistivity across the system. The generated heat removes the electrons from the gas molecules, which causes an ionized gas stream.

In plasma gasification, the untreated biomass is dropped into the gasifier, coming into contact with an electrically generated plasma, usually at atmospheric pressure and a temperature between 1 500 and 5 000 ºC. The organic matter is converted into high-quality syngas, and the inorganic matter is vitrified into inert slag. The plasma gasification process may reach temperatures from 2 000 to 30 000 ºC. The temperature is the main driving force for plasma gasification. As the temperature increases, both the energy production and the syngas quality increase. This also limits the production of tars. The particle size and moisture content of the biomass have large influences on the gasification process. Syngas production increases with smaller particle size and the efficiency of the gasification process decreases with high moisture contents (Canabarro, Soares *et al.*, 2013). (See Figure 2.19.)

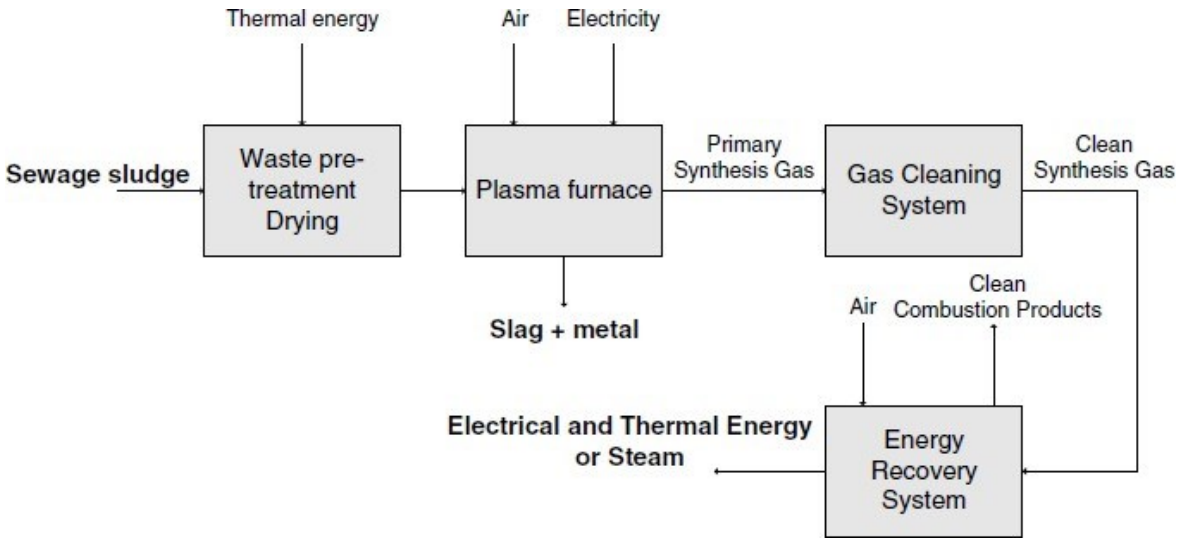

Figure 2.19: Block diagram of the plasma gasification process

Thermal plasma pyrolysis is regarded as a process of reacting a carbonaceous solid with limited amounts of oxygen at high temperature to produce gas and solid products. The highly reactive plasma zone consists of a large fraction of electrons, ions and excited molecules, as well as high radiation energy. The carbonaceous particles that are injected into a plasma are heated very rapidly by the plasma and the volatile matter is released and cracked. All the energy needed for gasification comes from the plasma and no energy for decomposition is produced by combustion. The process also acts as energy storage, since electrical energy is transformed to plasma energy and then stored in the produced syngas. The main advantage is better control of the composition of the produced gas, which has a high heat capacity and a reduction in unwanted contaminants such as tar, CO_2 and higher hydrocarbons. Thermal plasma offers a higher possibility for the production of light hydrocarbons such as methane and acetylene. Thermal plasma pyrolysis consists of four distinct processes, namely (Samal, 2017):

- Rapid heating of the particles from the heat transfer with the plasma jet
- An explosive liberation of volatile matter from the particles
- The fast gasification of the homogeneous phase, as well as rapid heat and mass exchange
- Further gasification of char particles with various gaseous components

Fast gasification of the homogeneous phase can be replaced by quench technology to achieve certain technical purposes, such as monomer recovery. The production of the syngas can be enhanced via further gasification of the char particles with various gaseous components by the

addition of water or steam. High heating rates, along with high temperatures of the plasma, result in the destruction of organic waste. A gas and a solid residue is then produced with various properties which depend on the feed characteristics and operating conditions. The amount of gas produced can reach up to 70–80 % of the total feed. The application of thermal plasma has increased ever since the discovery of the process in the 1980s. Throughout the years, research has led to great progress in understanding the application of material processing via thermal plasma. Plasma torches operate simultaneously as a plasma chemical and a thermal apparatus (these are explained further below). Energy is transferred to the particles being treated from the electrical energy of the torch, which then triggers a dual simultaneous reaction process in the plasma chemical reactor. The organic compounds are thermally decomposed into their constituent elements, while the inorganic materials are melted and converted into a dense, inert, non-leachable vitrified slag which does not require any controlled disposal. The advantages of thermal plasma are as listed below (Boulos, Fauchais *et al.*, 2013):

- High temperatures can be reached by conventional heat generators.
- Thermal plasmas are highly reactive and can reduce waste entering the environment. The process is non-polluting and capable of destroying substances harmful to health, and the products are predictable, harmless and acceptable for public health and the environment.
- They have very high energy density and high heat transfer efficiency, which allows large throughputs with shorter residence times.
- The plasma gas input per unit of heating power is lower than the gas flow of a classical burner, which results in lower energy loss related to the energy necessary for heating of the gas to the reaction temperature. There is also a lower amount of off-gases to be treated.
- There are none of the combustion gases generated by conventional incinerators.
- The plants are on a smaller scale than incinerators due to high energy densities, lower gas flows and volume reduction.

There is optimal control of the composition of the reaction gases. The heat source is electricity rather than energy liberated from combustion, and thus is independent of the treated substances. This enables flexibility, fast process control and more options in process chemistry, including the possibility of generating valuable co-products. There is efficient delivery of heat energy for the simultaneous rapid promotion of both the physical and chemical changes in the waste

material. The properties of plasma pyrolysis products are suitable for energy generation and material recycling. High and effective processing temperatures are easily achieved in very compact, high-throughput and fast response reactors. Thermal plasma for material processing applications is originated from electricity. Plasma torches are electrothermal devices that convert the electrical input energy to the thermal energy of the plasma. The primary source of electrical energy can be direct current (DC), alternating current (AC) at mains frequency or at radio frequency (RF) and they are referred to as DC, AC or RF torches. When an electric current is passed through a gas, plasmas are generated. Hybrid devices of the torch also exist. Plasma generated by DC electrical charge is normally used for the treatment of waste (Knoef and Ahrenfeldt, 2005).

2.5.4.1 The role of the gasifying/oxidizing agent

The choice of the best gasifying agent to use is vital as the agent is strongly linked to the purity of the produced syngas. (Knoef and Ahrenfeldt, 2005) investigated the effect of different oxidizing agents, namely air and pure O_2, on the purity and quality of the syngas produced. It was determined that using pure O_2 as an oxidizing agent lowers the calorific value of the syngas. The measured calorific value was 10 MJ. m^{-3} with pure O_2, while when air was used as an oxidizing agent, the calorific value of 4 $MJ.m^{-3}$ was obtained. This is due to the N_2 present in air flow, which dilutes the O_2 in the syngas. Using pure O_2 as a gasifying agent is rather expensive on an industrial scale. In cases where CO_2 was used as the oxidizing agent, the syngas tends to have a lower heating value. The reason is that during gasification with CO_2, most of the power required to produce syngas is used as energy to dissociate CO_2. In Figure 2.20, steam enthalpies are compared with commonly used gas plasma torches such as Ar, H_2 and N_2. Steam plasma has higher enthalpies due to steam's natural capacity to carry energy. Another advantage of using steam as a carrier gas for plasma processing is steam's high heat conductivity.

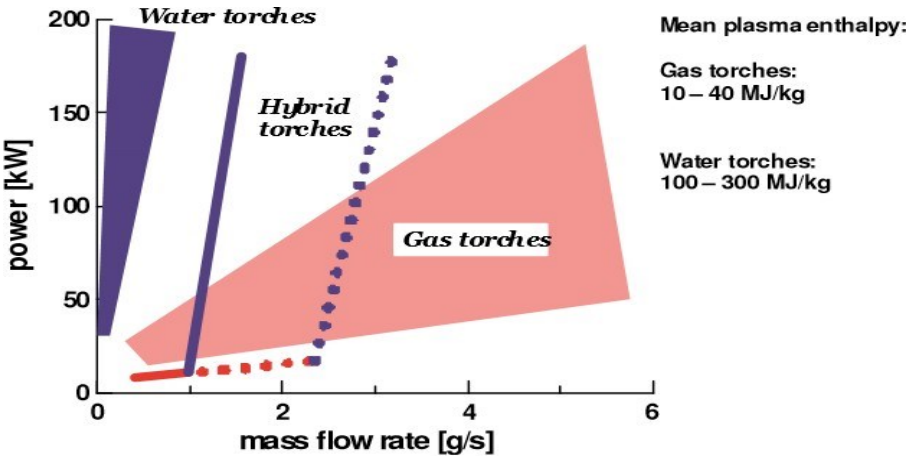

Figure 2.20: Operating regimes of DC plasma torches

The use of steam as a gasifying agent is better favoured because of the high yields of the desired products. Steam as a gasifying agent increases the H_2 ratio in the syngas, which is also beneficial in other processes, such as steam reforming reactions, which are rather endothermic and require operational temperatures of 1 100–1 700 K. A dual fluidized bed reactor is best suited when steam is used as a gasifying agent. This is mainly because fluidized bed reactors are designed to separate the gasification process from the combustion process. (Hrabovsky, 2011)

2.5.4.2 Factors that influence the quality of syngas

The performance and composition of syngas are strongly affected by the method applied to produce it, as well as the gasification parameters, the composition of the feedstock, and the type of waste or biomass used. These depend on the type of elements present, such as oxygen, hydrogen, carbon and various minerals. The moisture content in the feedstock stimulates the production of H_2 in the syngas. (Dong, Chi *et al.*, 2016) investigated the effect of operating parameters and moisture content on municipal solid waste pyrolysis and gasification. They found that at an average moisture of 20–25 %, the production of H_2 yield in the syngas increased. The rate of gasification is also largely affected by the particle size of the raw material. This rate increases with smaller particle sizes. (Hrabovsky, 2011) also concluded that the heating value of the produced syngas increased with higher feed rates, provided that the particle size of the feed material was also small. Heat was lost due to the anode, cathode, or radiation from poor insulation of the material. The rate of the quenching process for the syngas is also key in obtaining good-quality gas. The natural performance of the torch is affected by a number of factors: the plasma gas added (Ar, N_2, O_2, H_2O, etc.); the power injected from the

electricity supply; the specific enthalpy; the diffusion rate of the plasma; the thermal efficiency of the plasma torch; and the type of technology used for the plasma torch (DC, AC or RF). The yield of both H_2 and CO, the gas calorific value, the formation of tar, and the efficiency of the cold gas are the main parameters that govern the performance of a plasma torch (Fabry, Rehmet *et al.*, 2013).

2.5.4.3 DC torches

The most commonly used plasma device for material processing applications is the DC arc plasma torch (see Figure 2.21). A direct current is struck between a cathode rod and a nozzle anode and the energy from the arc is abstracted by the plasma gas injected in the inter-electrode region. Forced gas flow extends the arc in the anode nozzle which is strongly water-cooled. A thermal arc pinch effect is produced by the joint action of the cold wall arc channel and the cold gas sheath around a very high-temperature conducting core, the arc column. The DC arc in a plasma torch needs to be stabilized and should remain stationary against fluctuations. This is achieved by constricting the arc to a well-adjusted narrow, high temperature, highly conducting arc column (Trelles, Chazelas *et al.*, 2009).

The electric arc is stabilized by using a constricted anode nozzle and by the resultant aerodynamic effect in the streaming plasma gas. The stabilizing action of the vortex gas flow provides a cold boundary layer near the anode wall, to reduce the heat loss to the wall. This ensures the stability of the thermal energy, being highly concentrated with improved torch stability and efficiency. The localized heat flux at the nozzle can be as high as 160 W/mm^2. The material for the anode is normally copper, although molybdenum and graphite are also used. The anode losses range between 80 and 10 % of the energy input in the arc, depending on the nature of the gas and the working parameters. The cathode can be a thermionic type of material such as tungsten, carbon or molybdenum, which should be used in a non-oxidizing atmosphere. Under the conditions of an oxidizing atmosphere, the material of the cathode can be zirconium or hafnium. Heat losses at the cathode are generally lower, approximately less than 10 % of the input power compared with heat losses at the anode (Knoef and Ahrenfeldt, 2005).

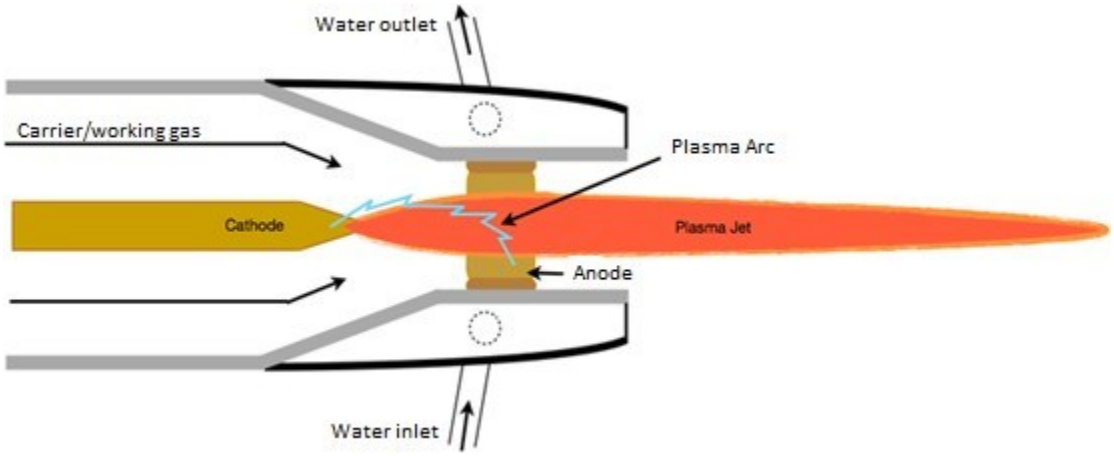

Figure 2.21: Schematic diagram of a typical DC torch

The torches can use different plasma gases/carriers such as O_2, N_2 and air and H_2O. The material of construction for the electrodes and the plasma gases should be correctly paired to avoid excessive corrosion and contamination while the torch is operating at ample power. A larger, more projecting plasma jet is achievable with a higher flow rate of plasma gas and an increase in arc current.

2.5.4.4 AC torches

For industrial application technologies, AC plasma torches are preferred. This is mainly because the power system is essentially cheaper and reliable. AC plasma torches also possess higher thermal efficiencies as reactive power losses are minimized with the aid of standard capacitor compensators. Each electrode alternately acts as the cathode and anode when AC at mains frequency is used in a two-electrode device. A DC discharge is established in each half-cycle once the breakdown potential is crossed, and the discharge is maintained if the applied voltage remains above the maintenance potential. The discharge gets extinguished when the voltage falls below the maintenance potential and the space charge gets swept away. The continuous alternation of the polarity of the electrodes places a strong limitation on the stability of the discharge and the choice of the electrode materials. The disadvantage of using AC technology in plasma torch technology is that the lifetime of the electrodes is short. It is limited to 200 hours, after which the electrodes start to degrade and erode (Fang, 2013).

2.5.4.5 RF torches

With radio frequency (RF) torches, inductive or capacitive coupling between 1 and 20 MHz can be used to generate a plasma column, which can be stabilized in a quartz tube. The main advantage of the RF torch technique is that the electrodeless feature allows the use of aggressive gases such as oxygen and chlorine, which cannot be used as plasma-carrying gases in DC plasma torches. The nature of the gas, its pressure and the frequency of the electromagnetic field determine the minimum power necessary to sustain the discharge (see Figure 2.22). The velocity of the gas in an RF plasma torch is lower than that encounted in DC torches. The energy density is also much lower than in plasma arc generators. RF plasma torches are capable of operating at high power levels of 1 MW and the lifetime of the torch is highly dependent on the type of material processing application. The electrothermal efficiency of an RF torch is, however, low, approximately 40–50 %, and its use in processing is mostly limited to specialized applications.

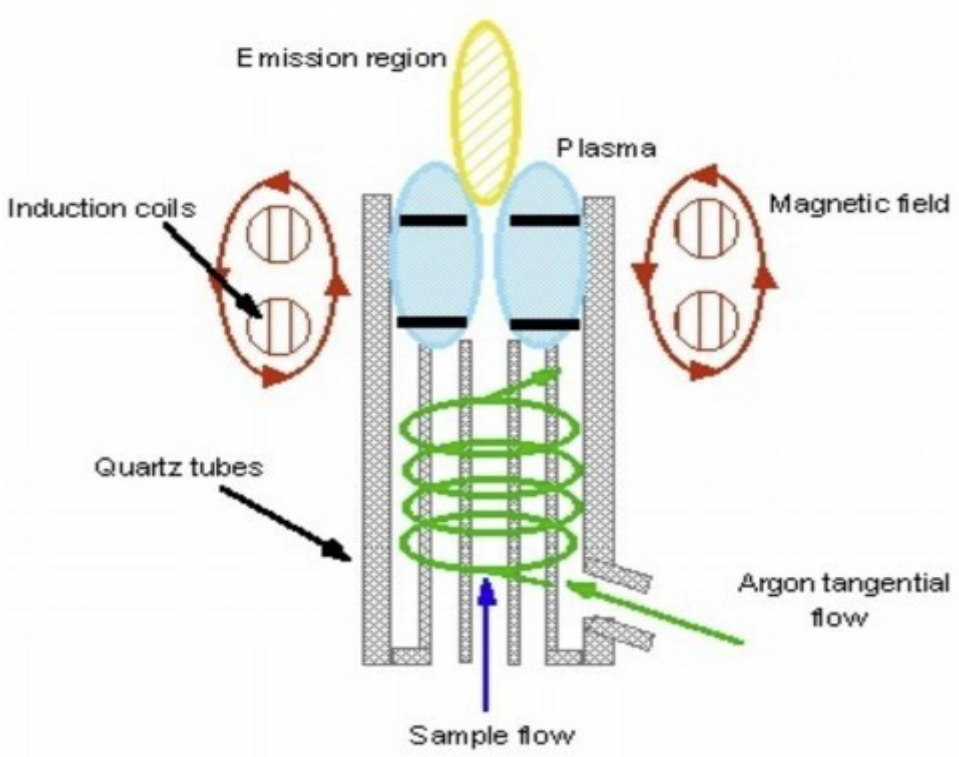

Figure 2.22: Schematic diagram of RF inductively coupled discharge

(Van Oost, Hrabovsky *et al.*, 2008) studied the plasma gasification of wood, using a plasma chemical reactor with a water-cooling system designed to operate at a wall temperature of up to 1 700 °C. The reactor was well insulated, with refractory ceramics of 400 mm thickness,

which prevented power losses to the wall. All the reactor chambers were water-cooled, and the material was continuously fed into the system at a controlled flow rate. Nitrogen flow was used to control the pressure inside the reactor, which prevented the reactor gas from flowing into the material supply system. The torch generated an oxygen-hydrogen-argon plasma jet that had extremely high plasma enthalpy and temperature. A quadrupole mass spectrometer (Balzers QMS 200) was used for the main gas analysis. FTIR, gas and liquid chromatography, and mass spectroscopy with cryofocusing were used to determine the content of tar, as well as the composition of the produced syngas. The results showed that the complete gasification of wood with the production of syngas yielded a high content of hydrogen and carbon monoxide. The main components of the produced syngas were H_2 (28–46 % vol), CO (44–68 %), CO_2 (2–8 %) and Ar (0.2–8 %). The tar content was below the sensitivity of the analysis method (1 mg/Nm^3).

(Hlina, Hrabovsky *et al.* , 2014) investigated the plasma gasification of biomass (spruce sawdust, wood pellets and waste plastics) by a plasma torch with a DC electric arc using hybrid stabilization. The plasma torch used involves the combination of arc stabilization by the gas, where the cathode is protected against oxidation by Ar flow, which is then followed by water stabilization of the arc. A vortex that surrounds the electric arc is formed from the water that is tangentially injected into the arc chamber of the torch. The input power of the torch was 100–110 kW and the mass flow rate of the gasified materials was varied. The plasma torch was mounted at the top of the reactor with a water-cooled jacket. The reactor was insulated with ceramic thermal insulation of 400 mm thickness with an inner volume of 0.22 m^3. The feed rate of the material into the reactor was controlled with a speed screw feeder from a 300 L volume hopper. The produced syngas was cooled down to 300 °C in a quenching chamber.

A quadrupole mass spectrometer (Pfeiffer Vacuum Omnistar GSD 301) was used as the main gas analyzer. The material used for the gasification process was wood sawdust (spruce, 10.5 % H_2O), wood pellets (spruce, 6 mm diameter, 7.4 % H_2O), waste plastic (1–6 mm, 89 % HDPE, 10 % PP, 1 % PET, CH 1.99 (mole composition)) and pyrolysis oil from the thermal decomposition of waste tyres consisting of aromatic hydrocarbons, $CH_{1.47}$ (mole composition). The oxidizing agents used were CO_2, O_2 and H_2O to achieve syngas with the optimal composition of CO and H_2. The feed throughput for gasification varied between 9 and 30 kg/h and consisted of tens to hundreds of slm (standard litres per minute) of CO_2 in the cases of sawdust, pellets and waste plastic. With regard to the pyrolysis oil, the feed throughput for

gasification was 11 kg/h of H_2O. In all the results, CO and H_2 formed approximately 90 % of the produced syngas. The raw material with smaller particle sizes showed some carbon yield, more particularly observed with sawdust. The reaction time and temperature in the reactor were sufficient when CO_2 was used as the oxidizing medium.

Very low concentrations of tar were measured, under 10 mg/Nm^3. The oil showed the lowest production of syngas, because the gasification of the pyrolysis oil is also partial oxidation due to the lack of oxygen in the oil. The gasification of pyrolysis oil is not energetically self-sufficient. This is primarily because the pyrolysis oil has a high heating value by itself, and its oxidizing agent (H_2O) has a high capacity, which caused a negative effect on the energy efficiency of the gasification.

(Marquesi, Filho *et al.*, 2015) studied the production of syngas by the reaction of coal and bagasse with air and steam in a plasma reactor. Thermodynamic equilibrium modelling and parametric analysis of the thermochemical conversion approach were performed for the gasification process. They used steam and air as their oxidizing agents for their analysis. They found that the maximum cold gas efficiency when using steam is close to 90 %, and in the case of air it is equal to 85 %. The electric energy efficiency based on the simplified model of a cogeneration system was established to be 0.52 with biomass feedstock, and 0.49 with coal feedstock when using air as an oxidizing agent. When steam is used as an oxidizing agent, the electric energy efficiency with biomass as feedstock is 0.54 and 0.51 with coal feedstock.

(Agon, Hrabovský *et al.*, 2016) studied the thermochemical conversion method using plasma gasification for the treatment of waste. The type of raw material used was RDF (refuse derived fuel) and it had a compositional analysis of 47 % plastic; 24 % wood and paper; 10 % textiles and 18 % fines. They performed experiments on a single-stage plasma gasification system using a PLASGAS reactor. The volume of the reactor was 0.22 m^3, and four layers of different refractory ceramic materials were used as insulation. The insulation thickness of 400 mm separates the inner surface of the reactor from the water-cooled outer walls to reduce heat loss from the reactor. The reactor was pre-heated with an electric rod prior to the experiments for 24 hours, reaching a temperature of about 1 200 K. A plasma torch provided any additional heating that was required, enabling the temperature in the reactor to reach 1 560 K. The DC water/argon plasma torch was mounted on top of the reactor and operated with currents between 350 and 550 A, using arc powers within a range of 90–160 kW. The raw material was

continuously fed and monitored by controlling the speed of the screw conveyor. The anode was a rotating water-cooled copper disc, situated outside of the arc chamber.

The oxidizing agents were O_2 and CO_2, with their flow rates being set using thermal gas mass flow controllers and H_2O. The water mass flow rate was controlled by measuring the difference in weight. The gas was then cooled to a temperature of 550 K in a quenching chamber by controlling the flow rate of the water spray. Thereafter the syngas was filtered using basalt filter bags before it entered the combustion chamber. The produced syngas was sampled for online composition analysis. A Pfeiffer Omnistar GSD 301 T3 mass spectrometer was used to measure the relative concentrations of CO, H_2, CH_4, O_2 and Ar. No air or nitrogen was added to the system.

The composition of the produced syngas was compared with the theoretical composition, assuming thermodynamic equilibrium. It was found from the results that the carbon conversion efficiency is relatively insensitive to the type of gasifying agent. The CO and H_2 yields in the syngas for using oxygen-steam as oxidizing gasifier were significantly higher than for the other cases. The tar analysis content varied from 132 to 543 mg/Nm^3, which is relatively high for tar measurements during biomass plasma gasification.

(Shie, Chen *et al.*, 2014) investigated the operating performance of a plasma torch on municipal solid waste mixed with raw wood. A 10 kW plasma torch was used for the gasification process. The process is a batch feed, with samples of approximately 10 g fed into the reactor. A gas chromatograph GC-TCD with a Supelco packing column was used to analyze the gas. The temperature of the reactor ranged from 573 to 873 K. The experiments resulted in higher temperatures, and the CO and H_2 yields also increased. When H_2O was used as an oxidizing agent, the concentration of H_2 production also increased.

(Byun, Cho *et al.*, 2011) performed experiments to illustrate that thermal plasma gasification is the most effective and environmentally friendly method for the treatment of solids and for energy utilization. They used a non-transferred thermal plasma torch with a power capacity of 100 kW. The solid waste was from a paper mill, and the material was fed into the reactor at 50 kg/h. The operating current and voltage were 200 A and 350 ± 10 V respectively. The temperature in the reactor was maintained at 1 400–1 450 °C, and heat exchange was used to decrease the flue gas temperature to 180 °C. The produced syngas was supplied to the H_2 recovery system, which was used primarily to combust the syngas. A water-gas shift unit was

used for the conversion of CO to H_2 and a pressure swing adsorption unit for the separation and purification of H_2. A gas analyzer and gas chromatography were used for the analysis of the gas components. The experiments produced H_2 of high purity, yielding a recovery of 99.9 % of H_2.

(Tamošiūnas, Valatkevičius *et al.*, 2016) conducted experiments in a plasma-chemical reactor using a water steam plasma torch for the conversion of biomass to hydrogen-rich synthesis fuels. Pure glycerol and crushed wood were used as biomass sources. Glycerol was supplied to the chemical reactor at a constant feed rate of 2 g/s, while wood with a known composition was supplied at 1.2 g/s. To protect the cathode of the plasma torch, argon was used as a shielding gas. In the course of the experiments, the plasma torch power was changed from 48 to 56 kW. The current was 200 A, the voltage was 240–280 V and the steam flow rate ranged between 2.63 and 4.48 g/s at a temperature of 500 K. The mean plasma temperature was 2800 K. The results of the experiments indicated that as the ratio of steam to glycerol increased, the concentrations of CO_2 and H_2 also increased, while that of CO decreased slightly. Another finding was that when the steam to glycerol ratio and the plasma torch power increased, the yield of the gas produced increased and the yield of char decreased significantly. The H_2 yield increased as the flow rate of steam increased. It was also concluded that the specific energy requirement for wood is higher than for glycerol. The H_2/CO ratio was close to 2 in both cases. This implies that the produced syngas is suitable for direct energy/heat or chemical production via Fisher-Tropsch synthesis.

Chapter 3 Experimental

3.1 TGA-FTIR experiments on glucose, sucrose and fructose

3.1.1 Materials

Sucrose (>99 %), fructose (>99 %) and glucose monohydrate (>99 %) were purchased from Merck South Africa (1 Friesland Drive, Longmeadow Business Estate, Modderfontein, 1645) and used as received.

3.1.2 Methods

The pyrolysis experiments were conducted using a Perkin Elmer TGA 4000 thermogravimetric analyser hyphenated to a Perkin Elmer Spectrum 100 FTIR spectrometer. Sucrose, fructose and glucose were subjected to identical pyrolysis procedures. Approximately 20 mg of sample material was placed in an α-alumina crucible and heated from 30 °C to 850 °C in a nitrogen atmosphere flowing at 50 mL/min. The experiments were performed at five different heating rates, namely 5, 10, 15, 20 and 50 °C/min.

The gases evolved from the TGA were transferred via a heated line (kept at 225 °C) to a heated infrared gas cell (kept at 225 °C) having an optical path length of 10 cm and equipped with KBr windows. The spectrometer was set to scan from 4000 cm^{-1} to 550 cm^{-1} with a resolution of 4 cm^{-1}, at a sampling rate of one spectrum every 6 seconds.

The glucose and fructose experiments were repeated twice to obtain sufficient data to test for repeatability, while the sucrose experiments were repeated only once, giving a total number of 23 experiments.

3.2 TGA-DTG analyses of macadamia nut shells

3.2.1 Materials

Figure 3.1 shows the macadamia nut shells prepared for the plasma gasification experiments. Unprocessed shells where was obtained from KwaZulu-Natal farms, via EPCM South Africa. The shells were crushed in an in-house laboratory shredder. The average particle diameter after crushing was approximately 10 mm.

Figure 3.1: Sample of the macadamia nut shells used during the experiments

3.2.2 Methods

The pyrolysis experiments were conducted using a Perkin Elmer TGA 4000 thermogravimetric analyser. Approximately 20 mg of sample, obtained by cutting a shell, was placed in an α-alumina crucible and heated from 30 to 1 000 °C in a nitrogen atmosphere flowing at 50 mL/min and then kept isothermal for 15 minutes. The experiments were performed at three different heating rates, namely 5, 10 and 20 °C/min. The experiments were repeated twice to obtain sufficient data to test for repeatability. The end temperature was close to the operating temperature of the gasification system. In total, six experiments were conducted.

3.3 Plasma gasification experiments

Figure 3.2 shows a photo of the plasma gasification system. The 15 kW pilot facility is situated at Necsa, Pelindaba, in the Applied Chemistry R&D Division. The two major components of the system are the plasma torch and gasification reactor. Inlets for the plasma torch, quench heat exchanger, feeder, thermocouple, oxidant feeder and viewing port are positioned on the top lid of the reactor. The plasma torch supplies power to the reactor. It consists of an anode and cathode, which can operate at a maximum power supply of 30 kW. To obtain the desired power output, both the current and power can be adjusted. The second inlet is the screw feeder which feeds the raw material into the reactor. The third inlet into the reactor is fitted with a quench probe heat exchanger for cooling the product gas. This is an annular device, that uses water as a cooling agent. The product gas is cooled to ambient temperature by passing through the quench probe before being filtered. The fourth inlet is fitted with a transparent quartz

window to enable the internal operation of the gasification reactor to be viewed during experiments. In addition, the window can be used to monitor the temperature in the reactor using an optical pyrometer. The main temperature measurement instrument is, however, a type R thermocouple for accurate measurement of the reactor temperature.

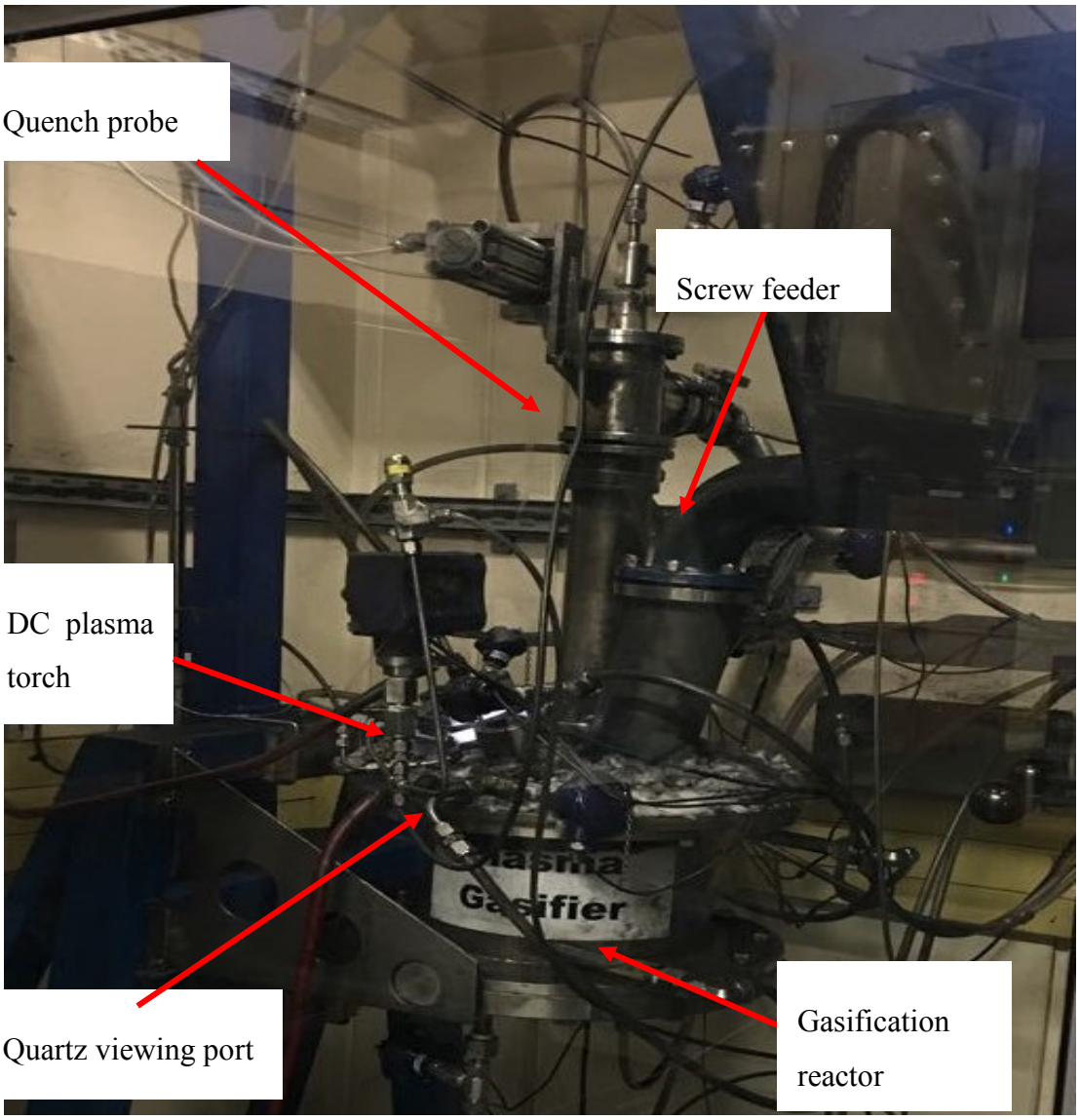

Figure 3.2: Plasma gasification reactor

During the gasification process, one of the by-products is water. After being cooled by the quench heat exchanger, the product gas enters the knockout vessel where water vapour condenses. The main function of the knockout vessel is to separate the syngas from the water and the larger particulates. These particulates and the water settle at the bottom of the vessel, while the syngas continues to flow towards the filter. The filter traps fine solid ash and any

particulates that did not settle in the knockout vessel. Figure 3.3 shows the knockout vessel connected to the filter.

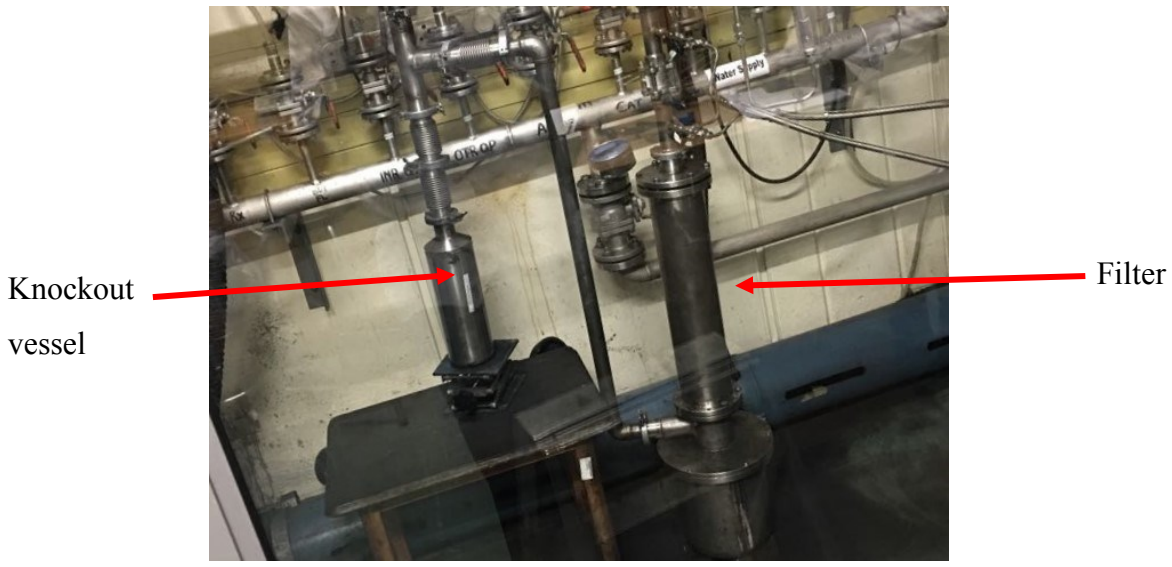

Figure 3.3: Knockout vessel and filter

After being cleaned, the product gas is sampled in a U-tube for offline analysis. The U-tube samples are taken manually. Figure 3.4 shows the U-tube sample collector.

Figure 3.4: U-tube sample collector

Gas samples were taken every 10 minutes during the gasification experiments. They were collected in the U-tubes. After each experimental run the gas samples were analysed offline by a gas chromatograph (GC). The GC system used is an Agilent 7890 GC (Santa Clara, California) coupled to the Fast RGA (refinery gas analyser) system from AC Analytical Controls (Rotterdam, the Netherlands) with six columns, six valves and three detectors, one flame ionization detector (FID) and two thermal conductivity detectors (TCD). All samples

were taken according to ASTM D 3588, ASTM D2598, DIN 51666, ISO 6976 and GPA 2172 standard methods. The actual molar composition of the gas was determined by means of calibration data and relative response factors. Figure 3.5 presents a flow diagram of the full system.

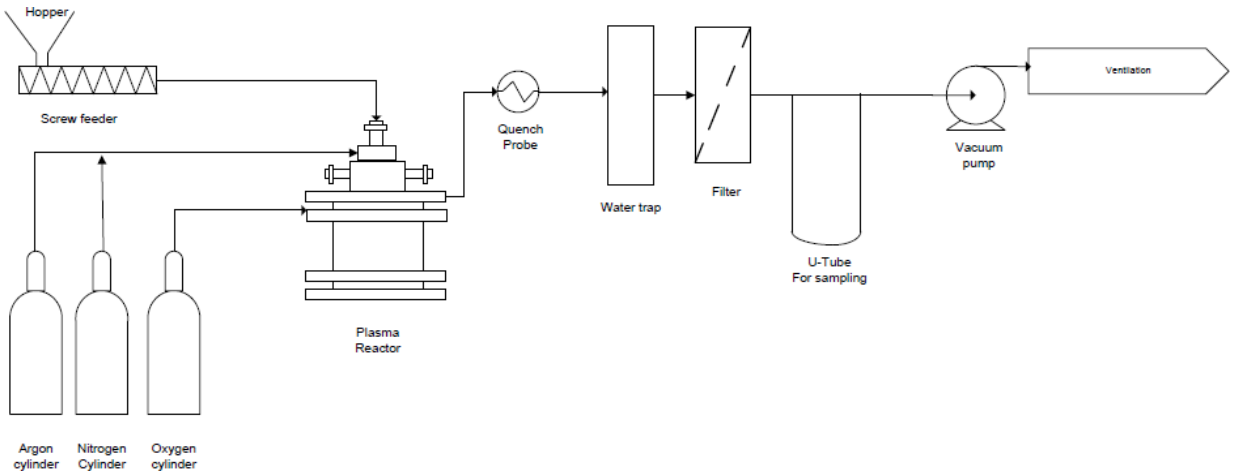

Figure 3.5: Flow diagram of the system

Cooling water is initially switched on before starting the plasma power supply. The plasma gasses supply in the torch is automated via control system of the customized built plasma power supply. Table 3.1 lists the phases of the start-up procedure of the plasma power supply

Table 3.1: List of all experiments conducted

Phase no.	Description
1	Purging phase with argon/nitrogen to flush out air form plasma torch
2	Starting of the plasma torch after the purging process. The argon gas is introduced into the plasma torch for 10 seconds.
3	Once the torch is operating, nitrogen gas is then slowly introduced into the plasma torch while the argon gas is slowly reduced simultaneously.
4	The last phase is considered as the operating phase. The argon gas flow is zero and the plasma torch operates at a nitrogen flow rate of ~40 slpm

3.3.1 Sucrose feed material

Table 3.2 lists some of the physical properties of sucrose. Sucrose a solid white odourless crystalline solid. It is considered to be a homogeneous material with a well-known composition of $C_{12}H_{22}O_{11}$. The average particle diameter of the sucrose used for this work was 0.4 mm.

Table 3.2: Physical properties of sucrose

Molecular weight	345.3 kg/kmol
Melting point	186 ^{o}C
Density	1.6 g/cm^{3}
Heats of combustion	-1.3 × 10^{6} cal/mol
Water solubility	2 100 mg/mL
LogP	-3.7
Crystalline structure	Monoclinic

3.3.2 Screw feeder calibration with sucrose

A simple plastic beaker was used for the calibration of the feeder. The hopper was filled with 30 kg of sucrose. The plastic beaker was placed at the outlet of the hopper, and average mass flow measurements were taken at different speed settings. For each speed setting, the experiment was repeated three times. Figure 3.6 presents the feeder calibration graph with a 5 % error margin. The feeder calibration showed a linear response over the feed range of 0.4 to 1.4 kg/h.

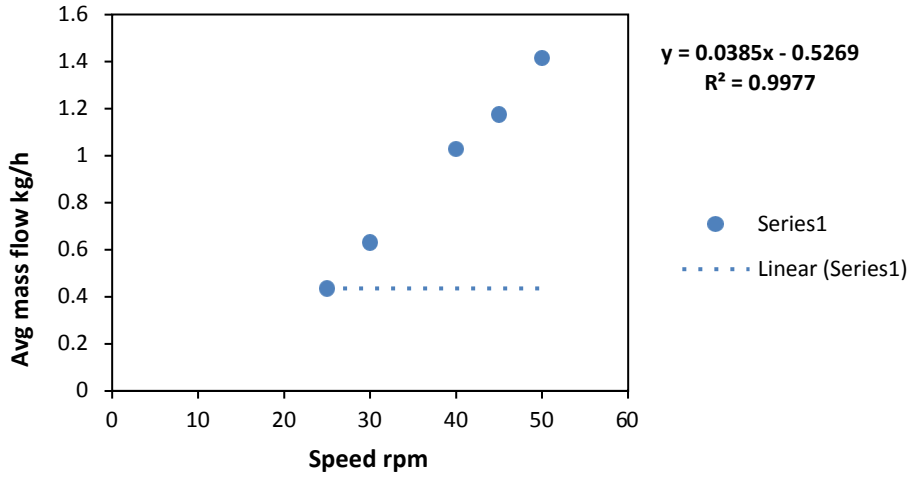

Figure 3.6: Screw feeder calibration of sucrose with mass feed rate with respect to speed

3.3.3 Screw feeder calibration with crushed macadamia nut shells

The procedure for obtaining the screw feeder calibration for the macadamia nut shells was the same as for the sucrose screw feeder calibration. An empty plastic beaker was initially measured for the calibration of the feeder. The hopper was filled with 30 kg of crushed macadamia nut shells. The plastic beaker was placed at the outlet of the hopper, and average mass flow measurements were taken at different speed settings. For each speed setting, the experiment was repeated three times. Figure 3.7 shows the feeder calibration graph with a 12 % error margin. The error margin is higher for the macadamia nut shells than for the sucrose. This is mainly attributed to sucrose being a homogeneous material and having a smaller particle diameter.

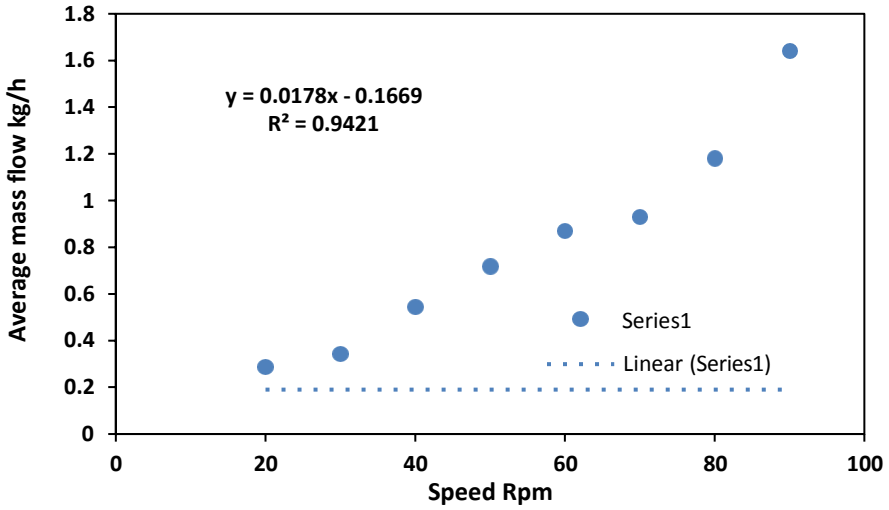

Figure 3.7: Screw feeder calibration of macadamia nut shells with mass feed rate with respect to speed

3.3.4 Ultimate analysis of macadamia nut shells

The elemental analysis was conducted using a Thermo Scientific Flash 2000 CHNS elemental analyzer (Thermo Fisher Scientific, Inc., Waltham, Massachusetts, USA) which is situated in the Chemistry Building at the University of Pretoria. For the CHNS determination, the macadamia shells nut samples were weighed in tin capsules and introduced into the combustion reactor. The furnace temperature was 900 ^{o}C and the oven temperature was 65 ^{o}C. After combustion, the resulting gases were carried by a helium flow at 130 mL/min to a layer filled with copper, then swept through a gas chromatograph (GC) column that provides separation of the combustion gases, and, finally, detected by a thermal conductivity detector (TCD).

(Bada, Falcon *et al.*, 2015) conducted ultimate and proximate analyses on macadamia nut shell samples. Their macadamia nut shells materials were sampled from the KwaZulu-Natal province in South Africa. Similar results were obtained and are shown in Table 3.3.

Table 3.3: Physico-chemical properties of raw macadamia nut shells

Proximate analysis (dry basis)	wt%
Fixed carbon	23.4
Volatile matter	76.25
Ash content	0.36
Moisture (as received)	7.97
Ultimate analysis (dry basis)	
Hydrogen	7.05
Nitrogen	0.27
Carbon	56.8
Sulphur	0.28
Oxygen	35.6

3.4 Summary of experiments performed

The TGA-FTIR experiments were performed at the Fluoro-materials Group laboratory, at the University of Pretoria. The gasification runs were performed at Necsa.

Plasma gasification experiments were carried out on sucrose. The experiments were conducted at a plasma torch power setting of 11 kW, the gasification reactor was kept constant at 1000 ^{o}C and the sucrose feed rate was kept constant at 1 kg/h. Two experiments were evaluated at equivalence ratios (ER) of 0.05 and 0.1. The experiments were repeated twice to obtain sufficient data to test for repeatability. In total, 4 experiments were conducted.

The experiments with macadamia nut shells were done at four different feed rates, namely 0.54, 0.72, 1 and 1.14 kg/h at torch power settings of 9, 11 and 14 kW. The conversion efficiency, syngas composition and low heating values were calculated for each run. A total number of 24 experiments were performed for these experimental parameters. These were repeated, and an average was reported. No oxygen was added during the experiments.

Finally, experiments were performed on macadamia nut shells to evaluate the effect of oxygen addition on the syngas quality. The experiments occurred at a constant power of 11 kW and constant macadamia nut shells feed rate of 1 kg/h. Three different oxygen mass flows were evaluated at 0 kg/h, 0.619 kg/h (14% oxygen added), and 0.652 kg/h (20% oxygen added).

Table 3.4 lists a summary of all experiments and the number of runs they were performed.

Table 3.4: List of all experiments conducted

Experiment no.	Description of experiment	Runs
1	TGA-FTIR for sucrose at heating rates 5,10, 15, 20, 50 ºC/min	5
2	TGA-FTIR for glucose at heating rates 5,10, 15, 20, 50 ºC/min	10
3	TGA-FTIR for fructose at heating rates 5,10, 15, 20 ºC/min	8
4	TGA-DTG for macadamia nut shells at heating rates 5, 10 and 20 °C/min.	6
5	Plasma gasification of sucrose evaluated at equivalence ratios (ER) of 0.05 and 0.1	4
6	Plasma gasification of macadamia nut shells evaluated namely 0.54, 0.72, 1 and 1.14 kg/h at each respective plasma power setting of 9, 11 and 14 kW	24
7	Plasma gasification of macadamia nut shells evaluated at 0, 0.619 and 0.652 kg/h oxygen added	4

Chapter 4 Results and discussion

4.1 Equilibrium thermodynamic analysis

Figure 4.1 shows the predicted species distribution as function of temperature using 1 kmol sucrose at 1 bar, in an inert atmosphere, generated using the commercial software package Outotec HSC Chemistry 7.1 (HSC Chemistry, 2019). A Gibbs-energy minimization routine for the system is implemented by the software. Only C, H, and O were selected as available elements in our case. The thermodynamic behaviour of sucrose is anticipated to represent the general behaviour of the other species investigated.

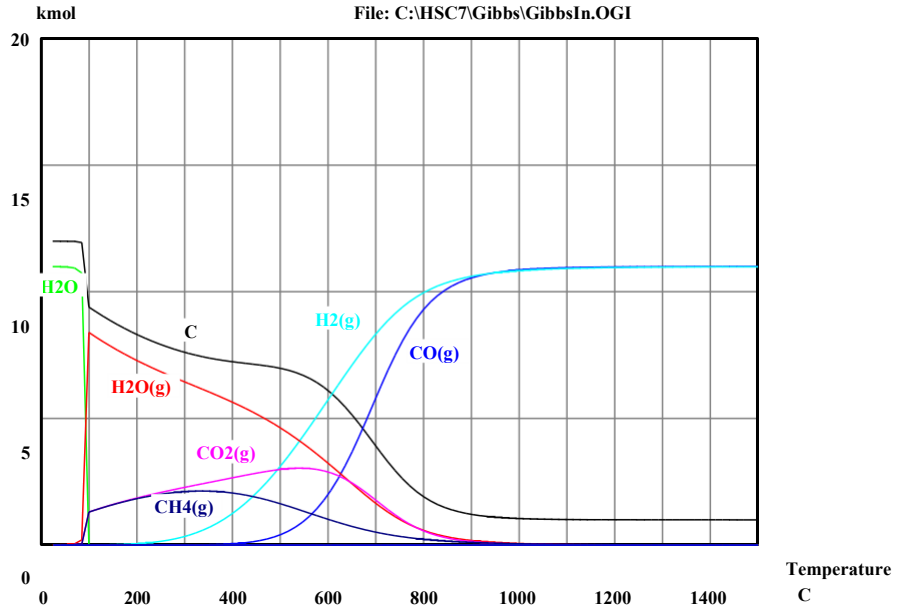

Figure 4.1: Equilibrium composition for kmol sucrose at 1 bar

Sucrose is thermodynamically unstable. Up to 100 ºC the stable products are solid carbon and liquid water. Above the boiling point of water, a mixture of methane, water vapour, and carbon dioxide is predicted. Above 900 ºC only carbon monoxide, hydrogen, and solid carbon (graphite is the stable phase) exist, and the system composition remains constant up to high temperatures. The temperature range is generally classified as: torrefaction up to 300 ºC; pyrolysis between 300 ºC and 900 ºC; and gasification above 900 ºC. In the pyrolysis region kinetics predominate, and numerous condensable organic species are obtained in practice.

With the addition of a 0.5 kmol of oxygen to react with the residual solid carbon the behaviour is largely identical to the pyrolysis case, as seen in Figure 4.2 below. In the intermediate

temperature region, more carbon dioxide forms, and of course all the solid carbon is mopped up as carbon monoxide above 900 °C.

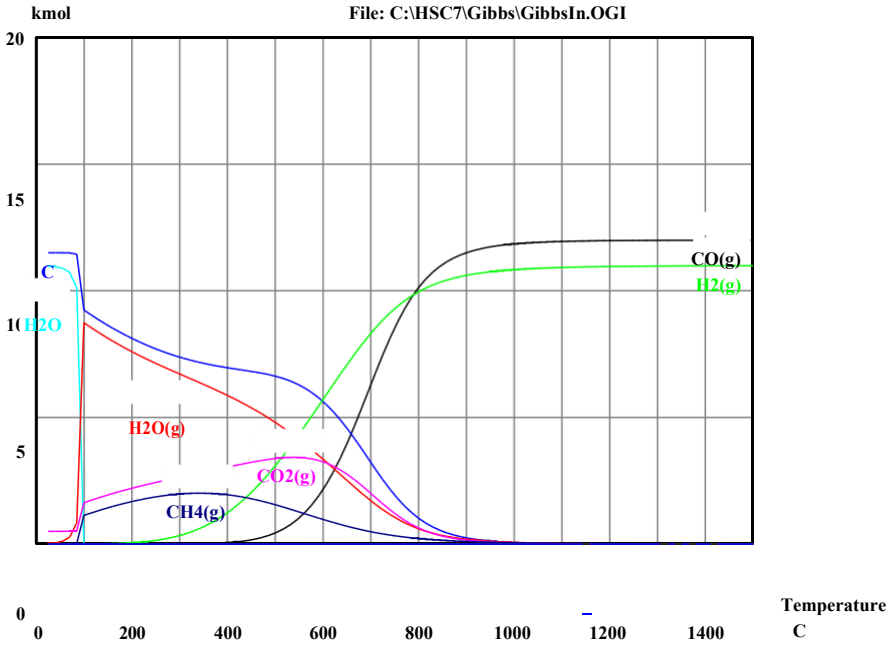

Figure 4.2: Equilibrium composition for kmol sucrose at 1 bar, with 0.5 kmol O_2

The three simplified stoichiometric reactions are: dehydration at low temperature, Equation (13); pyrolysis to syngas up to 900 °C, without oxygen, Equation (14); and pyrolysis with a 1-to-0.5 molar ratio of sucrose-to-oxygen to remove the residual solid carbon, Equation (15).

$$C_{12}H_{22}O_{11} \rightarrow 11H_2O + 12C \quad (13)$$

$$C_{12}H_{22}O_{11} \rightarrow 11CO + 11H_2 + 12C \quad (14)$$

$$C_{12}H_{22}O_{11} + 0.5O_2 \rightarrow 12CO + 11H_2 \quad (15)$$

The Ellingham diagrams for the three reactions are given in Figure 4.3. The values confirm the equilibrium calculations above: all three reactions are thermodynamically viable in the temperature region of interest.

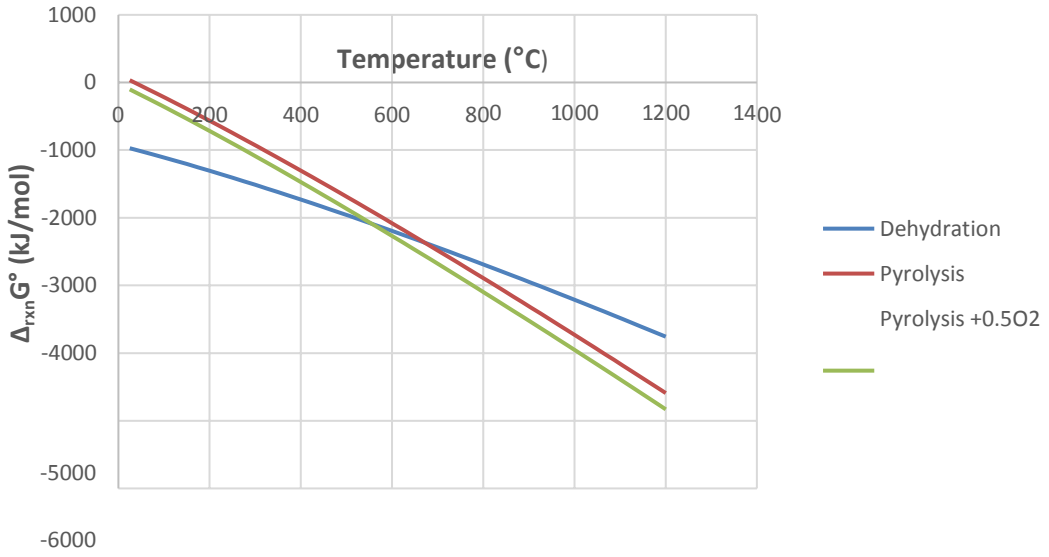

Figure 4.3: Gibbs free energy of the three dominant sucrose reactions

The enthalpy and entropy changes accompanying the three reactions, at room temperature, are listed in Table 4.1.

Table 4.1: Enthalpy and entropy changes for the sucrose reactions

Reaction	$\Delta_{rxn}H_{298}°$ (kJ/mol)	$\Delta_{rxn}S_{298}°$ (J/(K mol)
$C_{12}H_{22}O_{11} \rightarrow 11H_2O + 12C$	-922.429	478.335
$C_{12}H_{22}O_{11} \rightarrow 11H_2 + 11CO + C$	1005.745	3257.470
$C_{12}H_{22}O_{11} + 0.5O_2 \rightarrow 11H_2 + 12CO$	895.204	3346.816

The dehydration of sucrose is exothermic and also has a positive change in entropy. The formation of carbon monoxide is endothermic and driven by the increase in entropy. The reason for the endothermicity is attributable to the stability of the water molecule; its bonds have to be broken to form the carbon monoxide.

4.2 Thermogravimeteric analysis

4.2.1 Thermal decomposition of glucose, sucrose and fructose

The thermograms for sucrose, glucose, and fructose are presented in Figures 4.4, 4.5 and 4.6 respectively, at heating rates of 5, 10, 15, 20 and 50 °C/min each. The infrared spectra of the distinguishable mass loss events for each sugar were taken at the point of maximum absorbance at a heating rate of 10 °C/min and are presented in Figures 4.7 to 4.13.

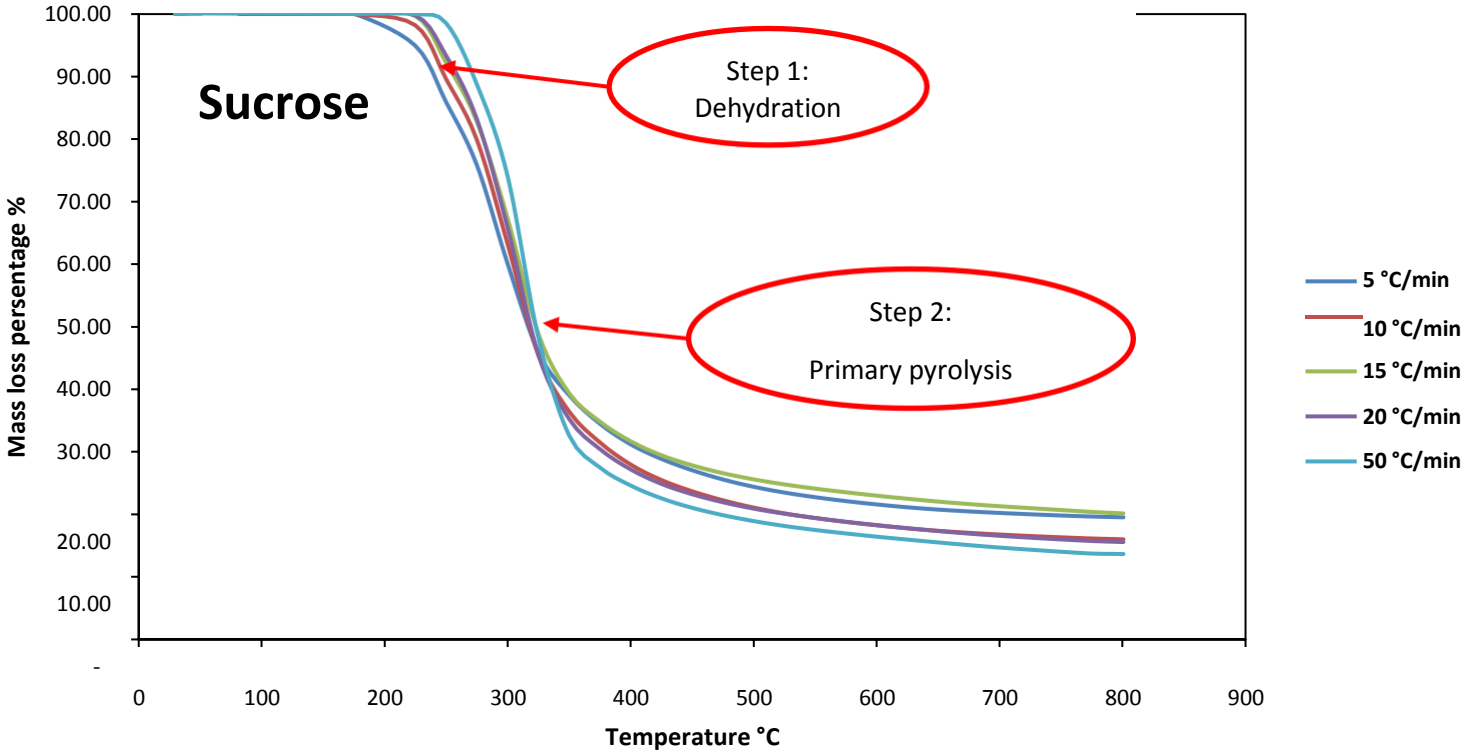

Figure 4.4: TGA curves for sucrose at heating rates 5, 10, 15, 20 and 50 ºC/min

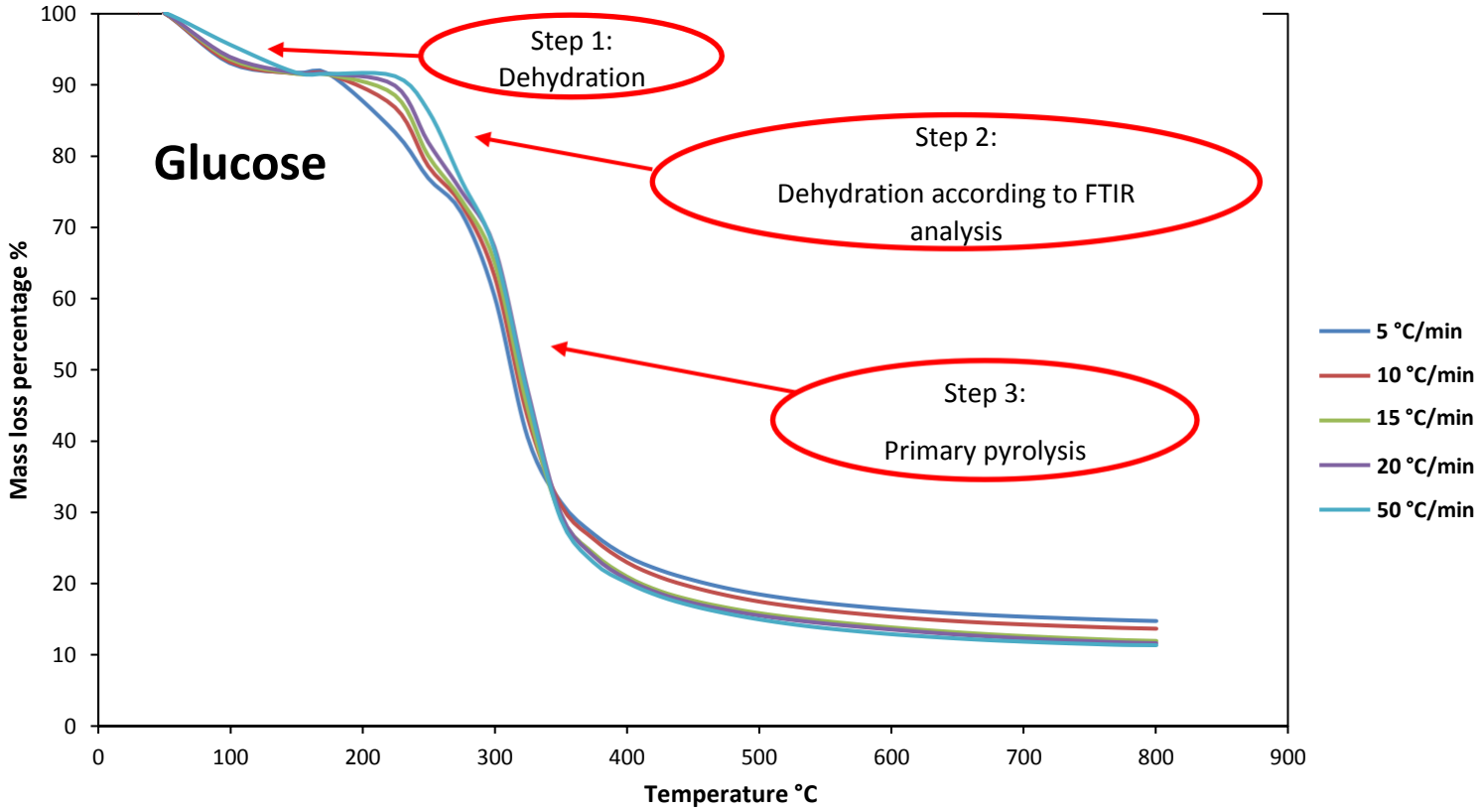

Figure 4.5: TGA curves for glucose at heating rates of 5, 10, 15, 20 and 50 °C/min

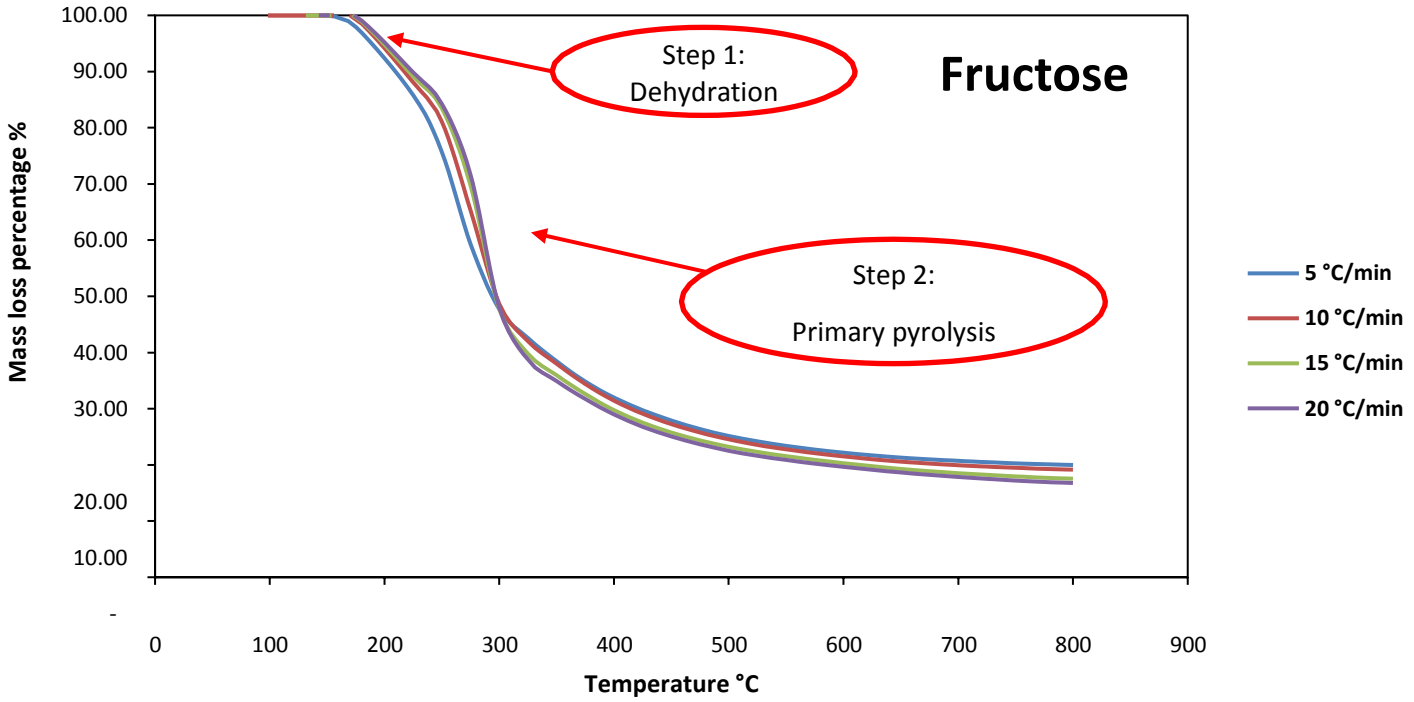

Figure 4.6: TGA curves for fructose at heating rates 5, 10, 15 and 20 ºC/min

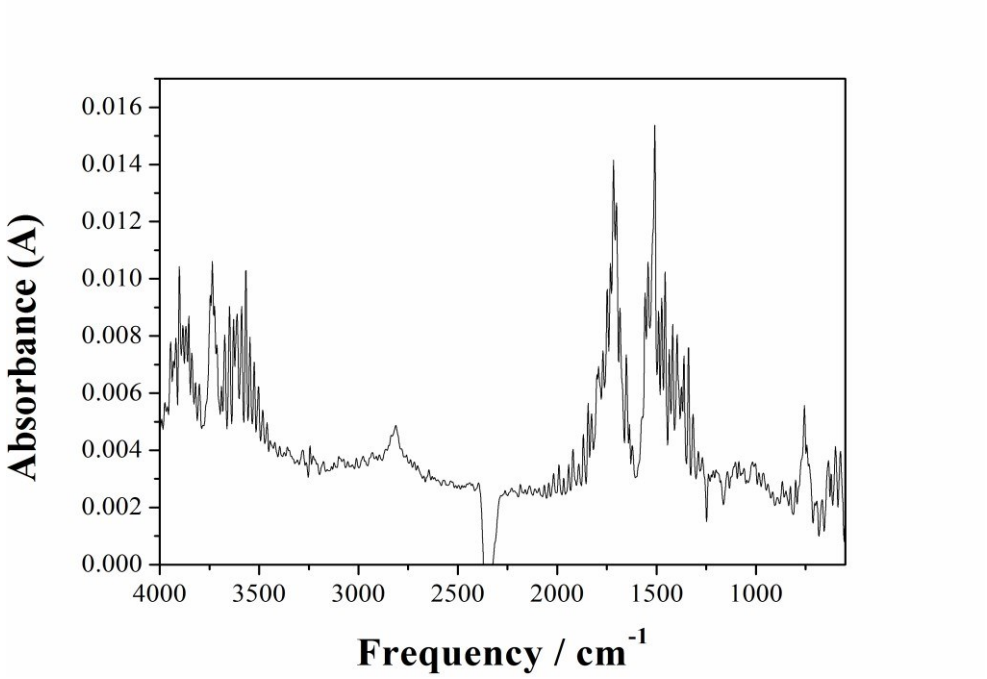

Figure 4.7: FTIR spectrum of the first mass loss event for sucrose at a thermal decomposition temperature of ~220 ºC

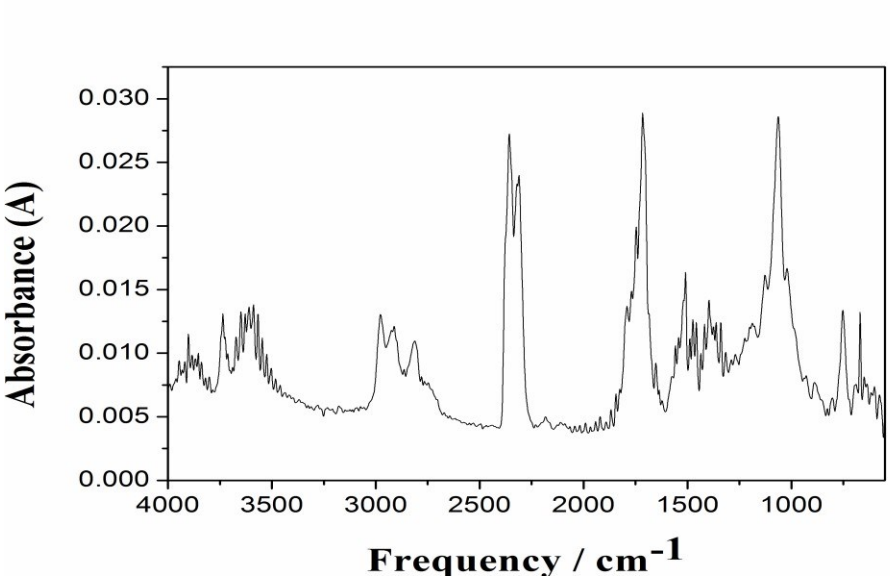

Figure 4.8: FTIR spectrum of the second mass loss event for sucrose at thermal decomposition temperature of ~300 ºC

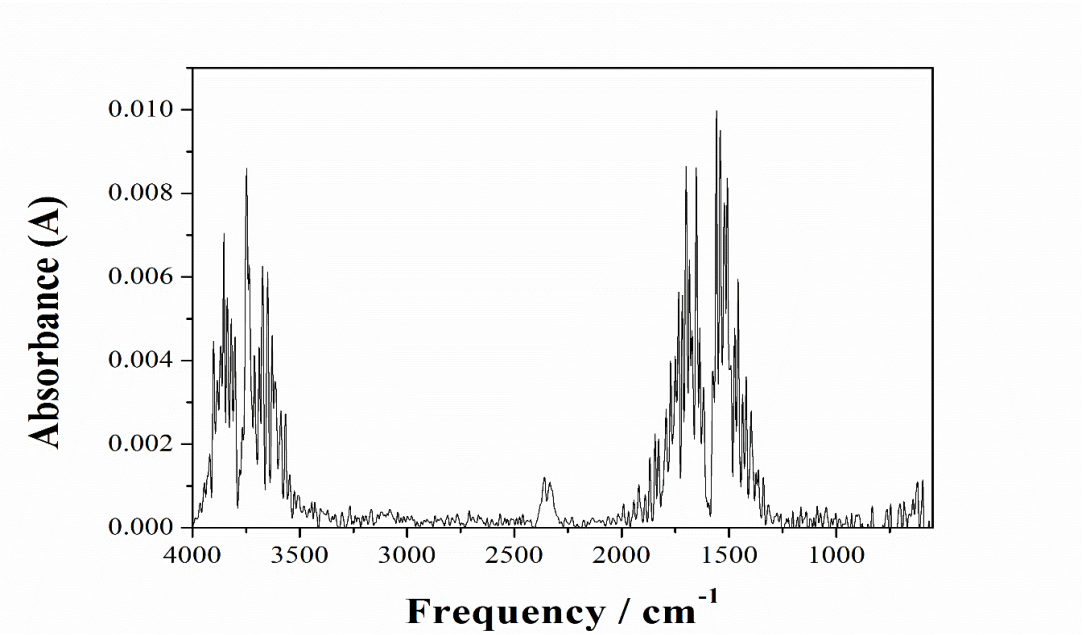

Figure 4.9: FTIR spectrum of the first mass loss event for glucose at thermal decomposition temperature of ~ 60 - 100 ºC

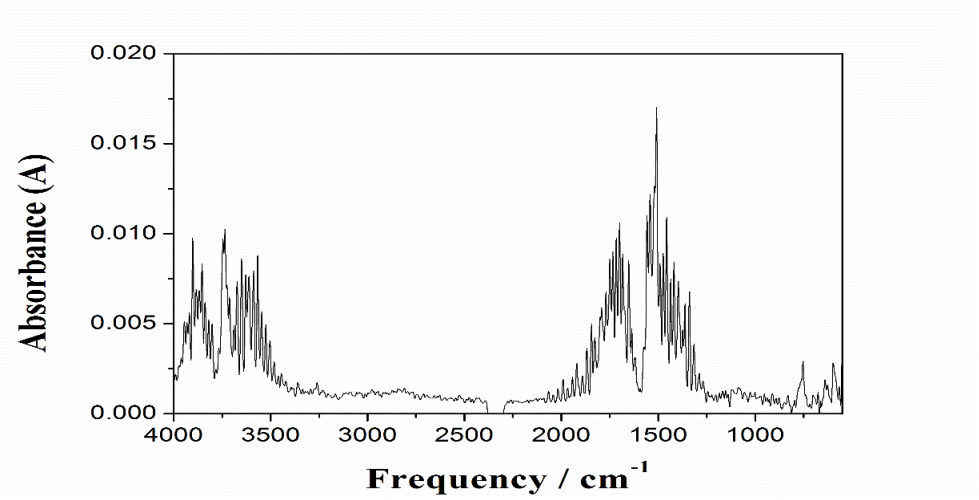

Figure 4.10: FTIR spectrum of the second mass loss event for glucose at thermal decomposition temperature of ~250 ºC

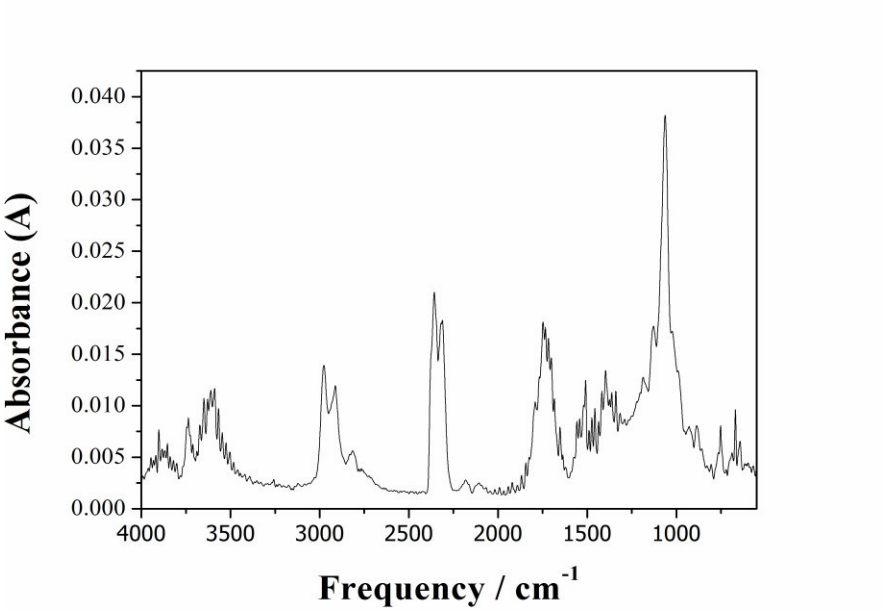

Figure 4.11: FTIR spectrum of the third mass loss event for glucose at thermal decomposition temperature of ~325 ºC

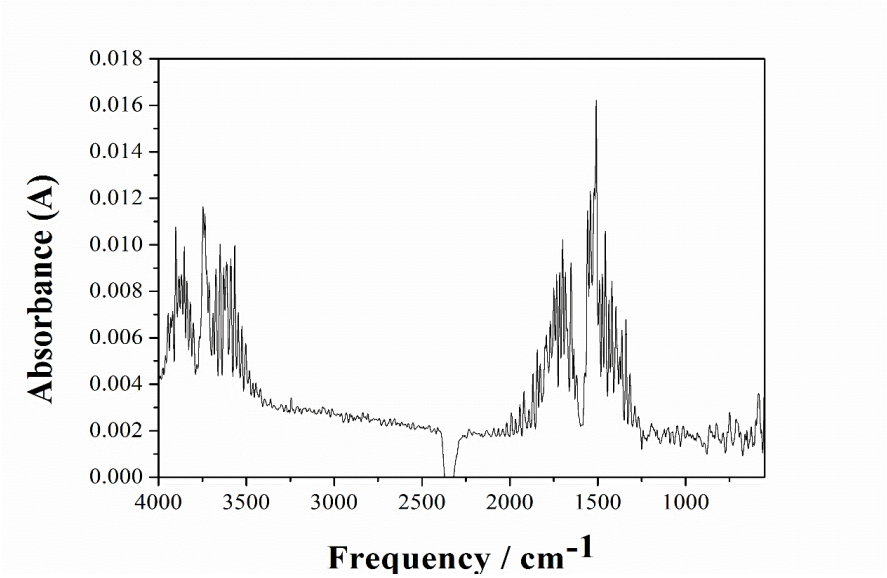

Figure 4.12: FTIR spectrum of the first mass loss event for fructose at thermal decomposition temperature of ~162 ºC

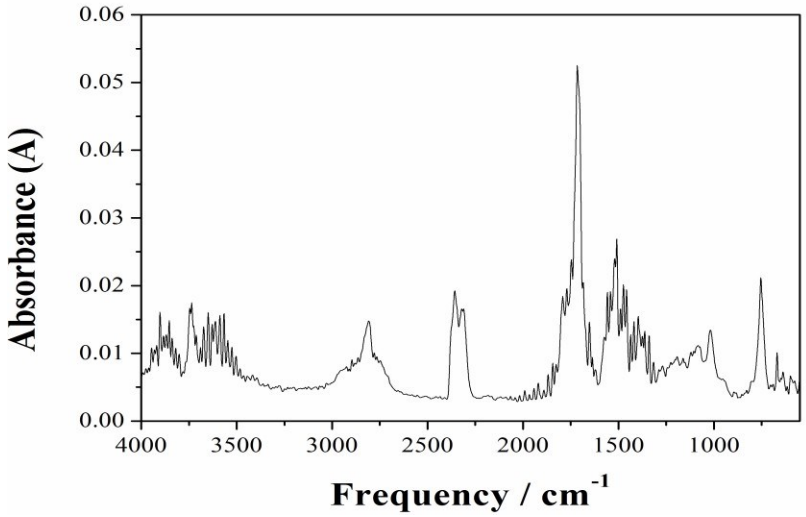

Figure 4.13: FTIR spectrum of the second mass loss event for fructose at thermal decomposition of ~ 296 ºC

Apart from the observation that glucose monohydrate loses its crystal water at around 100 °C, all three sugars display similar general thermal behaviour. Sub-stoichiometric dehydration, according to Equation 13, takes place in the region 150 °C to 250 °C. Between 250 °C and 450 °C primary pyrolysis with the formation of hydrocarbons takes place. Higher heating rates in general increase the degree of gasification, but the carbonaceous residue is never less than 15 %.

For sucrose, the theoretical mass loss from the dehydration process is 57 %. From Figure 4.4, the actual mass loss for from the dehydration process is ~12 %. The additional loss of ~ 45 % is due to in the formation of hydrocarbons in the primary pyrolysis process. The theoretical mass loss for the formation of CO and H_2 is 96 %. The actual mass loss for sucrose was about 80 % at 10 °C/min and went up to 86 % at 50 °C/min. Heating rates influence degradations reactions and the composition of by-products. Low heating rates increase the effect of heat and mass transfer which causes the likelihood of the formation of hydrocarbons. Low heating rates also decreases conversion to biochar (Surahmanto, 2017). Inspection of the mass percentage loss curve of sucrose reveals that there are two processes occurring and that they are strongly temperature-dependent. The first process is prominent at a heating rate of 5 °C/min, but almost completely gone at 50 °C/min. The dehydration process starts at a temperature of approximately 220 °C. The primary pyrolysis process proceeds and start flattening out at a temperature of approximately 350 °C. The mass of char residues after the experiments were

measured as 19.6, 15.8, 20.2, 15.6 and 13.7 % for respective heating rates of 5, 10, 15, 20 and 50 ^{o}C/min.

(Gaussling, 2008) conducted an experiment for the thermal decomposition of sucrose under a nitrogen atmosphere. The experiment was performed at a heating rate of 10 ^{0}C/min, with a TGA Q 500 thermogravimetric analyser. The mass loss for sucrose reported as 78.6 % at a heating rate of 10 °C/min. Figure 4.14 gives his result. The dehydration process started occurring at a temperature of 227 °C. The primary pyrolysis process concludes at 325 °C. There is an overall 6 % difference between this sucrose result from the literature and our experimental results.

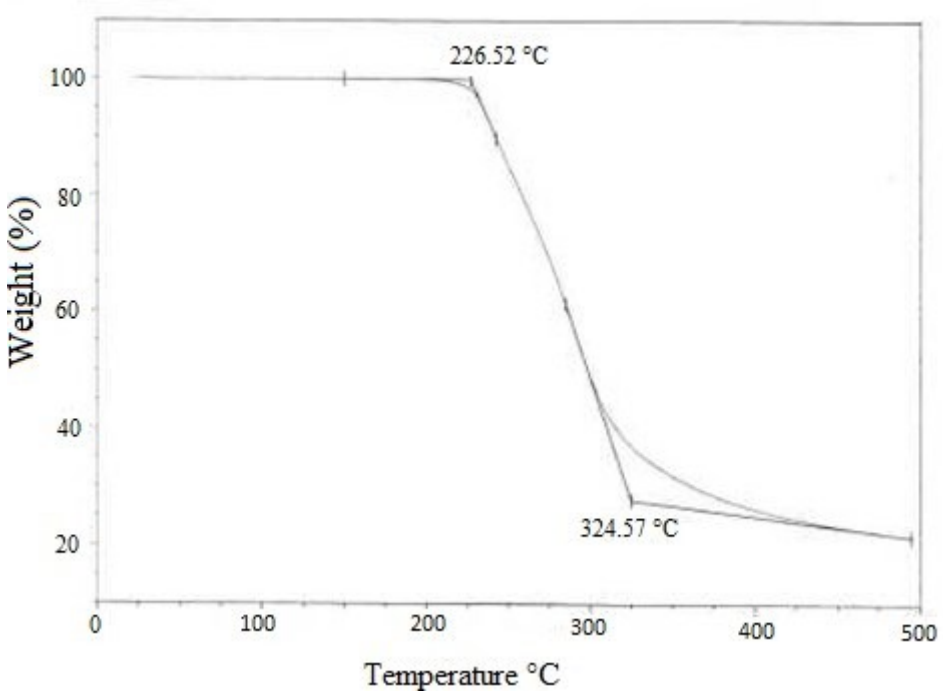

Figure 4.14: TGA curve for sucrose at heating rate 10 ^{o}C/min (Gaussling, 2008)

For glucose monohydrate, the theoretical mass loss for full dehydration process is 64 %. From Figure 4.5, the mass loss for the loss of the crystal water is ~8 % and can be observed to occur at a temperature of ~60 °C to 100 °C. Thereafter, dehydration results in the loss of another ~21 %, in the range 180 °C to 280 °C. After this the primary pyrolysis process results in a final mass loss of about 86% at 5 °C/min to 89 % at 50 °C/min. The pyrolysis process starts slowing after roughly 350 °C. The mass of char residues after the experiments were measured as 15.3,

13.7, 12.1, 11.7 and 11.3 % for respective heating rates of 5, 10, 15, 20 and 50 ºC/min. (Yann, 2019) investigated the thermal decomposition of glucose under argon atmosphere. The experiments were performed at heating rates of 1, 2, 5 and 10 ^{0}C/min, with a Netzsch TG 209 thermogravimetric analyser. Figure 4.15 shows the results of the experiments. Similarly, the thermal decomposition followed a triple step reaction, with the primary and secondary pyrolysis steps occurring at 225 °C and 311 °C.

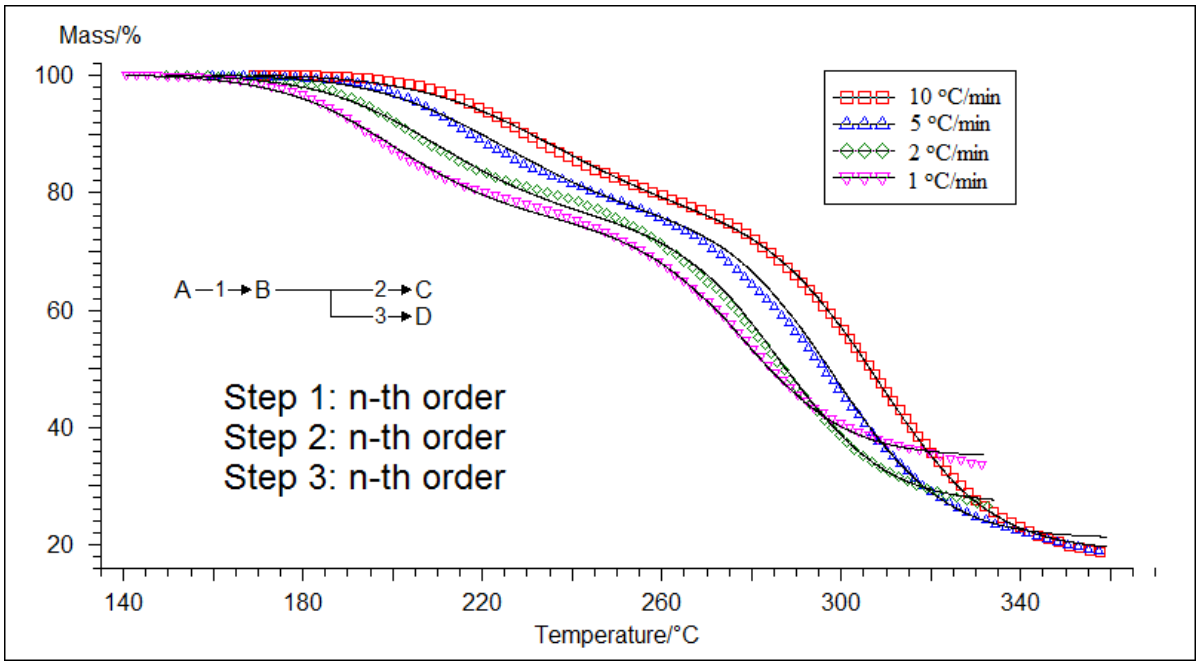

Figure 4.15: TGA curves for glucose at heating rate 1, 2, 5 and 10 ºC/min (Yann, 2019)

For fructose, the theoretical mass loss for the dehydration process is 60 %. In Figure 4.6 the actual mass loss for dehydration process is ~15 %. The actual mass loss due to pyrolysis about 80 % at 5 °C/min and went up to 85 % at 50 °C/min. The dehydration process starts at a temperature of approximately 162 °C, much lower than that of sucrose and glucose samples. The pyrolysis process of fructose proceeds up to ~300 °C, liberating H_2O, CO, CO_2 and volatile organics. The mass of char residues after the experiments were measured as 13.5, 16.8, 17.5, 19.1 and 11.3 % for respective heating rates of 5, 10, 15, and 20 ºC/min.

In the IR spectrum of the first mass loss event for sucrose is given in Figure 4.7, for the first two mass loss events of glucose monohydrate in Figure 9 and Figure 10, and for the first event for fructose in Figure 4.11. Of course, the first low-temperature event for glucose monohydrate is the loss of the one water of crystallisation. In all cases the spectra only clearly show water. Background carbon dioxide is also observed, either as a positive peak in Figure 9, or as negative

peaks in the other figures, due to background subtraction. The O-H symmetric and asymmetric stretching vibrational are observed as the rotation-vibration absorbance peaks between 3500 and 4000 cm^{-1}. The H-O-H bending vibrations, also seen as rotation-vibration absorbance peaks, are found between 1300 and 1910 cm^{-1} (Bonner, 1934). The spectra for the pyrolysis streams generated by the primary pyrolysis processes are depicted in Figure 4.8, Figure 4.11, and Figure 4.13 for sucrose, glucose, and fructose respectively. In all cases water is still clearly visible. The two absorbance peaks in a frequency range of 2250 to 2350 cm^{-1} represent the C=O stretching vibrations of carbon dioxide. Their intensities have become much more prominent, well above background values. CO_2 is thus a well-defined pyrolysis product.

The regions of interest which appear in all spectra during pyrolysis are: 1000 to 1250 cm^{-1}; 1600 to 1800 cm^{-1}, superimposed on the water bending peaks; and 2700 to 2900 cm^{-1}. The modes in the region 1000 to 1250 cm^{-1} may be attributable to the C-O stretches of a variety of alcohols, ethers, esters—aryl or alkane. Absorption by the C=O functional group, contained in a wide range of organic compounds, takes place between 1600 and 1800 cm^{-1}. The wavenumber region between 2700 and 2900 cm^{-1} in its turn are indicative of C-H stretching modes.

Unambiguous identification of organic compounds is clearly not possible from the spectra. Comparison with the NIST database indicated the following possibilities: furfural ($C_5H_4O_2$); ethylene (C_2H_2); cyclotetradecane ($C_{14}H_{28}$); maltol ($C_6H_6O_3$).

The main conclusion to be drawn from the IR analysis is that during the primary pyrolysis process observed during TGA experiments, water, carbon dioxide, along with a variety of organic compounds—predominantly oxygen containing—are produced.

4.2.2 Thermal decomposition macadamia nut shells

Figure 4.16 shows the results of the TGA for the macadamia nut shells at heating rates 5, 10, AND 20 ^{o}C/min. As for the sugars, it is evident that lower heating rates yields more char.

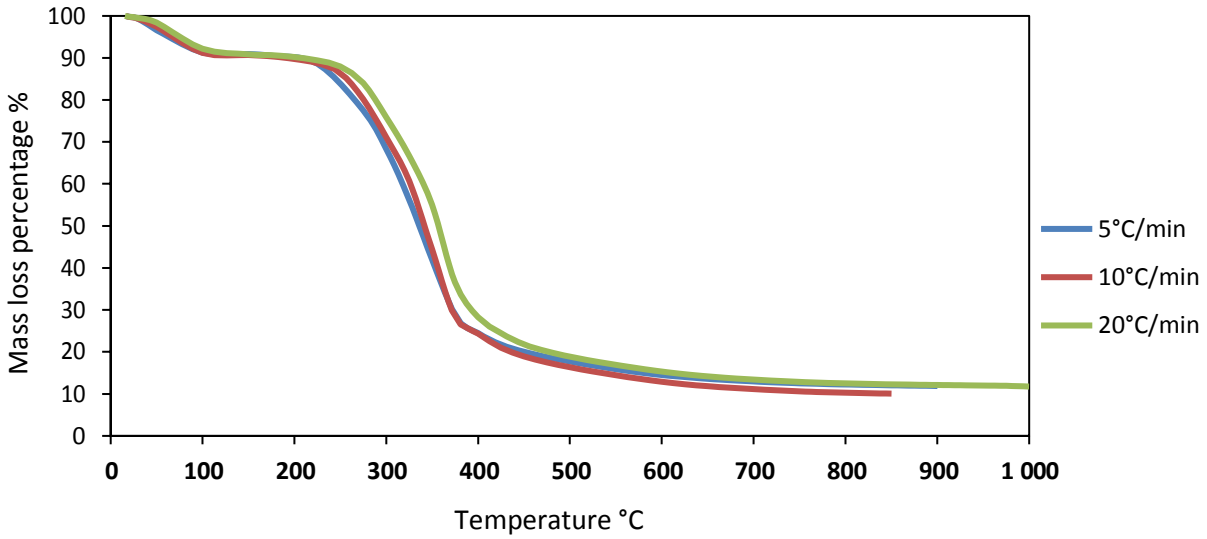

Figure 4.16: TGA curves of macadamia nut shells at heating rates 5, 10 and 20 ^{o}C/min

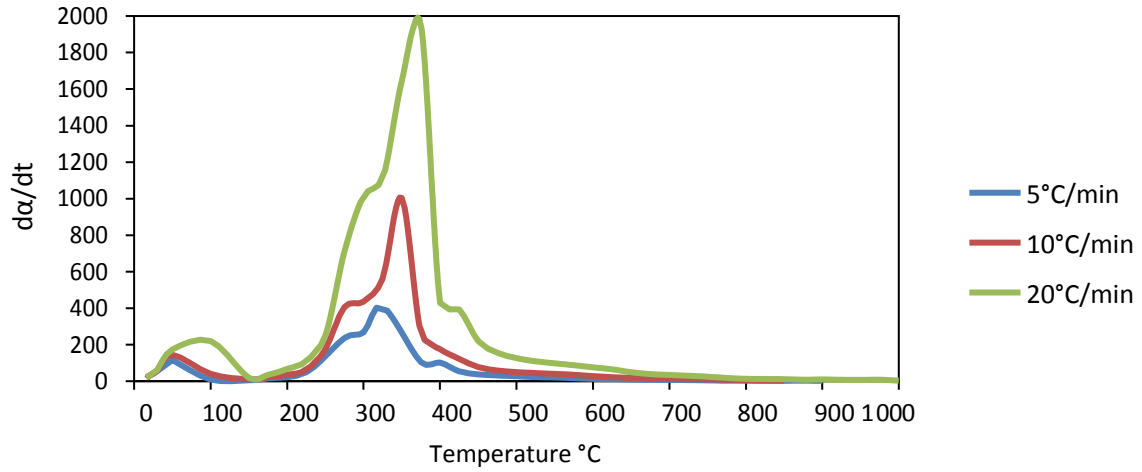

Figure 4.17: DTG curves for macadamia nut shells at heating rates 5, 10 and 20 ^{o}C/min

From the DTG curve in Figure 4.16 it is evident that the initial dehydration step peaks at roughly 55 °C at a heating rate of 5 °C/min, at 58 °C for a heating rate of 10 °C/min, and then at 107 °C at a heating rate of 20 °C/min. Heat transfer and/or kinetic effect may be the cause for this drift. The final mass loss for the shells was about 88 % at 10 °C/min. The DTG curves suggest that for all heating rates, the decomposition of macadamia nut shells occurs in three steps, as represented by the clearly identifiable peaks. This is in accordance with the observation of (Xavier, Lira *et al.*, 2016). At around 250 °C to 300 °C lignin starts decomposing, along with various extractives. The decomposition of hemicellulose and cellulose follow, with the position of the highest peaks representing cellulose, at roughly

between 330 and 380 °C. The last peaks above 400 °C indicate the final stages of the decomposition of lignin. Compared to the well-defined sugars, the decomposition of the macadamia nut shells is thus substantially more complex. Surprisingly, though, the final solid residue appears to be lower than for the sugars.

4.3 Plasma gasification

4.3.1 Plasma torch efficiency and energy losses

An energy balance around the torch anode and cathode was conducted at power settings of 9, 10, 11, 12, 13 and 14 kW. The aim was to determine the electrical energy introduced into the system by the plasma torch. Sensible heat losses occurred through water cooling at the torch anode and cathode. Equations 18 to 20 were used to calculate the plasma torch efficiency.

$$Q_{anode} = \dot{m}_{water} \times C_{p,water} \times \Delta T_{anode} \tag{18}$$

$$Q_{cathode} = \dot{m}_{water} \times C_{p,water} \times \Delta T_{cathode} \tag{19}$$

$$Efficiency = \frac{IV - (Q_{anode} + Q_{cathode})}{IV} \tag{20}$$

Here I and V are the current drawn and the voltage applied to the torch, respectively. The efficiency of the laboratory plasma torch was calculated to be ~30 % as shown in Figure 4.17.

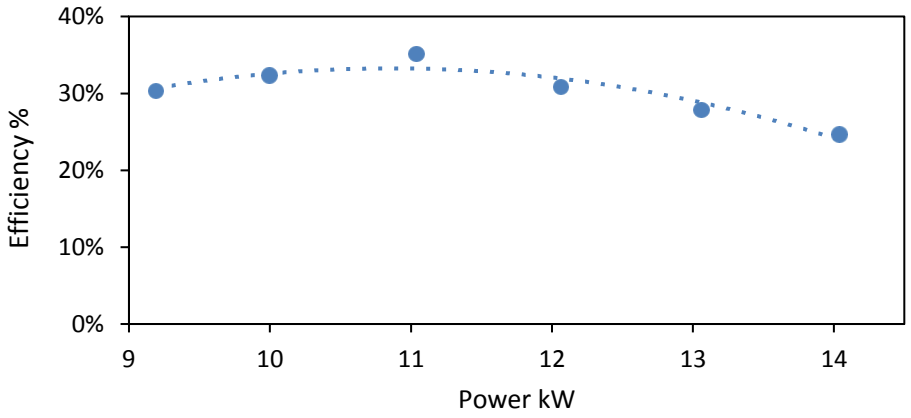

Figure 4.18: Efficiency of plasma torch relative to power settings

At a power setting of 11 kW, the efficiency is 34 % and the highest. It was also observed that the efficiency decreases at power settings greater than 12 kW. Similar torches operate at

efficiencies of 70 % and sometimes higher. One important reason may be that there is no heat shield between the anode housing and gasification reactor, resulting in higher radiation heat transfer from the reactor to the anode.

Sensible heat losses were also calculated for other various components as shown in Table 4.2. This was done without material feed. All components except the flange were water cooled. Its loss was estimated by difference.

Table 4.2: Average energy loss for plasma gasification

DC torch component	Power loss %
Cathode	4 %
Anode	68 %
Inner quench	4 %
Outer quench	6 %
Reactor wall	11 %
Flange	7 %

4.3.2 Plasma gasification of sucrose

Biomass gasification consists of the overlapping processes of drying, pyrolysis and partial oxidation. (Sikarwar, Zhao *et al.*, 2016) reported a simple way of representing the gasification reaction is shown in Equation 21:

$$\text{Biomass} + \text{heat} \rightarrow H_2 + CO + CO_2 + CH_4(g) + C_mH_n + \text{Biochar} \quad (21)$$

The equivalence ratio (ER) as in Equation 22, written for sucrose, is defined as the ratio of actual oxygen supplied to the stoichiometric amount for complete combustion-gasification to form carbon monoxide.

$$ER = \frac{\left[\frac{oxygen}{sucrose}\right]_{actual}}{\left[\frac{oxygen}{sucrose}\right]_{stoichiometric}} \quad (22)$$

Equation 23 shows the complete combustion of sucrose to CO_2, and has an ER of 24.

$$C_{12}H_{22}O_{11} + 12O_2 \rightarrow 12CO_2 + 11H_2O \quad (23)$$

Equation 24 presents the reaction of when H_2 and CO are only the desired gas products. Per definition the ER value here is one.

$$C_{12}H_{22}O_{11} + 0.5O_2 \rightarrow 12CO + 11H_2 \quad (24)$$

Plasma gasification experiments were carried out on pure sucrose. The experiments were conducted at a plasma torch power setting of 11 kW, yielding a constant gasification-reactor temperature of 1000 ºC after thermal equilibrium had been reached. The sucrose feed rate was kept constant at 1 kg/h. During these experimentations, clogging of the screw feeder was experienced due to the low melting temperature of sucrose, 186 ºC and the resulting reduction of flow-ability of the sucrose. A single point comparison was made due to this experimental difficulty. The first experiment had an ER of 1, at an oxygen feed rate of 0.0468 kg/h. The second experiment had an ER of 2, at an oxygen feed rate of 0.0936 kg/h. During experimentation gas samples were taken every 10 minutes. The gas samples were collected in U-tubes. After each experimental run the gas samples were analysed offline by a gas chromatograph (GC). Figure 4.18 presents the results of the gas produced for the two experiments.

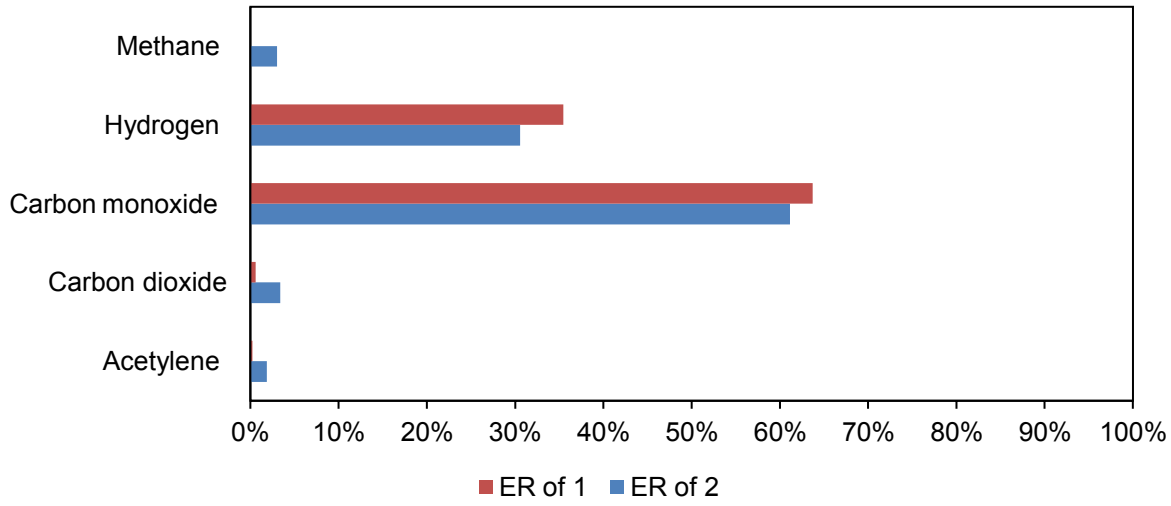

Figure 4.19: Produced gas for the plasma gasification of sucrose with at a constant power of 11 kW and two ER values

In the first experiment with an ER of 1, the CO/H_2 ratio was 1.8 and the CO/CO_2 ratio was 109. In the second experiment with an ER of 2, the CO/H_2 ratio was 1.73 and the CO/CO_2 ratio 18. An increase in ER enhances the formation of hydrocarbons such as C_2H_2 and CH_4. (Pellegrini and De Oliveira, 2007) obtained similar results. Thus, it can be concluded that a stoichiometric ER ensures high syngas quality. The degree of conversion of the plasma gasification was calculated by weighing the char residue after each experiment and comparison with the amount fed. The mass of char residue measured for the plasma gasification of sucrose with an ER of 1 was 8 %. The mass of char residue measured for the plasma gasification of sucrose with an ER of 2 was 12 %. This difference may not be significant, and is probably within experimental error. From the results of the TGA experiments with sucrose, the mass of char residue was varied between 20 % and 14 % for heating rates from 5 ^oC/min to 50 ^oC/min. Plasma gasification with its anticipated much faster heating rate, thus has higher conversions than TGA experiments. More importantly, the pyrolysis stream contains predominantly syngas, and none of the complex organic compounds observed for conventional pyrolysis. This is anticipated for the temperature at which the experiments were performed, viz., 1000 ^oC. Heat transfer and other transient effects did thus not interfere with the product distribution, although complete conversion to gas was not achieved. The power balance of the process can be written as in Equation 25:

$$\Delta Qr = \eta\ W_{torch} - Q_{losses} \tag{25}$$

Where ΔQr is the power available for gasification, η is the efficiency and W_{torch} is power of the torch. Q_{losses} is power losses carried out of the gasification reactor. At 100 % conversion efficiency, the plasma gasification of sucrose is converted to CO and H_2 as in Equation 24. Thus, the theoretical energy requirement for 100 % conversion efficiency as a function of sucrose feed rate

$$\begin{aligned}\Delta Qr &= \Delta_{rxn}H_c^\circ \times \dot{m}_{sucrose} \\ &= 20.378\ (kJ/g) \times \dot{m}_{sucrose}\ (kg/h) \times (h/3600\ s)\end{aligned}$$

4.3.3 Plasma gasification of macadamia nut shells

The plasma gasification of macadamia nut shells at four different feed rates were evaluated, namely 0.54, 0.72, 1 and 1.14 kg/h at plasma power settings of 9, 11 and 14 kW. The conversion efficiency, syngas composition and low heating values were calculated for each run. A total

number of 24 experiments were performed for these experimental parameters. These were repeated, and an average is reported. No oxygen was added during the experiments.

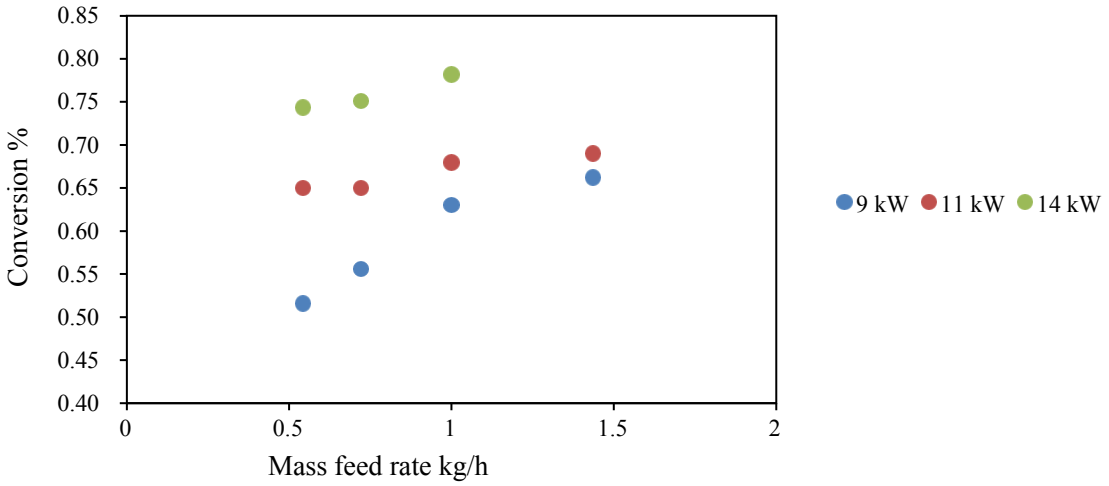

Figure 4.20: Conversion of the macadamia nut shells to syngas relative to mass feed rate and respective constant power of 9, 11 and 14 kW

Figure 4.20 shows the conversion of the produced syngas relative to the four mass feed rates of macadamia nut shells and constant powers of 9, 11 and 14 kW. The conversion efficiency of the plasma gasification process for the macadamia nut shells was calculated by weighing the residue after each experiment and comparing with the amount fed, as for the sucrose experiments. During experimentation gas samples were taken every 10 minutes. The gas samples were collected in U-tubes. After each experimental run the gas samples were analysed offline by a gas chromatograph (GC). As expected, it was observed that as the power increases, conversion increases; from 48 % at 9 kW to higher than 80 % conversion at 14 kW. This is obviously due to the increase in available energy.

Unexpectedly, however, it was also observed that higher mass feed rates increase conversion. This could be an indication that higher feed rates result in better mixing, and thus improved heat transfer, inside the reactor. The exit of the feeder is localized around the striking angle and there is an uneven distribution of feed inside the reactor.

Table 4.3 to Table 4.5 presents the calorific values of the syngas for the above feed rates and power levels. The LHV_{syngas} (low heating value of syngas) was calculated using Equations 26 and 27, for energy content and power content respectively.

$$LHV_{syngas}\left(\frac{kJ}{mol}\right) = \sum_{i} x_i \times \Delta H_c^{\circ} \qquad (26)$$

$$\text{LHV}_{\text{syngas}}(\text{kW}) = \text{LHV}_{\text{syngas}}\left(\frac{\text{kJ}}{\text{mol}}\right) \times \dot{m}_{syngas} \quad (27)$$

Here x_i is defined as the mass fraction of the i^{th} gaseous components in the syngas, and $\Delta_c H°$ is the heat of combustion of these components.

The calorific values of the syngas increased with higher feed rates. The calorific value of the syngas also increases with higher plasma power. The calorific value is dependent on the composition of products in the syngas. However, an increase in the feed rates gives rise to an increased concentration of contaminants such as methane and CO_2. This inadvertently affects the quality of the syngas w.r.t. the calorific value.

Table 4.3: Calorific values of produced syngas for macadamia nut shells at different feed rates and a constant power of 9 kW

Feed rate (kg/h)	Syngas (kg/h)	Conversion to syngas	H_2 (mol%)	CO (mol%)	CO_2 (mol%)	CH_4 (mol%)	Syngas avg molar mass (g/mol)	LHVsyngas (kJ/mol)	LHVsyngas (kJ/g)	LHVsyngas (kW)
0.543	0.28	0.52	40	60			17.60	284.20	16.15	1.26
0.72	0.4	0.56	39	59	1	1	17.90	287.42	16.06	1.78
1	0.63	0.63	39	58	2	1	18.06	284.59	15.76	2.76
1.435	0.95	0.66	39	57	2	2	17.94	290.67	16.20	4.28

Table 4.4: Calorific values of produced syngas for macadamia nut shells at different feed rates and a constant power of 11 kW

Feed rate (kg/h)	Syngas (kg/h)	Conversion to syngas	H_2 (mol%)	CO (mol%)	CO_2 (mol%)	CH_4 (mol%)	Syngas avg molar mass ($g/mol_)$	LHV_{syngas} ($kJ/mol_)$	LHV_{syngas} (kJ/g)	LHV_{syngas} (kW)
0.543	0.351	0.65	40	60			17.60	284.20	16.15	1.57
0.72	0.47	0.65	41	59			17.34	284.23	16.39	2.14
1	0.68	0.68	39	58	2	1	18.06	284.59	15.76	2.98
1.435	0.9	0.69	39	57	2	2	17.94	290.67	16.20	4.05

Table 4.5: Calorific values of produced syngas for macadamia nut shells at different feed rates and a constant power of 14 kW

Feed rate (kg/h)	Syngas (kg/h)	Conversion to syngas	H_2 (mol%)	CO (mol%)	CO_2 (mol%)	CH_4 (mol%)	Syngas avg molar mass (g/mol)	LHV_{syngas} (kJ/mol)	LHV_{syngas} (kJ/g)	LHV_{syngas} (kW)
0.543	0.4	0.74	40	60			17.60	284.20	16.15	1.81
0.72	0.54	0.75	37	58	3	2	18.62	287.78	15.46	2.32
1	0.78	0.78	37	57	3	3	18.51	293.86	15.88	3.45

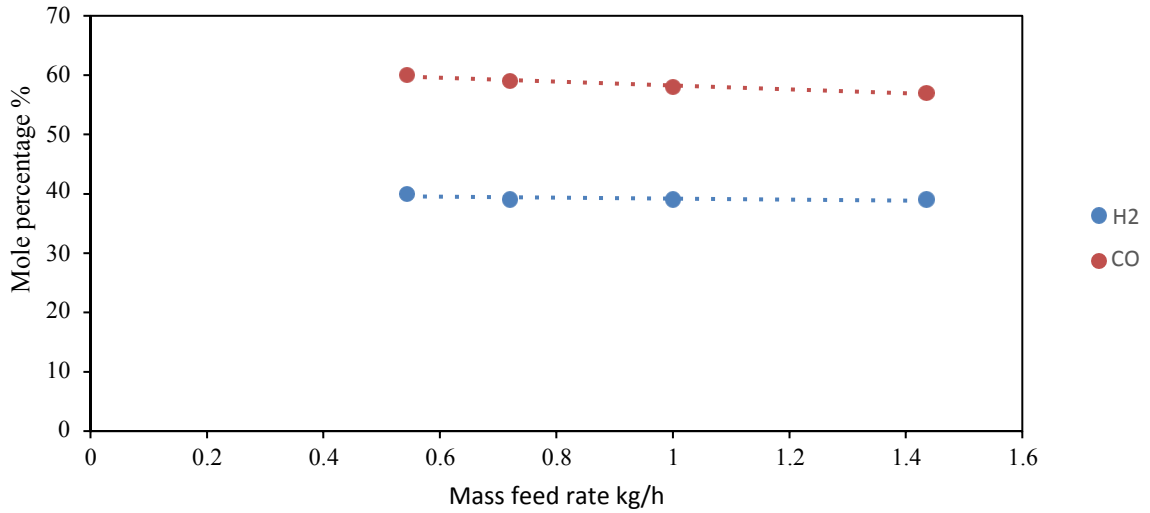

Figure 4.21: Syngas product yield relative to mass flow rate at constant power of 9 kW

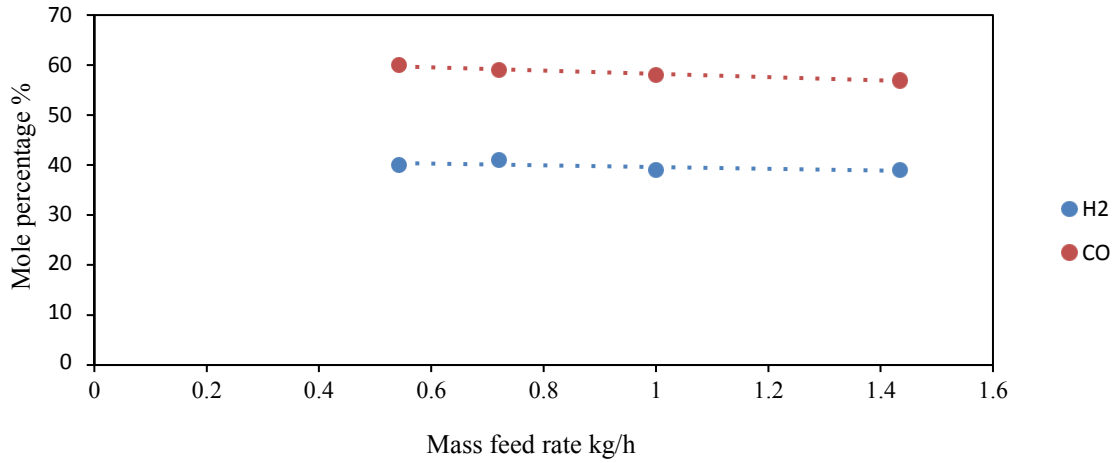

Figure 4.22: Syngas product yield relative to mass flow rate at a constant power of 11 kW

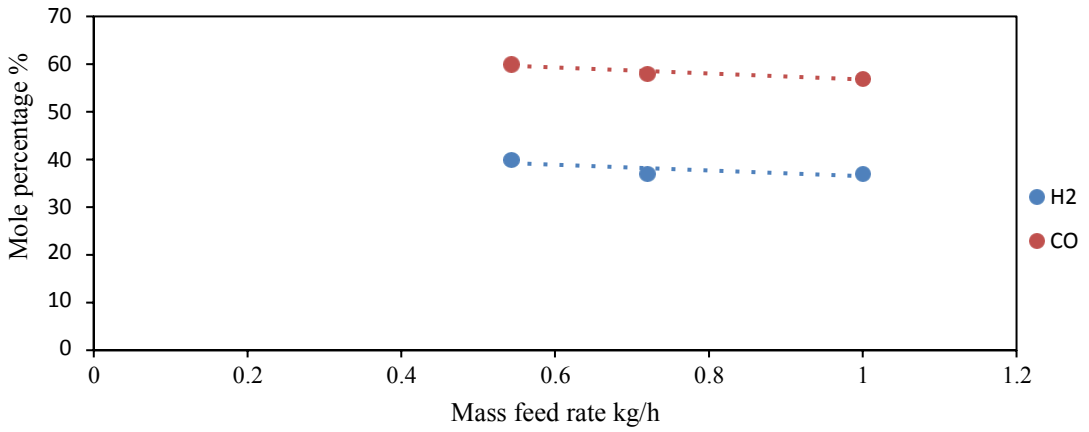

Figure 4.23: Syngas product yield relative to mass flow rate at constant power of 14 kW

Figure 4.21 to Figure 4.23 show the syngas product yield relative to mass flow rate power settings of 9, 11, and 14 kW. The figures show the same decreasing trend for CO and H_2 at higher mass feed rates, with their ration remaining roughly the same. Higher mass flow rates give rise to the formation of hydrocarbons resulting in a decrease in the quality of the syngas decreases. For power settings of 9 and 11 kW, at a mass rate higher than 1 kg/h, the yields of CO and H_2 both decreases. The main reason for this may be poor mixing of the macadamia nut shells when entering the reactor. This simply means that there is a larger bulk of material entering the reactor and insufficient power for full conversion into syngas. Thus, it can be concluded that the mass flow of 1 kg/h for macadamia nut shells is the optimal feed rate. For syngas products at power settings of 14 kW, product yields of CO and H_2 both starts decreasing at a mass rate higher than 0.543 kg/h. This is primarily because the plasma torch efficiency decreases at power settings greater than 12 kW. This is because radiation heat loss increases with increasing power. There is no shield between the anode housing and the gasification reactor.

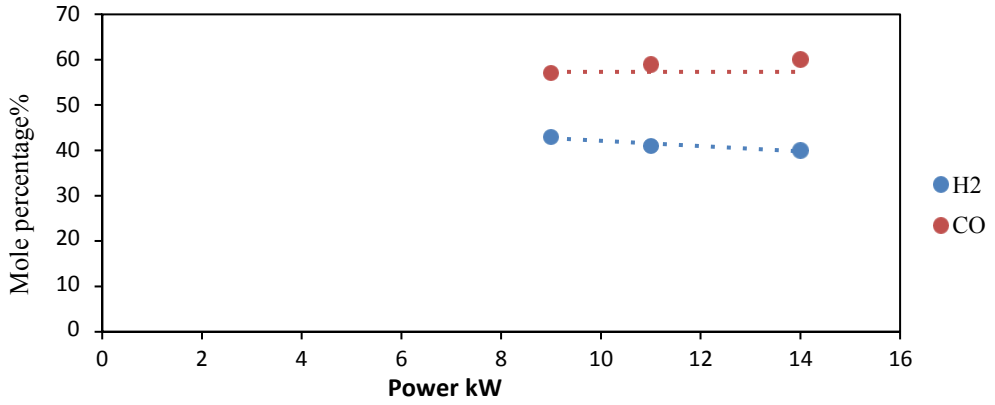

Figure 4.24: Syngas product yield relative to power and a constant feed rate of 1 kg/h

Figure 4.24 shows the mole percentages of H_2 and CO respectively, as function of variation in power and a constant feed rate of 1 kg/h. The produced syngas increases with increasing power to the DC torch. (Diaz, Leal-Quiros *et al.*, 2014) similarly observed that the mole fractions tend to increase with temperature by directly increasing the power.

The solid mass decrease for plasma gasification of the macadamia nut shells was less than that obtained by TGA. The TGA mass loss was 85 % to 90 %, depending on the heating rate. For the TGA experiments, the residence time for heating rates 15 ºC/min and 20 ºC/min was approximately 55 and 41 minutes respectively. Conversion with plasma gasification experiments reached ~80 %. The residence time for the plasma gasification experiments was an hour. The most likely explanation is that the large crushed macadamia shell particle diameter of 10 mm. Also, the residence time for the plasma gasification experiments were slightly longer than that of the TGA experiments despite having the gasification reactor temperature at 1000 ºC. The sample size for TGA experiments is ~20 mg, which is a tiny sub-mm slither. Thus the ratio of the particle size to the residence time in the gasification reactor needs optimisation. For obvious reasons, courser feed particles are cheaper to produce, thus finding a balance between particle size and cost of production is essential for future work.

Expressed as power, the best energy yield recorded in this set of experiments, is just higher than 4 kW. The effective power input into the reactor is the 14 kW electric consumed by the DC torch, with the cathode and anode losses subtracted. The 30 % efficiency of the torch thus reduces the reactor power input to just above 4 kW. The system thus runs at approximately its break-even point. If the torch efficiency could be improved, the performance of the system could similarly be improved, yielding a net energy gain. The main cause of torch inefficiency is anode losses. As noted before, this may be due to the close proximity of the anode to the

reactor. Other torch design issues might also be important. This should be a priority for future work.

4.3.4 Comparison of the sucrose and macadamia feed streams

The sucrose samples are homogenous, with known composition, while the macadamia nut shells are less so. In Figure 4.24, the gaseous product yields of sucrose and macadamia nut shells are compared, for a constant mass feed rate of 1 kg/h, the gasification reactor was kept constant at 1000 °C, and a constant power of 11 kW.

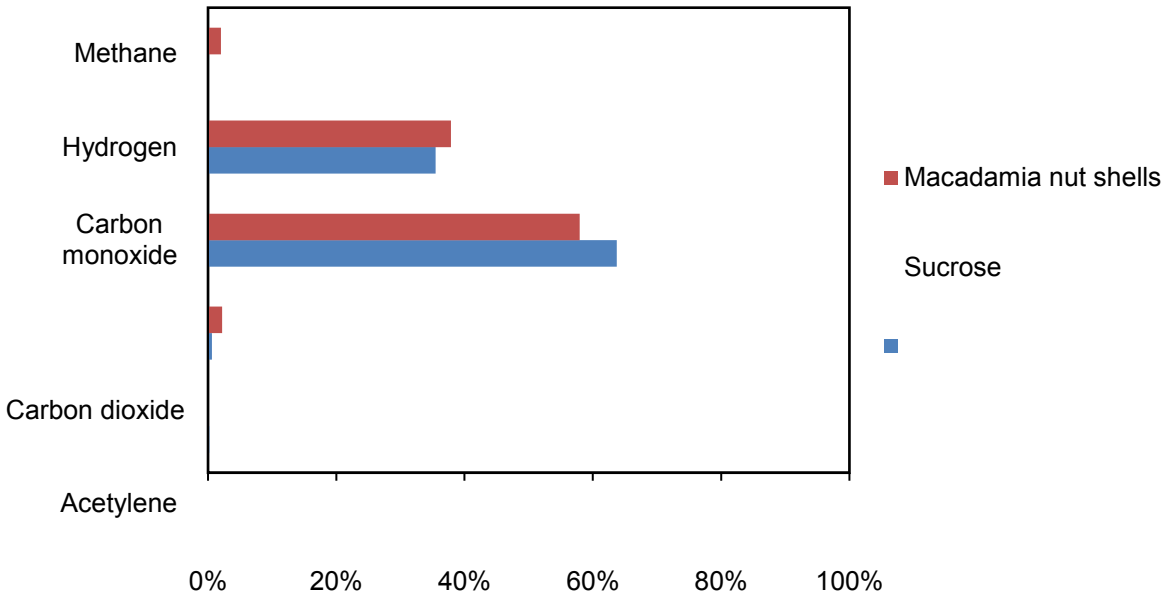

Figure 4.25: Produced gas composition of plasma gasification of sucrose and macadamia nut shells without the presence of oxygen at a constant power of 11 kW

This analysis indicates that the CO/CO_2 ratio for the sucrose experiments is 109, while the CO/CO_2 ratio for the macadamia nut shells is 29. Sucrose thus yields a better quality syngas. (Beneroso, Bermúdez *et al.,* 2015) made the observation that higher CO/CO_2 ratios implies better syngas quality. One of the factors contributing to this may be that the particle diameter of the sucrose is 0.4 mm, while that of the macadamia nut shells is 10 mm. Sucrose crystals, because of not much more than heat transfer effects, should thus gasify more quickly, leaving the gaseous species formed more time to reach thermodynamic equilibrium. (Kumar, Guangul *et al.*, 2016) also investigated the effect of particle size and biomass blending ratio on syngas composition. Similarly, the syngas they produced consisted mainly of CO, H_2, CH_4 and CO_2. The results showed that smaller particle size leads to higher conversion to CO, H_2 and CH_4. The reason for the higher yields is the better heat transfer within smaller particle sizes and the larger surface area of the particles. The larger the particle size, the less effective the surface area for gasification, which consequently produces syngas with low H_2 and CO content.

(Hrabovsky, 2011) also observed that the particle diameter substantially influences both the surface temperature and the gasification rate. An increase in the diameter results in a reduction in heat transfer to the particle due to more intensive shielding of the particle by the gas sheath formed from volatilized material. Another contributing factor could be that the available carbon in the macadamia nut shells structure are more strongly bonded than in sucrose.

4.3.5 Effect of oxygen addition on plasma gasification of macadamia nut shells

Two more additional experiments were conducted to investigate the effect of oxygen addition on the plasma gasification of macadamia nut shells. The experiments were performed at a constant power of 11 kW and constant macadamia nut shells feed rate of 1 kg/h. Three different oxygen mass flows were evaluated, at 0 kg/h, 0.619 kg/h (14% oxygen added), and 0.652 kg/h (20% oxygen added). The objective was to investigate the effect of oxygen addition on the quality of syngas. Figure 4.25 shows the gas species distribution at these input values.

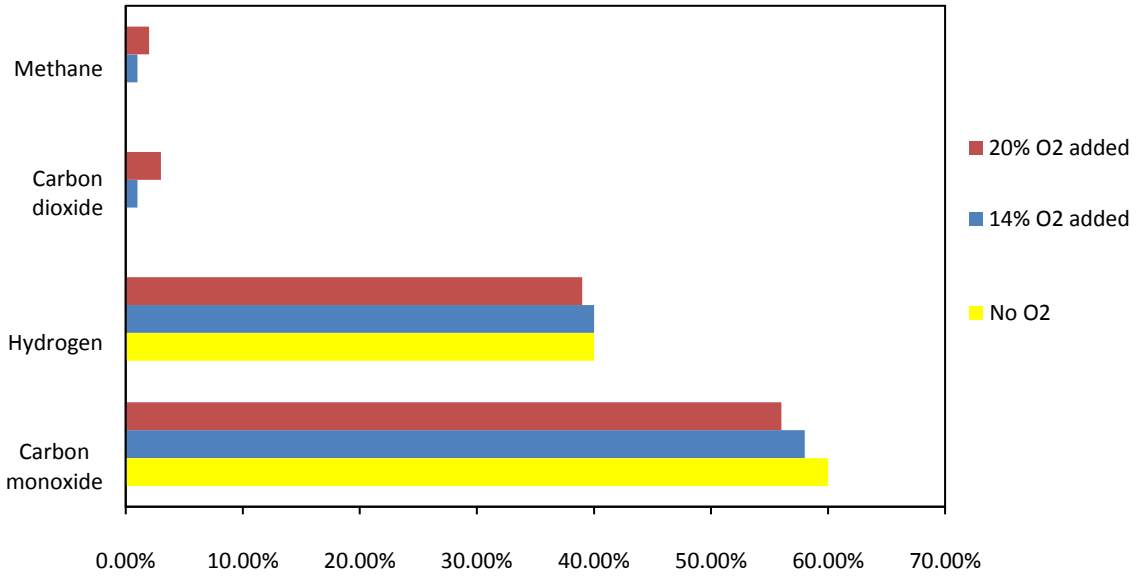

Figure 4.26: Producer gas composition of plasma gasification for macadamia nut shells at a constant power of 11 kW

The gas consists of CO, H_2, CO_2 and CH_4. It is evident that an increase in oxygen decreases the quality of the syngas. (Gray, 2014) also came to a similar conclusion, namely that as the amount of air increases, the quality of the syngas and the efficiency of the conversion decreases. High oxygen addition give rise to the formation hydrocarbons and carbon dioxide. The absence of oxygen in the plasma gasification of macadamia nut shells improves the quality of syngas, as only CO and H_2 are the predominant products.

4.4 Technical performance of the system

(Hrabovsky, 2011) summarized the advantages of plasma gasification methods over conventional methods as follows:

a) The energy for gasification is supplied by the plasma torch rather than the energy liberated from the combustion process. The energy input is thus is independent of the heated of combustion of the treated substances. This provides flexibility and fast process control. A broad range of biomass feedstock can be thus treated.
b) The combustion gases generated in conventional autothermal reactors are minimal.
c) The temperature in the reactor can be easily controlled by the independent variation of the plasma power and material feed rate.
d) The high temperatures required for gasification and a homogeneous temperature distribution can easily be achieved and maintained in the whole reactor volume. The production of higher hydrocarbons, tars, and other complex organic molecules is minimised.
e) High energy density and high heat transfer efficiency can be achieved, allowing shorter residence times and higher material throughputs.
f) Easy control of composition of reaction products.
g) Low thermal inertia and easy feedback control.
h) Much lower plasma gas input per unit heating power than the gas flow of classical reactors and thus lower energy loss corresponding to the energy necessary for heating of plasma to reaction temperature; also lower amount of gases diluting produced syngas.
i) Smaller plants than for conventional reactors due to high energy densities, lower gas flows, and volume reduction.

The majority of these claims can be confirmed from the experience obtained during this project. Point by point, comments on the above claims are as follow: a) The temperature in the reactor was indeed easily controlled by adjusting the power settings of the torch and controlling the material feed. This can only be done within the limits of the hardware. For example the torch cannot operate below 6–7 kW. And although trivial sounding, the solid feed into the reactor is not necessarily that easy. Although anything can be fed in principle, treatment of the solids to optimal size and flowability is critical for a hopper to operate. b) The combustion gases, predominantly carbon dioxide and methane were maximally 6 %. c) The experiments

were performed in the range 900 to 1100 °C. Higher temperature were found to be possible. d) Optimisation of the temperature distribution inside the reactor is an ongoing project. Nevertheless, from the work done to date, cold spots and/or areas without adequate gas flow have not been intractable problems, and certainly fixable common-sense design improvements. e) Relatively fast feeds are possible, within the limits reported here. It is clear that full conversion of the solids was not obtained and careful optimisation is still required. f) The composition of the gasification stream predominantly carbon monoxide and hydrogen, in a more or less consistent ratio, with minimal amounts of methane and carbon dioxide—in the parameter range investigated. Some variation would be possible, if for example water is used as oxidant. Consistency rather than variability should probably be claimed. g) The system takes roughly 45 min to reach thermal equilibrium. This is two step process: first a constant temperature is sought with only the torch gas; once solid feeding starts a new equilibrium is reached and power has to be adjusted. This final torch setting and internal temperature was used for this research. Since it was important for this work to obtain consistent results, this was found necessary. For practical industrial work, this may not be the case, and the system is certainly less cumbersome than a conventional autothermal setup. h) The plasma gas flow for this system was 26.7 to 40 slpm. The torch itself may be turned on and off at will. i) The total footprint of the gasification system is 1×2 m^2, and that of the power supply another 1×2 m^2. The PSU, reactor system, and utilities are all mountable on a 2×m^2 skip, and may be easily moved to the biomass point of source.

Commercially available non-transfer arc plasma torches have energy efficiencies of ~ 65 % (Hrabovsky, 2006). The efficiency of the torch used here is 30 %. This may not only be attributable to torch design, but also to the closeness of the node to the hot reactor internal volume. Optimisation of this will result in a net energy gain, in the form of syngas.

Chapter 5 Conclusions and recommendations

The main aim of the project was to investigate the performance of a pilot-scale plasma gasification system comprising a plasma torch and PSU, with a nominal rating of 30 kW, but in practice run at 15 kW and below, a gasification reactor, a hopper, and all necessary utilities.

Plasma gasification experiments were conducted on sucrose and crushed macadamia nutshells. The pilot-scale plasma gasification system used comprises a 15 kW DC plasma torch fitted to a 5 L gasification reactor. The DC plasma torch has an efficiency of ~30 % with most of the energy lost in the torch anode.

For the macadamia nutshells, the plasma input-power was set at 9, 11 and 14 kW. At each power input setting, four different feed rates were investigated, namely 0.5, 0.7, 1.04 and 1.14 kg/h. It was observed that as the power increases, conversion increases from 48 % at 9 kW to higher than 80 % at 14 kW. It was also observed that higher mass feed rates increase the conversion. The lower heating values of the syngas produced during gasification increased with higher power inputs and higher feed rates. At a feed rate of 1 kg/h, the maximum calorific power value was 3.45 kW, at a torch setting of 14 kW. The highest power values obtained was slightly more than 4 kW.

The effect of equivalence ratio (ER) was evaluated on the plasma gasification of sucrose. ER values of 1 and 2 were investigated. With an ER of 1, the CO/H_2 ratio was 1.8 and the CO/CO_2 ratio was 109. With an ER of 2, the CO/H_2 ratio was 1.73, and the CO/CO_2 ratio 18. As expected, an increase in ER enhances the formation of CO_2. A low ER thus results in higher syngas quality.

At equivalent conditions the homogenous, crystalline sucrose yielded a CO/CO_2 ratio of 109, significantly higher than the 29 for plasma gasification of the macadamia nut shells. A contributing factor to having better quality syngas, was the smaller the average particle diameter of the sucrose, 0.4 mm, compared to the 10 mm of the crushed macadamia nut shells was. Another contributing factor could be that the available carbon in the macadamia nut shells structure are more strongly bonded than in sucrose.

For additional insight, kinetic data for the pyrolysis of sucrose, fructose and glucose were obtained using a TGA-FTIR hyphenated system, at much lower heating rates than anticipated in plasma system, and TGA-DTG experiments on macadamia nut shells. Dynamic studies were

performed on sucrose, fructose and glucose at heating rates of 5, 10, 15, 20 and 50 °C/min in an atmosphere of nitrogen flowing at 50 mL/min, and for the macadamia shell at heating rates of 5, 10 and 20 °C/min in an atmosphere of nitrogen flowing at 50 mL/min. The sugars yielded 80 % to 85 % conversion into gaseous products, while the conversion of the shells approached 90 %; the residue was biochar. The FTIR spectra showed the major products that form from the pyrolysis of sugars to be CO_2, H_2O, along with large quantities C-H-O-containing compounds, amongst them $C_5H_4O_2$ and $C_6H_6O_3$. The latter two compounds are probably condensible.

The system overall was found to be robust and functional. At best, however, there is no net energy gain, and the energy content of the syngas yield is equal to the energy introduced into the reactor, the latter value not including anode losses. For optimisation the point below are suggested.

An increase in the yield of syngas produced can be achieved by optimizing the angle at which the torch strikes the raw material from the screw feeder. Maintaining direct contact of the energy from the torch with the raw material will ensure maximum conversion. The best operating approach entails feeding the raw material at the optimal set point for the mass feed rate, as well as ensuring sufficient power of the DC torch.

Ideally, the aim of any cost-intensive project is to operate at a gain. One of the interventions to save costs would be to operate the plasma gasification system during the summer months and outside Eskom's peak hours, i.e. when electricity is cheapest.

Insulators such as ceramics around the reactor wall can be used to reduce heat losses. Insulating flanges can also be installed to reduce heat losses by means of conduction and radiation. The heat loss due to the outer quench can be reduced by minimizing the outlet temperature from the quench. If the design permits, one could consider installing a heat exchanger.

We observed that the largest heat loss for the whole system occurs at the torch anode. One avenues to be explored should be optimisation of the swirl ring. The main objective of swirl rings is to ensure efficient swirling of the plasma gas around the electrode, creating a jet/nozzle. This aids the gas flow through the nozzle to deliver the best edge angularity. In future work, it would be beneficial to investigate the design of the swirl rings and to find the optimal way to reduce the heat loss due to the anode. Figure 5.1 shows a swirl ring.

Figure 5.1: Four-hole swirl ring

Finally the position of the torch exit, i.e. its anode, needs to be reconsidered, and ways of shielding it from the glare of the reactor investigated..

References

Agon, N, M Hrabovský, O Chumak, M Hlína, V Kopecký, A Masláni, A Bosmans, L Helsen, S Skoblja and G Van Oost (2016). "Plasma gasification of refuse derived fuel in a single-stage system using different gasifying agents." *Waste Management* **47**, 246-255.

Ahrenfeldt, J, TP Thomsen, U Henriksen and LR Clausen (2013). "Biomass gasification cogeneration – A review of state of the art technology and near future perspectives." *Applied Thermal Engineering* **50**(2), 1407-1417.

Alonso Pippo, W, CA Luengo, L Alonsoamador Morales Alberteris, P Garzone and G Cornacchia (2011). "Energy Recovery from Sugarcane-Trash in the Light of 2nd Generation Biofuel. Part 2: Socio-Economic Aspects and Techno-Economic Analysis." *Waste and Biomass Valorization* **2**(3), 257-266.

Bada, S, R Falcon, L Falcon and M Makhula (2015). "Thermogravimetric investigation of macadamia nut shell, coal, and anthracite in different combustion atmospheres." *Journal of the Southern African Institute of Mining and Metallurgy* **115**(8), 741-746.

Bassilakis, R, RM Carangelo and MA Wójtowicz (2001). "TG-FTIR analysis of biomass pyrolysis." *Fuel* **80**(12), 1765-1786.

Basu, P (2013). Biomass Gasification, Pyrolysis and Torrefaction: Practical Design and Theory, *Elsevier Science*.

Battacharya, SC, AH Siddique and HL Pham (1999). "A study on wood gasification for Low-Tar Gas production." *Energy* **24**.

Beneroso, D, JM Bermúdez, A Arenillas and JA Menéndez (2015). Comparing the composition of the synthesis-gas obtained from the pyrolysis of different organic residues for a potential use in the synthesis of bioplastics.

Bocci, E, A Di Carlo and D Marcelo (2009). "Power plant perspectives for sugarcane mills." *Energy* **34**(5), 689-698.

Boulos, MI, P Fauchais and E Pfender (2013). Thermal Plasmas: Fundamentals and Applications, *Springer US*.

Bridgwater, AV (2003). "Renewable fuels and chemicals by thermal processing of biomass." *Chem Eng J* **91**.

Bridgwater, AV and GVC Peacocke (2000). "Fast pyrolysis processes for biomass." *Renewable and Sustainable Energy Reviews* **4**(1), 1-73.

Bulut, A and S Karagoz (2013). "Pyrolysis of table sugar." *ScientificWorldJournal* **2013**, 172039.

Byun, Y, M Cho, JW Chung, W Namkung, HD Lee, SD Jang, Y-S Kim, J-H Lee, C-R Lee and S-M Hwang (2011). "Hydrogen recovery from the thermal plasma gasification of solid waste." *Journal of hazardous materials* **190**(1), 317-323.

Canabarro, N, JF Soares, CG Anchieta, CS Kelling and MA Mazutti (2013). "Thermochemical processes for biofuels production from biomass." *Sustainable Chemical Processes* **1**(1), 22.

Cangialosi, F, G Intini, L Liberti, M Notarnicola and P Stellacci (2008). "Health risk assessment of air emissions from a municipal solid waste incineration plant – A case study." *Waste Management* **28**(5), 885-895.

Chang, AC, H-F Chang, F-J Lin, K-H Lin and C-H Chen (2011). "Biomass gasification for hydrogen production." *International Journal of Hydrogen Energy* **36**(21), 14252-14260.

Chen, H, B Dou, Y Song, Y Xu, Y Zhang, C Wang, X Zhang and C Tan (2012). "Pyrolysis characteristics of sucrose biomass in a tubular reactor and a thermogravimetric analysis." *Fuel* **95**(0), 425-430.

Curley, R (2011). Fossil Fuels, *Britannica Educational Pub.*

Demirbas, A (2004). "Combustion characteristics of different biomass fuels." *Progress in energy and combustion science* **30**(2), 219-230.

Demirbas, A (2004). "Effects of temperature and particle size on bio-char yield from pyrolysis of agricultural residues." *Journal of Analytical and Applied Pyrolysis* **72**(2), 243-248.

Demirbas, MF (2009). "Biorefineries for biofuel upgrading: a critical review." *Applied Energy* **86**, S151-S161.

Demirbas, MF, M Balat and H Balat (2011). "Biowastes-to-biofuels." *Energy Conversion and Management* **52**(4), 1815-1828.

Department of Agriculture, FaF (2017). "Trends in the Agricultural Sector 2016." Retrieved 2018/5/2, 2016, from http://www.daff.gov.za/Daffweb3/Portals/0/Statistics%20and%20Economic%20Analysis/Statistical%20Information/Trends%20in%20the%20Agricultural%20Sector%202016.pdf.

Diaz, G, E Leal-Quiros, R Smith, J Elliott and D Unruh (2014). Syngas generation from organic waste with plasma steam reforming. Journal of Physics: Conference Series, *IOP Publishing*.

Dong, J, Y Chi, Y Tang, M Ni, A Nzihou, E Weiss-Hortala and Q Huang (2016). "Effect of Operating Parameters and Moisture Content on Municipal Solid Waste Pyrolysis and Gasification." *Energy & Fuels* **30**(5), 3994-4001.

Downie, A, A Crosky and P Munroe (2009). "Physical properties of biochar." *Biochar for environmental management: Science and technology*, 13-32.

Eff, C (1973). Solid waste incinerator, *Google Patents*.

Fabry, F, C Rehmet, V Rohani and L Fulcheri (2013). "Waste gasification by thermal plasma: a review." *Waste and Biomass Valorization* **4**(3), 421-439.

Fang, Z (2013). Pretreatment Techniques for Biofuels and Biorefineries, *Springer Berlin Heidelberg*.

Fiorese, G, M Catenacci, V Bosetti and E Verdolini (2014). "The power of biomass: Experts disclose the potential for success of bioenergy technologies." *Energy Policy* **65**(0), 94-114.

Funino, J, K Yamaji and H Yamameto (1999). "Biomass-balance table for evaluating bioenergy resources." *Appl Energy* **63**.

Garbelini, R, EO Ono, JD Rodrigues, EC Camili and ARB da Silva (2016). "Plant growth regulators and shade on emergence in macadamia nut tree." *Bioscience Journal*.

Gaussling, P (2008).” Thermal decomposition of sucrose in nitrogen atmosphere”, *Lamentations of chemistry*, *Editorial of scientist political*.

Giudicianni, P, G Cardone and R Ragucci (2013). Cellulose, hemicellulose and lignin slow steam pyrolysis: thermal decomposition of biomass components mixtures. J Anal Apllied Pyrolysis.

Gómez-Barea, A, P Ollero and B Leckner (2013). "Optimization of char and tar conversion in fluidized bed biomass gasifiers." *Fuel* **103**.

Govender, M (2011). "COP17 and renewable energy." *South African Sugar Journal* **95**, 202-203.

Gray, L (2014). "Plasma Gasification as a Viable Waste-to-Energy Treatment of Municipal Solid Waste." *Solid and Hazardous Waste Prevention and Control Engineering*.

Hlina, M, M Hrabovsky, T Kavka and M Konrad (2014). "Production of high-quality syngas from argon/water plasma gasification of biomass and waste." *Waste management* **34**(1), 63-66.

Hrabovsky, M (2011). “Thermal plasma gasification of biomass. Progress in Biomass and Bioenergy Production”. S Shaukat, *InTech***,** 41-62.

Hrabovsky, M (2011). Thermal Plasma Gasification of Biomass.

Jin, W, K Singh and J Zondlo (2013). "Pyrolysis Kinetics of Physical Components of Wood and Wood-Polymers Using Isoconversion Method." *Agriculture* **3**(1), 12-32.

Johnson, RR, ED Alford and GW Kinzer (1969). "Formation of sucrose pyrolysis products." *Journal of Agricultural and Food Chemistry* **17**(1), 22-24.

Kim, KH, J-Y Kim, T-S Cho and JW Choi (2012). "Influence of pyrolysis temperature on physicochemical properties of biochar obtained from the fast pyrolysis of pitch pine (Pinus rigida)." *Bioresource Technology* **118**, 158-162.

Knoef, H and J Ahrenfeldt (2005). Handbook biomass gasification, *BTG biomass technology group The Netherlands*.

Koçar, G and N Civaş (2013). "An overview of biofuels from energy crops: Current status and future prospects." *Renewable and Sustainable Energy Reviews* **28**(0), 900-916.

Koumi Ngoh, S and D Njomo (2012). "An overview of hydrogen gas production from solar energy." *Renewable and Sustainable Energy Reviews* **16**(9), 6782-6792.

Kumar, A, F Guangul, M Inayat and S Sulaiman (2016). "Effect of fuel particle size and blending ratio on syngas production and performance of co-gasification." *Journal of Mechanical Engineering and Sciences* **10**(2), 2188-2200.

Kumar, U, S Maroufi, R Rajarao, M Mayyas, I Mansuri, RK Joshi and V Sahajwalla (2017). "Cleaner production of iron by using waste macadamia biomass as a carbon resource." *Journal of Cleaner Production* **158**, 218-224.

Leal, MRLV, MV Galdos, FV Scarpare, JEA Seabra, A Walter and COF Oliveira (2013). "Sugarcane straw availability, quality, recovery and energy use: A literature review." *Biomass and Bioenergy* **53**, 11-19.

Lede, J and O Bouton (1999). Flash pyrolysis of biomass submitted to a concentrated radiation. Application to the study of the primary steps of cellulose thermal decomposition. Division of fuel chemistry; reprints of symposia, vol. 44(2), 217th ACS meeting, 21–25 march. USA, *Anaheim*.

Loh, YR, D Sujan, ME Rahman and CA Das (2013). "Sugarcane bagasse—The future composite material: A literature review." *Resources, Conservation and Recycling* **75**, 14-22.

Luo, Z, S Wang, Y Liao, J Zhou, Y Gu and K Cen (2004). "Research on biomass fast pyrolysis for liquid fuel." *Biomass Bioenergy* **26**.

Makaringe, N, I van der Walt, G J. Puts and P L. Crouse (2017). TGA-FTIR Characterisation of Bamboo Wood, Napier Grass, Pine Wood and Peach Pips for Gasification Applications.

Mandl, C, I Obernberger and F Biedermann (2009). Updraft fixed-bed gasification of softwood pellets: mathematical modelling and comparison with experimental data. Proceedings of the 17 th European Biomass Conference & Exhibition, ETA-Renewable Energies.

Marquesi, A, GP Filho, A Gorbunov, A Halinouski, A Essiptchouk and B Sismanoglu (2015). "THEORETICAL ASSESSMENT OF PLASMA GASIFICATION PROCESS OF LOW-GRADE COAL AND BIOMASS FEEDSTOCK." *ADVANCES IN CHEMISTRY RESEARCH*, 57.

McKendry, P (2002). "Energy production from biomass (part 3): gasification technologies." *Bioresource Technology* **83**(1), 55-63.

Merola, R (2011). Reactor for pyrolysis of biomass.

Mohan, D, CU Pittman and PH Steele (2006). "Pyrolysis of wood/biomass for bio-oil: acritical review." *J Energy Fuels* **20**.

Molino, A, S Chianese and D Musmarra (2016). "Biomass gasification technology: The state of the art overview." *Journal of Energy Chemistry* **25**(1), 10-25.

Nagao, MA (2011). "Farm and forestry production and marketing profile for macadamia nut (Macadamia integrifolia and M. tetraphylla)." *Specialty crops for pacific island agroforestry. Holualoa, Hawaii: Permanent Agriculture Resources*.

Obernberger, I and G Thek (2008). Combustion and gasification of solid biomass for heat and power production in Europe-state-of-the-art and relevant future developments. Proc. of the 8th European Conference on Industrial Furnaces and Boilers (keynote lecture).

Oelofse, SH and A Nahman (2013). "Estimating the magnitude of food waste generated in South Africa." *Waste Management & Research* **31**(1), 80-86.

Ozcan, M (2014). "Assessment of renewable energy incentive system from investors' perspective." *Renewable Energy* **71**(0), 425-432.

Pellegrini, LF and S De Oliveira (2007). "Exergy analysis of sugarcane bagasse gasification." *Energy* **32**(4), 314-327.

Pennington, NL and CW Baker (1990). Sugar: User's Guide To Sucrose, *Springer US*.

Ponder, GR and GN Richards (1993). "Pyrolysis of inulin, glucose and fructose." *Carbohydrate research* **244**(2), 341-359.

Popp, J, Z Lakner, M Harangi-Rákos and M Fári (2014). "The effect of bioenergy expansion: Food, energy, and environment." *Renewable and Sustainable Energy Reviews* **32**(0), 559-578.

Rubel, FN (1974). Incineration of solid wastes / Fred N. Rubel. Park Ridge, N.J, *Noyes Data Corp*.

Ruiz, JA (2013). "Biomass gasification for electricity generation: review of current technology barriers." *Renew Sustain Energy Rev* **18**.

Samal, S (2017). "Thermal plasma technology: The prospective future in material processing." *Journal of Cleaner Production* **142, Part 4**, 3131-3150.

SASA (2014). "Cane Growing in South Africa." Retrieved 11 November, 2014, from http://www.sasa.org.za/sugar_industry/CaneGrowinginSA.aspx.

Serio, MA, E Kroo and MA Wójtowicz (2003). "Biomass pyrolysis for distributed energy generation." *ACS Division of Fuel Chemistry Preprints* **48**(2), 584.

Shie, J-L, L-X Chen, K-L Lin and C-Y Chang (2014). "Plasmatron gasification of biomass lignocellulosic waste materials derived from municipal solid waste." *Energy* **66**, 82-89.

Siedlecki, M, W De Jong and AHM Verkooijen (2011). "Fluidized Bed Gasification as a Mature And Reliable Technology for the Production of Bio-Syngas and Applied in the Production of Liquid Transportation Fuels—A Review." *Energies* **4**(3), 389.

Sikarwar, VS, M Zhao, P Clough, J Yao, X Zhong, MZ Memon, N Shah, EJ Anthony and PS Fennell (2016). "An overview of advances in biomass gasification." *Energy & Environmental Science* **9**(10), 2939-2977.

Šimkovic, I, I Šurina and M Vričan (2003). "Primary reactions of sucrose thermal degradation." *Journal of Analytical and Applied Pyrolysis* **70**(2), 493-504.

Sinha, S, A Jhalani, M Ravi and A Ray (2000). "Modelling of pyrolysis in wood: A review." *SESI Journal* **10**(1), 41-62.

Smithers, J (2014). "Review of sugarcane trash recovery systems for energy cogeneration in South Africa." *Renewable and Sustainable Energy Reviews* **32**, 915-925.

Southern African Macadamia Growers's Association (2018). "Overview of macadamia crop." Retrieved 2018/5/2, 2018.

Srirangan, K, L Akawi, M Moo-Young and CP Chou (2012). "Towards sustainable production of clean energy carriers from biomass resources." *Applied Energy* **100**(0), 172-186.

Tamošiūnas, A, P Valatkevičius, V Valinčius and R Levinskas (2016). "Biomass conversion to hydrogen-rich synthesis fuels using water steam plasma." *Comptes Rendus Chimie* **19**(4), 433-440.

Tang, H, Y Zhang and Y Chen (2013). Method and apparatus for pyrolysis and gasification of biomass.

The Chamber of Mines Coal Leadership Forum (2018, 2018). "National coal strategy for South Africa." Retrieved 2018/5/2, 2018, from http://www.chamberofmines.org.za/component/jdownloads/send/25-downloads/535-coal-strategy-2018.

Trazzi, P, J Leahy, M Hayes and W Kwapinski (2016). "Adsorption and desorption of phosphate on biochars." *Journal of Environmental Chemical Engineering* **4**(1), 37-46.

Trelles, JP, C Chazelas, A Vardelle and JVR Heberlein (2009). "Arc Plasma Torch Modeling." *Journal of Thermal Spray Technology* **18**(5), 728.

Van Oost, G, M Hrabovsky, V Kopecky, M Konrad, M Hlina and T Kavka (2008). "Pyrolysis/gasification of biomass for synthetic fuel production using a hybrid gas–water stabilized plasma torch." *Vacuum* **83**(1), 209-212.

Wang, C, B Dou, Y Song, H Chen, M Yang and Y Xu (2014). "Kinetic Study on Non-isothermal Pyrolysis of Sucrose Biomass." *Energy & Fuels* **28**(6), 3793-3801.

Wang, S, Q Liu, Z Luo, L Wen and K Cen (2007). "Mechanism study on cellulose pyrolysis using thermogravimetric analysis coupled with infrared spectroscopy." *Frontiers of Energy and Power Engineering in China* **1**(4), 413-419.

Wienese, A and B Purchase (2004). Renewable energy: an opportunity for the South African sugar industry? Proc S Afr Sug Technol Ass, *Citeseer*.

Xavier, T, T Lira, M Schettino Jr and M Barrozo (2016). "A STUDY OF PYROLYSIS OF MACADAMIA NUT SHELL: PARAMETRIC SENSITIVITY ANALYSIS OF THE IPR MODEL." *Brazilian Journal of Chemical Engineering* **33**(1), 115-122.

Yang, H, R Yan, H Chen, DH Lee and C Zheng (2007). "Characteristics of hemicellulose, cellulose and lignin pyrolysis." *Fuel* **86**(12–13), 1781-1788.

Yang, Z, X Liu, Z Yang, G Zhuang, Z Bai, H Zhang and Y Guo (2013). "Preparation and formation mechanism of levoglucosan from starch using a tubular furnace pyrolysis reactor." *Journal of Analytical and Applied Pyrolysis* **102**(0), 83-88.

Yanik, J, C Kornmayer, M Saglam and M Yüksel (2007). "Fast pyrolysis of agricultural wastes: Characterization of pyrolysis products." *Fuel Processing Technology* **88**(10), 942-947.

Appendix A – Cooling water during plasma gasification

Table A: Operating conditions for cooling water per compartment during plasma gasification experiments

Cathode (liters/min)	Anode (liters/min)	Inner quench (liters/min)	Outer quench (liters/min)	Reactor (liters/min)	Flange (liters/min)	Feeder (liters/min)
17	17	5	5	5	5	5

Appendix B – Plasma gasification of macadamia nut shells operating conditions

Table B: Operating conditions for the plasma gasification of macadamia nut shells at constant power 9 kW and 0.543 kg/h feed rate

Cooling water (In)	Cooling water (Out)	Volts	Current	Cathode CW out(°C)	Anode CW out(°C)	Inner quench CW out(°C)	Outer quench CW out(°C)	Reactor CW out(°C)	Flange CW out(°C)	Reactor Gas temp. (°C)	N_2 flow (slpm)
15.2	19.8	88.5	103	15.6	21.2	16.5	16.4	20.3	18.3	1032.8	26.6

Table C: Operating conditions for the plasma gasification of macadamia nut shells at constant power 9 kW and 0.72 kg/h feed rate

Cooling water (In)	Cooling water (Out)	Volts	Current	Cathode CW out(°C)	Anode CW out(°C)	Inner quench CW out(°C)	Outer quench CW out(°C)	Reactor CW out(°C)	Flange CW out(°C)	Reactor Gas temp. (°C)	N_2 flow (slpm)
17.62	18.2	83.5	109	18.4	22.2	18.5	18.7	18.8	18.7	961.5	26.6

Table D: Operating conditions for the plasma gasification of macadamia nut shells at constant power 9 kW and 1 kg/h feed rate

Cooling water (In)	Cooling water (Out)	Volts	Current	Cathode CW out(°C)	Anode CW out(°C)	Inner quench CW out(°C)	Outer quench CW out(°C)	Reactor CW out(°C)	Flange CW out(°C)	Reactor Gas temp. (°C)	N_2 flow (slpm)
17.1	21.1	70	130	17.3	21.8	18.9	19	24.5	19.7	1002.8	26.6

Table E: Operating conditions for the plasma gasification of macadamia nut shells at constant power 9 kW and 1.435 kg/h feed rate

Cooling water (In)	Cooling water (Out)	Volts	Current	Cathode CW out(°C)	Anode CW out(°C)	Inner quench CW out(°C)	Outer quench CW out(°C)	Reactor CW out(°C)	Flange CW out(°C)	Reactor Gas temp. (°C)	N_2 flow (slpm)
17.4	22.1	72	131	17.6	22.4	19.1	18.6	23.4	18.6	1023.2	26.6

Table F: Operating conditions for the plasma gasification of macadamia nut shells at constant power 11 kW and 0.543 kg/h feed rate

Cooling water (In)	Cooling water (Out)	Volts	Current	Cathode CW out(°C)	Anode CW out(°C)	Inner quench CW out(°C)	Outer quench CW out(°C)	Reactor CW out(°C)	Flange CW out(°C)	Reactor Gas temp. (°C)	N_2 flow (slpm)
19.6	23.7	115	100	19.7	26.4	20.8	21.3	22.7	21.7	1063	26.6

Table G: Operating conditions for the plasma gasification of macadamia nut shells at constant power 11 kW and 0.72 kg/h feed rate

Cooling water (In)	Cooling water (Out)	Volts	Current	Cathode CW out(°C)	Anode CW out(°C)	Inner quench CW out(°C)	Outer quench CW out(°C)	Reactor CW out(°C)	Flange CW out(°C)	Reactor Gas temp. (°C)	N_2 flow (slpm)
19.9	24.5	115	100	20.3	26.3	20.6	21.5	22.7	21.1	1042	26.6

Table H: Operating conditions for the plasma gasification of macadamia nut shells at constant power 11 kW and 1 kg/h feed rate

Cooling water (In)	Cooling water (Out)	Volts	Current	Cathode CW out(°C)	Anode CW out(°C)	Inner quench CW out(°C)	Outer quench CW out(°C)	Reactor CW out(°C)	Flange CW out(°C)	Reactor Gas temp. (°C)	N_2 flow (slpm)
19.7	24.8	115	100	20.2	27	20.9	21.6	24.2	22.1	1107	26.6

Table I: Operating conditions for the plasma gasification of macadamia nut shells at constant power 11 kW and 1.435 kg/h feed rate

Cooling water (In)	Cooling water (Out)	Volts	Current	Cathode CW out(°C)	Anode CW out(°C)	Inner quench CW out(°C)	Outer quench CW out(°C)	Reactor CW out(°C)	Flange CW out(°C)	Reactor Gas temp. (°C)	N_2 flow (slpm)
20.1	24.5	115	100	20.2	26.8	16.5	21.5	24.1	21.9	1076	26.6

Table J: Operating conditions for the plasma gasification of macadamia nut shells at constant power 14 kW and 0.543 kg/h feed rate

Cooling water (In)	Cooling water (Out)	Volts	Current	Cathode CW out(°C)	Anode CW out(°C)	Inner quench CW out(°C)	Outer quench CW out(°C)	Reactor CW out(°C)	Flange CW out(°C)	Reactor Gas temp. (°C)	N_2 flow (slpm)
17.1	23.1	72	195	20.7	26.4	18.6	18.2	19.6	19.1	1049	26.6

Table K: Operating conditions for the plasma gasification of macadamia nut shells at constant power 14 kW and 0.72 kg/h feed rate

Cooling water (In)	Cooling water (Out)	Volts	Current	Cathode CW out(°C)	Anode CW out(°C)	Inner quench CW out(°C)	Outer quench CW out(°C)	Reactor CW out(°C)	Flange CW out(°C)	Reactor Gas temp. (°C)	N_2 flow (slpm)
18.2	23.9	72	195	21	26.8	18.6	18.5	19.6	19.8	1086	26.6

Table L: Operating conditions for the plasma gasification of macadamia nut shells at constant power 14 kW and 1 kg/h feed rate

Cooling water (In)	Cooling water (Out)	Volts	Current	Cathode CW out(°C)	Anode CW out(°C)	Inner quench CW out(°C)	Outer quench CW out(°C)	Reactor CW out(°C)	Flange CW out(°C)	Reactor Gas temp. (°C)	N_2 flow (slpm)
18.3	24.1	73	195	21.3	26.7	18.8	18.6	20.3	20.1	1103	26.6

Appendix C – Plasma gasification of macadamia nut shells & oxygen

Table M: Operating conditions for the plasma gasification of macadamia nut shells at constant power 11 kW and 1 kg/h feed rate

Cooling water (In)	Cooling water (Out)	Volts	Current	Cathode CW out(°C)	Anode CW out(°C)	Inner quench CW out(°C)	Outer quench CW out(°C)	Reactor CW out(°C)	Flange CW out(°C)	Reactor Gas temp. (°C)	O_2 flow (slpm)
17.2	19.5	115	100	20.5	26.8	21.3	20.4	23.4	22.6	1115	1.58

Table N: Operating conditions for the plasma gasification of macadamia nut shells at constant power 11 kW and 1 kg/h feed rate

Cooling water (In)	Cooling water (Out)	Volts	Current	Cathode CW out(°C)	Anode CW out(°C)	Inner quench CW out(°C)	Outer quench CW out(°C)	Reactor CW out(°C)	Flange CW out(°C)	Reactor Gas temp. (°C)	O_2 flow (slpm)
19.6	22.8	115	100	20.5	27.4	21.6	21.7	24.8	23.4	1124	1.67

Appendix D – Plasma gasification of sucrose with ER of 1

Table O: Operating conditions for the plasma gasification of sucrose at constant power 11 kW, 1 kg/h feed rate & ER of 1

Cooling water (In)	Cooling water (Out)	Volts	Current	Cathode CW out(°C)	Anode CW out(°C)	Inner quench CW out(°C)	Outer quench CW out(°C)	Reactor CW out(°C)	Flange CW out(°C)	Reactor Gas temp. (°C)	O_2 flow (slpm)
21.7	26.4	115	100	24.8	28.8	23.4	23.8	25.8	24.8	1053	0.12

Appendix E – Plasma gasification of sucrose with ER of 2

Table P: Operating conditions for the plasma gasification of sucrose at constant power 11 kW, 1 kg/h feed rate & ER of 2

Cooling water (In)	Cooling water (Out)	Volts	Current	Cathode CW out(°C)	Anode CW out(°C)	Inner quench CW out(°C)	Outer quench CW out(°C)	Reactor CW out(°C)	Flange CW out(°C)	Reactor Gas temp. (°C)	O_2 flow (slpm)
22.2	26.8	115	101	23.2	29.6	24.6	24.5	26.9	25	1163	0.24